POTENTIAL APPLICABILITY OF STRESS WAVE VELOCITY METHOD ON PAVEMENT BASE MATERIALS AS A NON-DESTRUCTIVE TESTING TECHNIQUE

By

MASRUR MAHEDI

Presented to the Faculty of the Graduate School of

The University of Texas at Arlington in Partial Fulfillment

of the Requirements

for the Degree of

MASTER OF SCIENCE IN CIVIL ENGINEERING

THE UNIVERSITY OF TEXAS AT ARLINGTON

December 2015

Acknowledgements

First, I would like to express my deepest gratitude to my supervisor Dr. Sahadat Hossain, for his valuable time, guidance, encouragement, help and unconditional support throughout my Master's studies. Without his guidance and support, this thesis would not have been completed.

I would like to give my special thanks to Dr. Xinbao Yu and Dr. Mohsen Shahandashti, for their time and participation as my committee members and for their valuable suggestions and advice.

My utmost appreciation to Texas Department of Transportation (TxDOT) for their constant help and collaboration.

I am really grateful to Dr. Mohammad Sadik Khan for his constant guidance, valuable input, cooperation and assistance in all stages of my work.

Special thanks extended to Dr. Sonia Samir, Mohammad Faysal, Ahmed Nawal Ahsan, Asif Ahmed, MD Ashrafuzzaman Khan and all my colleagues for their active cooperation and assistance. Finally, and most of all, I would like to thank my parents for their love, encouragement, and great support.

November 18, 2015

Abstract

POTENTIAL APPLICABILITY OF STRESS WAVE VELOCITY METHOD ON PAVEMENT BASE MATERIALS AS A NON-DESTRUCTIVE TESTING TECHNIQUE

Masrur Mahedi

The University of Texas at Arlington, 2015

Supervising Professor: Sahadat Hossain

Aggregates derived from natural sources have been used traditionally as the pavement base materials. But in recent times, the extraction of these natural aggregates has become more labor intensive and costly due to resource depletion and environmental concerns. Thus, the uses of recycled aggregates as the supplementary of natural aggregates are increasing considerably in pavement construction. Use of recycled aggregates such as recycled crushed concrete (RCA) and recycled asphalt pavement (RAP) reduces the rate of natural resource depletion, construction debris and cost. Although recycled aggregates could be used as a viable alternative of conventional base materials, strength characteristics and product variability limit their utility to a great extent. Hence, their applicability is needed to be evaluated extensively based on strength, stiffness and cost factors. But for extensive evaluation, traditionally practiced test methods are proven to be unreasonable in terms of time, cost, reliability and applicability. On the other hand, rapid non-destructive methods have the potential to be less time consuming and inexpensive along with the low variability of test results; therefore improving the reliability of estimated performance of the pavement.

In this research work, the experimental program was designed to assess the potential application of stress wave velocity method as a non-destructive test in evaluating recycled base materials. Different combinations of cement treated recycled concrete aggregate (RAP) and recycled crushed concrete (RCA) were used to evaluate the applicability of stress wave velocity method. It was found that, stress wave velocity method is excellent in characterizing the strength and stiffness properties of cement treated base materials. Statistical models, based on P-wave velocity were derived for predicting the modulus of elasticity and compressive strength of different combinations of cement treated RAP, Grade-1 and Grade-2 materials. Two, three and four parameter modeling were also done for characterizing the resilient modulus response. It is anticipated that, derived correlations can be useful in estimating the strength and stiffness response of cement treated base materials with satisfactory level of confidence, if the P-wave velocity remains within the range of 500 ft/sec to 1500 ft/sec.

Table of Contents

List of Illustrations

List of Tables

Chapter 1

INTRODUCTION

1.1 Background

Pavement is a layered system which limits the stress induced by the wheel loads to an acceptable level for the in-situ subgrade soil. A typical pavement system consists of a surface layer, a base course, optionally a subbase course and the subgrade. Among all the layers, base layer plays the most prominent role in transferring the induced stress to the underlying layers. Base layer is a layer of selected materials of designed thickness constructed in between the surface layer and the subbase or subgrade layer. A properly designed base layer provides drainage to water entering the pavement system, provides the insulation to frost susceptible subgrade, prevents the intrusion of fine grained particles into the surface layer and overall; provides a working platform for the construction operation. The rate of load distribution is also significantly affected by the quality of the base course materials (Potturi, 2006). Therefore, the base layer must have sufficient strength to meet the design specifications without any trace of failure.

Aggregates obtained from a variety of natural sources have been traditionally used for the pavement base construction. But with the urbanization sprawls, heavy construction, repair and reconstruction have constrained the extraction of these natural aggregate by depleting the resources, increasing costs, labor and environmental concerns (Hoyos, 2011). Along with these facts, waste generation from the pavement rehabilitation projects and declination of landfill spacing have raised the importance in pavement industry to find an alternative way of reusing these materials (Ordonez, 2006). Thus in recent times, recycled materials such as reclaimed asphalt pavement (RAP), recycled crushed concrete (RCA) have become a potential alternative to highway engineers by both reducing the depletion rate of natural aggregates and construction wastes. Additionally, recycled mate-

rials have also been reported to be the most effective solution in reducing pavement construction and maintenance costs (Ordonez, 2006).

Generally, demolition of existing structures such as concrete pavements, bridge, curb and gutter are the main sources of recycled concrete aggregates (Griffiths, 2002) which may also be generated from concrete over-runs associated with new constructions (Hansen, 1992). On the other hand; to maintain the functionality and to impede the loss of structural reliability, asphalt concrete pavements are often need to rehabilitate by milling the upper distressed layer which generates huge amount of Asphalt Pavement as by product (Taha, 2002). According to The National Asphalt Pavement Association (NAPA), in 2013 approximately 350.7 million tons of plant mix asphalt was produced in the United States of America and the total reported RAP generation was around 76.1 million tons (Annual Asphalt Pavement Industry Survey on Recycled Materials and Warm-Mix Asphalt Usage: 2009–2013). This huge quantity of RAP generated each year leads to the necessity to investigate the further use of RAP in pavement construction (FDOT, October 2012) that will provide significant reduction in use of virgin aggregates and offers financial savings in term of cost. Though in recent years, a large portion of this RAP is recycled in hot mix and cold mix processes (NAPA 2013), still huge quantities of RAP materials remain unutilized especially in Texas. Whatsoever, use of RAP and RCA as the base course materials would provide a viable cost effective alternative of utilizing this huge portion of reclaimed materials.

Most recycled materials when used as the substitute of natural aggregates in pavement base construction, do not meet the minimum strength standards designated by AASHTO and local state guidelines (Rana, 2004). In such cases, various forms of chemical and mechanical stabilizations are performed to establish the minimum strength requirements (Sobhan, 2003). But still, product variability plays a significant role in limiting the applica-

bility of these recycled materials (Goonam and Wilburn, 1998). Hence, the materials should be evaluated based on strength and stiffness factors before using in pavement construction.

1.2 Problem Statement

Pavement base layer quality is currently evaluated by specifying the levels of measurable material characteristics such as, strength and stiffness. Minimum limits for these design parameters have been specified in different standards which are anticipated to yield the desirable level of performance. In case of using the recycled materials in pavement construction, more extensive investigation of these controlling parameters is required because of the source dependence nature and strength variability of the aggregates. But for extensive evaluation, traditionally practiced test methods have been proven unreasonable in terms of time, cost, reliability and applicability. On the other hand, rapid non-destructive methods have the potential to be less time consuming and inexpensive along with the low variability of test results, therefore improving the reliability of estimated performance. This research work was motivated with this potential applicability of non-destructive tests in QC/QA programs of recycled pavement base materials.

In this study, different combinations of recycled concrete aggregate (RAP) and recycled crushed concrete (RCA) treated with different dosage levels of cement were used. Seven different combinations were tested at 0, 2, 4 and 6% cement contents for unconfined compressive strength (UCS) test. Among these combinations, four different combinations were considered for resilient modulus (M_R) test based on the material availability and time. All the specimens prepared for unconfined compressive strength and resilient modulus tests were subjected to impact echo/ sonic echo test to measure the P-wave velocity through the specimens. The P-wave velocity was then utilized to characterize the strength and stiffness properties of cement treated recycled base materials.

1.3 Research Objective

The main objective of this experimental study is to assess the potential application of stress wave velocity method (Impact echo/ sonic echo) as a non-destructive test in evaluating recycled pavement base materials. Focusing this objectives the research work has been done by following steps:

- Reviewing the existing literature on different non-destructive and destructive tests such as impact echo, impulse response, pulse velocity, unconfined compressive strength and resilient modulus tests.
- Collecting recycled materials such as recycled asphalt pavement (RAP) and recycled crushed concrete (RC) from different sources.
- Preparing experimental specimens of different combination of recycled asphalt pavement (RAP) and recycled crushed concrete (RC) mixtures stabilized with cement as per standard specifications.
- Performing stress wave velocity (impact echo) test, UCS test and resilient modulus test on prepared samples.
- Comparing data analysis to evaluate the applicability of stress wave velocity method in accessing strength and stiffness parameters of pavement base materials.
- Modeling stress wave velocity test results by utilizing conventional UCS test results and resilient modulus test results.
- Performing statistical analysis to access the acceptance of derived trends and correlations in term of statistical significance.
- Providing recommendations for future works to improve the test results and correlations.

1.4 Thesis Organization

The experimental study presented in this thesis has been organized in 5 chapters. A brief description of the chapters is given below:

Chapter 1 introduces the necessity of present research, objective and scope of this work.

Chapter 2 briefly presents the literature review on different non-destructive and destructive test methods that has been done to outline the objectives and experimental setup for this research work.

Chapter 3 describes the materials properties, experimental setup, test variables and methodologies that were implemented in this study.

Chapter 4 presents the test results that were conducted it this experimental program. Comparison, modeling and statistical analysis are also presented in this chapter.

Chapter 5 provides the summary and conclusions of the current study and also provides further directions for future work.

Chapter 2

LITERATURE REVIEW

2.1 Introduction

The main objectives of this chapter are to present a brief review on pavement structure, materials used, strength and stiffness characterization methods of the pavement construction materials. First, an introduction on the pavement layers is presented which will be followed by a brief review on different conventional and recycled materials used in pavement base and subbase construction. Finally, a discussion on different test methods for strength and stiffness characterization of pavement base materials will be presented. Since the main focus of this research study is to assess the potential applicability of non-destructive tests in pavement evaluation, the last part of this literature review will mostly describe the implementation of non-destructive tests in evaluating material strength and stiffness properties. The literature review presented in this chapter is a compilation of previous works found from different books, journals, conference proceedings and internet sources which are used as the theoretical support of the present experimental work.

2.2 Pavement Structure

The main function of a pavement is to limit the stresses to a acceptable level for the subgrade. A pavement structure undergoes stresses induced by wheel loads and distributes them to the lower layers. Classification of pavement is done using its load distribution pattern. There are three types of pavements such as rigid pavement, flexible pavement and composite pavement. Flexible pavement generally consists of prepared or stabilized subgrade, subbase or base course and surface course. Flexible pavement has higher deflection at the edges and lower deflection at center. On the other hand, rigid pavement consists of a prepared subgrade, base or subbase course and a pavement slab. Pavement slab is usually a concrete slab which settles uniformly under loading. Composite

pavement is a combination of both rigid pavement and flexible pavement. Rigid section is overlain by flexible pavement which includes hot mix asphalt (HMA), open graded friction course or rubberized asphalt (Potturi, 2006). This flexible overlay works as a thermal and moisture blanket and reduces the deflection and wearing of the rigid pavement layer. A brief description on typical pavement layers are given below.

2.3 Typical Pavement Layers

2.3.1 Surface Course

Surface course is the top layer of the pavement, constructed on the base or subbase course and stays in contact with the traffic wheel. For this reason, it has to provide smooth riding surface, adequate drainage, must have the capacity to resist the high traffic load, rutting, skidding.

2.3.2 Base Course

Base course is constructed immediately below the surface course and above the subbase if there is any, otherwise directly on the subgrade to provide structural support. This layer consists of crushed virgin aggregates such as: crushed limestone, crushed gravel, crushed slag or recycled aggregates such as: recycled asphalt pavement (RAP), recycled concrete aggregates (RCA) treated with Portland cement, lime or other binder materials. Base materials are to be selected in accordance with the specifications. Using recycle materials in base course with adequate treatments will reduce the cost significantly by decreasing the thickness of the layer. Hence, it is necessary to study and find the optimum binder content to get the desired performance of the base layer.

2.3.3 Subbase Course

This layer is usually constructed beneath the base layer to support the surface and base course. Generally, it consists compacted granular materials with or without treatment of stabilizer. It prevents fines from the subgrade to move into the base layer. The material

qualities of the subgrade are usually lower than the base layer as it requires less strength. If the strength of the base layer is high enough to sustain under the wheel load then subbase layer is neglected for economy. As the stresses induced by the wheel load reduce with depth especially in flexible pavement, top layers are usually stronger and hence expensive than the bottom layers. While designing a pavement it is important to consider the load induced by the traffic and type of materials to be used to ensure the most economic and sustainable design. A typical cross section of pavement structure is shown in Figure 2-1 (Ordonez, 2006).

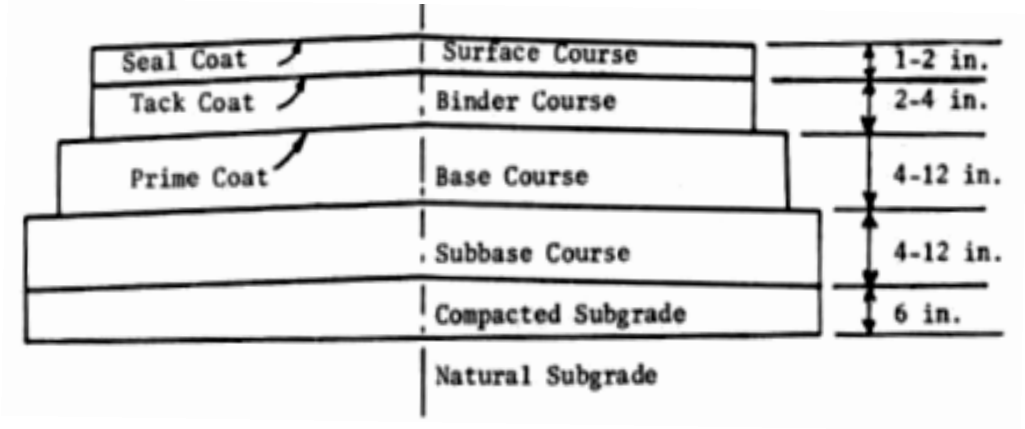

Figure 2-1 Typical pavement structure (Ordonez, 2006)

2.4 Pavement Design Criteria

Typically the strength of the natural soil is not high enough to support the wheel load which introduces the implementation of pavements. So, the main purpose of a pavement is to distribute the wheel load in such a way that the stress on the natural soil remains within its capacity. This objective is accomplished mainly by varying the thicknesses of different pavement layers which generally depends on following criteria:

2.4.1 Imparted Load on the Pavement

Equivalent single axle load (ESAL) is projected by using a fourth power formula which is used to estimate the imposed load on the pavement. The concept of ESAL is developed

by American Association of State Highway and Transportation Officials (AASHTO). The ESAL reference axle load is 18 kip single axle with two tires hence, the ESAL value varies with different types of vehicle. The amount of traffic is predicted and totaled over a design or analysis period and then converted into equivalent number of 18 kip single axle loads. For an example, an 18-wheeler with one single axle and two tandem exerts ESAL equivalent to 2.44. Different trucks have different wheel load conditions which can be found in any pavement design guide book.

2.4.2 Strength and Stiffness of Subgrade

One of the most important parameters in pavement design is the strength and stiffness values of the subgrade soil. In past, triaxial parameters, R-value, CBR and Soil Support Value (SSV) were used as pavement design parameters. These parameters mostly simulate the static load condition so the failure load does not represent the actual dynamic traffic load of the pavement. Soil failure does not occur in fields on a regular basis which is usually done in laboratory tests. Considering these factors, AASHTO 1993 recommended the use of resilient modulus (M_R) of base, subbase and subgrade materials as the most important pavement design parameter. Resilient modulus represents the dynamic modulus of soil and also considers the plastic deformation.

2.4.3 Design Parameters

The design parameters required for the pavement structure are: design variables, performance criteria, material properties, structural characteristics and reinforcement variables. Design variables include traffic, performance period, reliability and environmental effects. Performance criteria include serviceability, allowable rutting, loss of aggregates etc. Structural characteristics refer to the detachment between the pavement surface and subgrade and drainage load transfer. Material properties include compressive strength, resilient modulus, effective subgrade modulus, modulus of rupture of Portland Cement

Composites (PCC) etc. Reinforcement variables include different types of joints in concrete slab of rigid pavements.

2.5 Cement Treated Bases

Cement treated aggregate base (CTAB) is defined as a mixture of aggregates, measured amount of Portland cement and water that hardens after compaction and curing to form a durable paving material (Skokie, 1979). It is the most used base course for both rigid and flexible pavements. CTAB usually contains coarse aggregates with higher cement content which results in higher strength and stiffness. It acts like slab under the application of load and its performance depends largely on the elastic modulus and strength of the materials. These properties are useful to develop design procedures based on stress-strain relationship and fatigue characteristics parameters (George, 1990). Unconfined Compressive Strength (UCS) of the CTAB is used largely to determine the useful mix design parameters such as optimum water and cement contents (Croney and Croney, 1997). In previous studies, empirical relationships were developed between the compressive strength and shear modulus, resilient modulus, flexural or tensile strength of the CTAB materials to be used in the design of the pavement layers.

2.6 Recycled materials in Pavement Application

20^{th} century has experienced a tremendous growth in core structures such as roads and bridges including the repair and replacement of deteriorated structures. The heavy construction endeavor, repair and renewal have simultaneously increased the construction waste generation and an overall depletion of the resources. Recycling of the waste seems to be a viable alternative of these problems by both reducing the amount of waste and depletion of natural resources.

2.6.1 Reclaimed Asphalt Concrete (RAP)

Reclaimed Asphalt Concrete (RAP) is the granular pavement material containing a mixture of bitumen and aggregates removed or reprocessed as the part of pavement reconstruction and resurfacing. To maintain the functionality and to impede the loss of structural reliability, asphalt concrete pavements are often needed to rehabilitate by milling the upper distressed layer which generates a huge amount of asphalt pavement materials as by product. If rhino horn bulldozer is used for the full depth reclamation, it will break the whole top layer into segments. In a central processing plant, these broken pieces are crushed, screened and stacked in stockpiles. Cold in-place recycling (CIR) and hot in-place (HIR) recycling are two ways of reclaiming asphalt in fields. The reclaimed materials are used with or without chemicals. In hot in-place recycling process upper 2 inches layer is heated layer using equipment shown in Figure 2-2. The cold in-place recycling process is shown in the Figure 2-3.

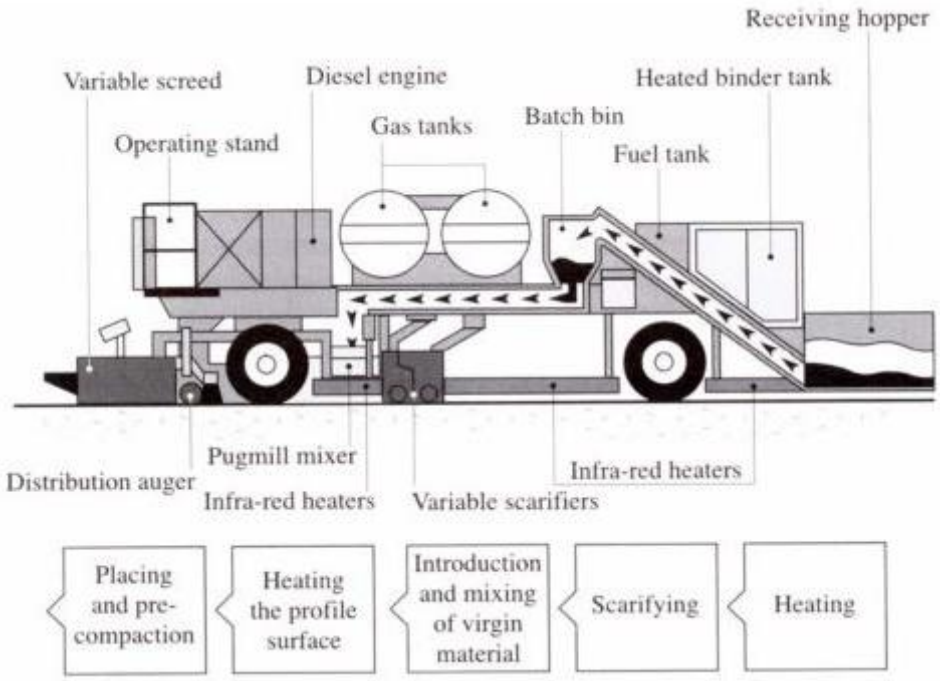

Figure 2-2 Schematic of Hot-In Place Recycling Machine (Sherwood, 1995)

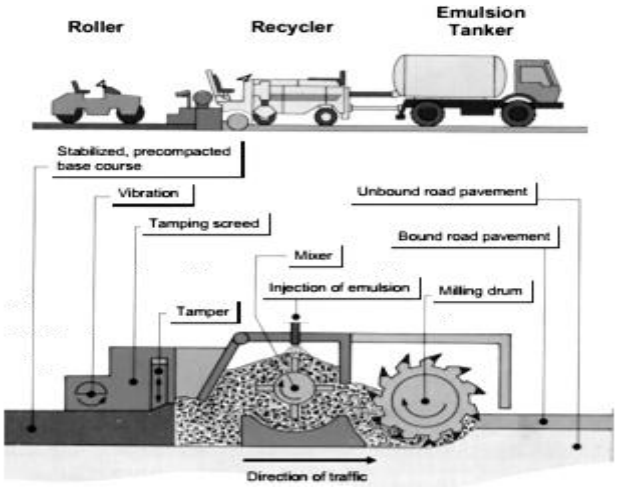

Figure 2-3 Schematic of Cold-In Place Recycling Machine (from Sherwood, 1995)

2.6.1.1 Mechanical Properties of RAP

In the following Table 2-1, the physical and mechanical properties of the RAP are indicated. The typical unit weight of RAP ranges from 120 to 140 pcf and the moisture content

varies from 5 to 8%. California Bearing Ratio (CBR) ranges from 20 to 25. Typically RAP material contains about 3 to 7% of hardened asphalt content. Hardening of asphalt content might have occurred because of oxidation, thixotropic effect etc.

Table 2-1 Properties of RAP materials (Potturi, 2006)

Property	Typical Range
Unit Weight	19.4 to 23 kN/m^3 (120 to 140 pcf)
Moisture Content	5 to 8%
Asphalt Content	3 to 7%
Asphalt Penetration	10 to 80 at 25˚C
Absolute Viscosity	4000 to 25000 poise at 60˚C
Compacted Unit Weight	16 to 20 kN/m^3
California Bearing Ratio (CBR)	20 to 25% for 100% RAP

.

2.6.2 Cement treated RAP and RCA

Recycled Asphalt pavement (RAP) consists of asphalt and aggregates which are generated by cold milling of the removed hot mix asphalt (HMA) pavement. Recycled Concrete Aggregates (RCA) are produced by crushing of concrete to meet the specific grade requirements. Its properties are different from the aggregates as cement is attached on the surface of the natural aggregates. Both RAP and RCA have been drawing the interest of the researchers as these could be a cost saving alternative to the virgin aggregates. RAP and RCA materials must meet the minimum design criteria provided by the AASHTO guidelines and state transportation departments. Addition of cement to the base materials improves the strength and stiffness. But this higher value of stiffness may not ensure the proper performance and durability of the pavement against problems such as rutting and cracking.

2.6.2.1 Compressive Strength of Cement Treated RAP and RCA

Though in recent years, a large portion of this RAP is recycled in hot mix and cold mix processes (NAPA 2013), still huge quantities of RAP remain unutilized especially in Texas. Whatsoever, use of RAP as the base course material would provide a viable cost effective alternative of utilizing this huge portion of unused RAP. This potential use of RAP was felt in early 90's and since then mechanical properties of RAP are being investigated extensively (Kolias et al. 1996). Kolias investigated the compressive strength, tensile strength and modulus of elasticity of different RAP mixes with unbound granular materials and recommended further research on RAP mixes. Croney and Croney (2007) based on the laboratory study reported that 70% of the strength of cement treated base gains in the first seven days. Later on, a substantial amount of research on mechanical properties of different cement treated RAP mixes were reported in various studies (Taha et al. 2002; Guthrie et al. 2009; Grilli et al. 2013). Taha (2002) investigated the compaction and compressive strength of different RAP- virgin aggregate mixes treated by different amount of cement contents and conclude that, compressive strength increases with the increase of cement content and percentage of virgin aggregates. Test result from Taha et al. (2002) has been presented in Figure 2-4. Hoyos et al. (2011) investigated the influence of fiber inclusion to the cement treated RAP mixes and the result is presented in Figure 2-5. Hoyos conclude that inclusion of fiber has limited beneficial effect on the compressive strength of cement treated RAP. Modulus of elasticity as the secant modulus was also investigated by Hoyos and reported that secant modulus of cement treated RAP tends to increase as the cement dosage increases. Figure 2-6 shows the variation of secant modulus with cement dosages reported by Hoyos (2011).

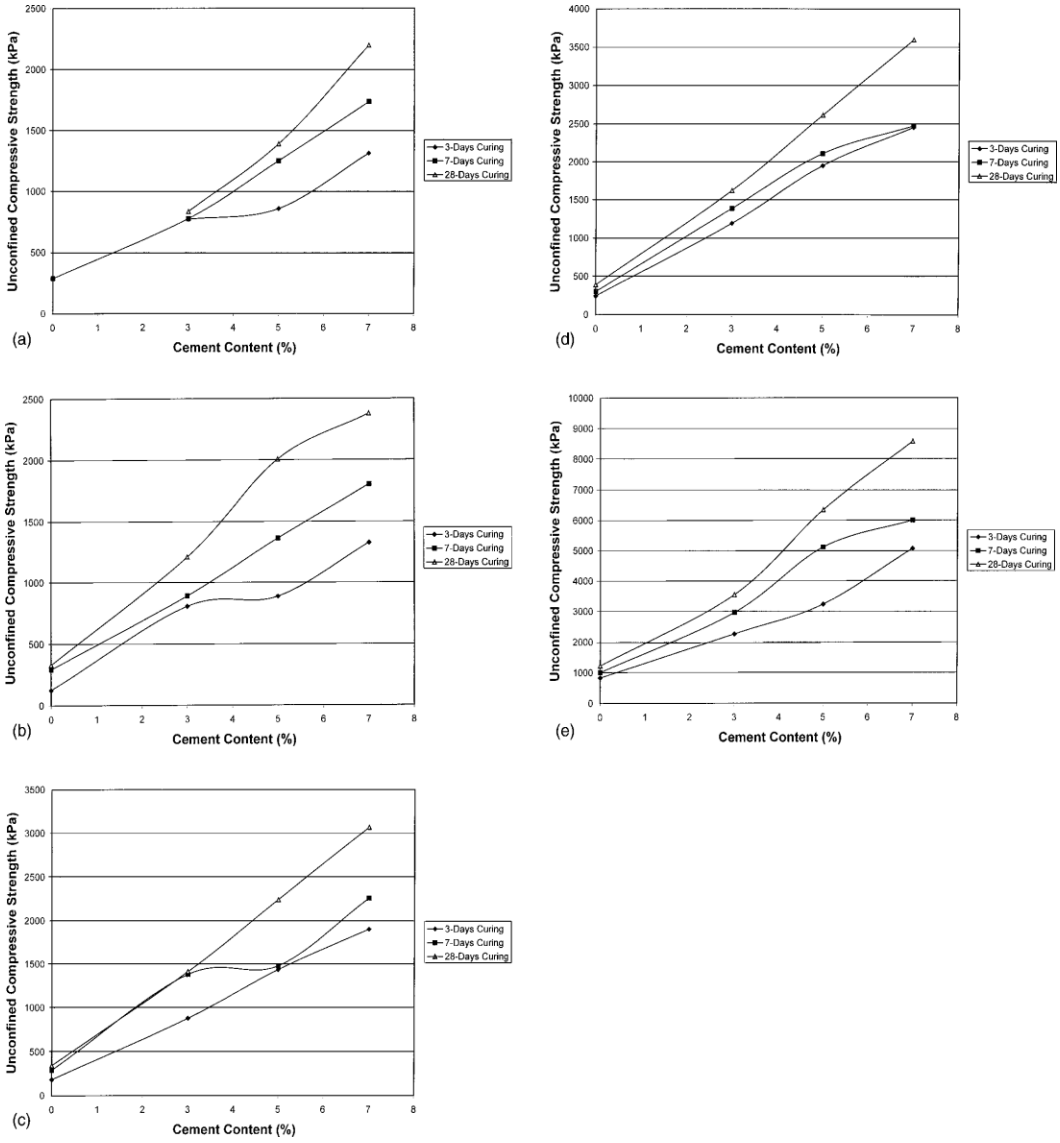

Figure 2-4 Unconfined compressive strength (UCS) test results (Taha, 2002)

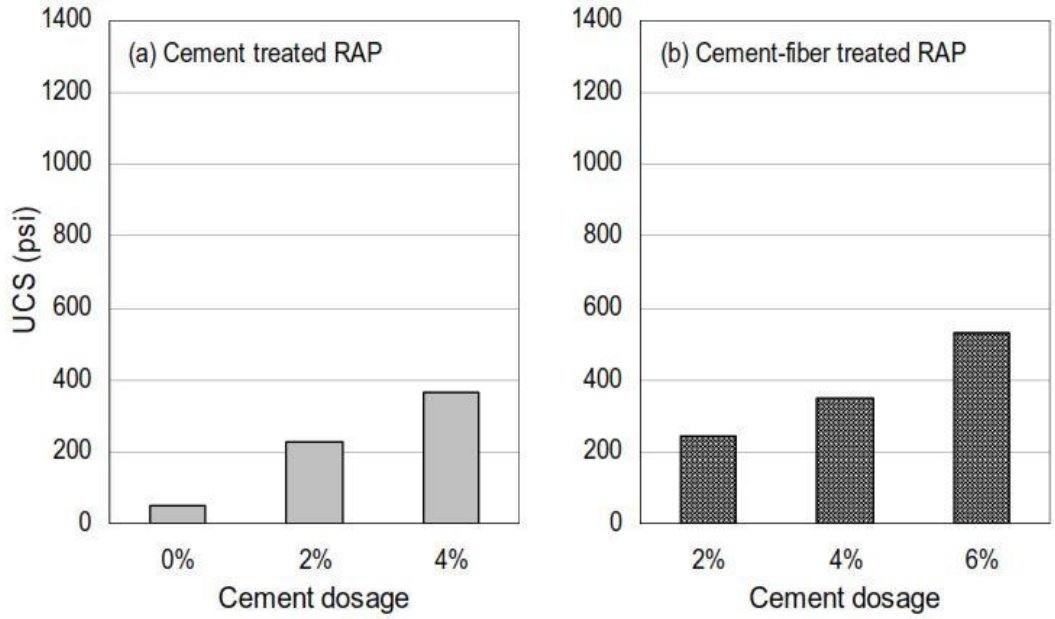

Figure 2-5 Unconfined compressive strength (UCS) test results (Hoyos, 2011)

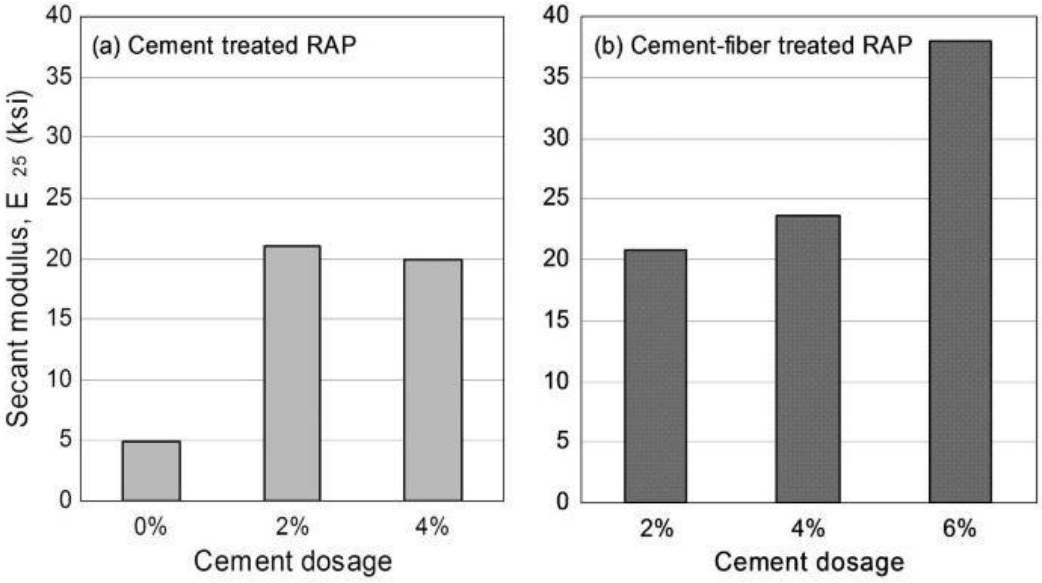

Figure 2-6 Secant modulus of elasticity of cement treat RAP materials (Hoyos, 2011)

Compressive strength of cement treated recycled concrete (RCA) and crushed limestone (CL) were investigated by Lim and Zollinger (2003). Table 2-2 shows the test variables for their experimental setup and Table 2-3 shows the complete factorial of the test matrix where low and high application levels of the test variables are indicated by (-) and (+) signs (Lim and Zollinger, 2003).

Table 2-2 Test variables and application levels (Lim and Zollinger, 2003)

Test Variables	Designation	Application Levels	
		Low (-)	High (+)
Content of Coarse Aggregates	A	48%	58%
Content of Fines	F	5%	10%
Cement Content	C	4%	8%

Table 2-3 Factorial of test mixtures for each aggregate type (Lim and Zollinger, 2003)

Mix ID	Test Variables and Application Levels			Mix ID	Test Variables and Application Levels		
	A	F	C		A	F	C
1	…	…	…	5	..	…	+
2	+	…	…	6	+	…	+
3	..	+	…	7	…	+	+
4	+	+	…	8	+	+	+

From the test results as presented in Table 2-4, it can be observed that strength of recycled concrete mixtures (RC) is more than 30% lower when compared to the strength of crushed limestone (CL). Higher water demand and higher water cement ratio of recycled concrete might be the reason of the lower strength (Lim and Zollinger, 2003). But still, all the mixtures tested in this study satisfied the minimum design strength requirement of cement treated aggregate base.

Table 2-4 Compressive strength at different Curing times (Lim and Zollinger 2003)

Aggregate	Mix ID	Compressive Strength (psi)			
		1 day	3 days	7 days	28 days
Recycled Concrete (RC)	1.0	257.8	243.8	397.4	603.7[e]
	2.0	195	282	455	646.6[e]
	3.0	257.7	286.3	454.5	550.8[e]
	4.0	208.2	400.2[b]	398.8	527.4[f]
	5.0	290.3	534.6	759.8[d]	1070.3
	6.0	345.1	647.3	886.6	1220.5
	7.0	289.1	…	797	963
	8.0	395.9	676.5	819.6	908.6
Crushed Limestone (CL)	1.0	378.9	524.3	630.6	1012.1
	2.0	318.1	490	519.7	556.9
	3.0	472.2[a]	598.7	508.3	908.5[a]
	4.0	278.7	543.8[c]	461.4	734.2[h]
	5.0	630.7	1083.8	1221.1	1709.5
	6.0	606.8	988	1224	1319.3
	7.0	648	1224.3	1501.7[d]	1556.5
	8.0	550.5	921.7[c]	1190.4	1292.8

[a] tested at 2 days
[b] tested at 5 days
[c] tested at 4 days
[d] tested at 8 days
[e] tested at 34 days
[f] tested at 33 days
[g] tested at 29 days
[h] tested at 22 days

2.6.2.2 Resilient Modulus of Cement Treated RAP and RCA

Resilient modulus and pavement deformation are the two important parameters used for the pavement performance evaluation. AASTO guideline 307-99 is the most common way to determine the resilient properties by repeated triaxial test. Accurate knowledge on resilient modulus of pavement materials enables to determine the actual response of the pavement layers to traffic loading. Generally, resilient modulus is defined as the ratio of repeated deviator stress to the recoverable or resilient strain. Resilient strain is the portion of the deformation that may be recoverable by the exclusion of applied stress. Figure 2-7 (Buchanan, 2007) represents the stress- strain response of loading and unloading cycles of a typical triaxial test.

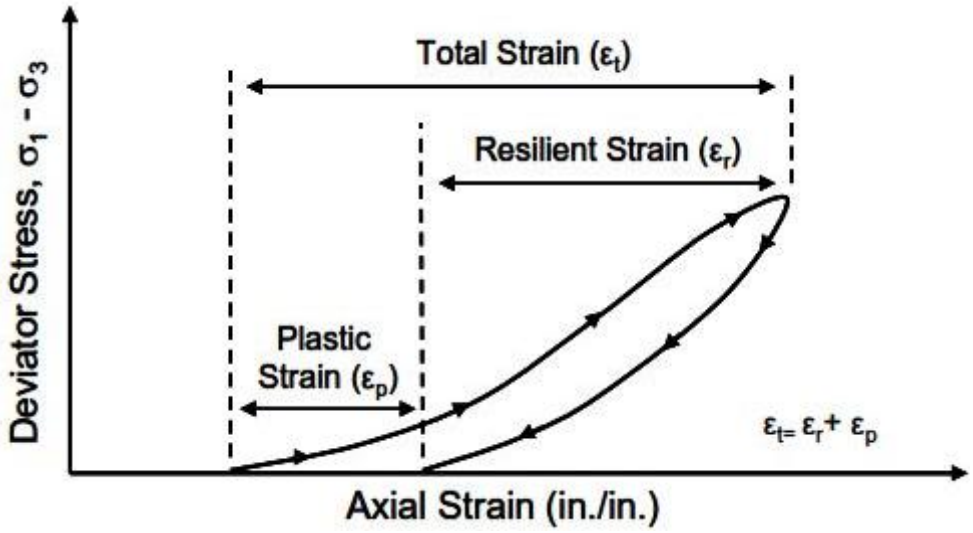

Figure 2-7 Specimen response during axial loading (Buchanan, 2007)

One of the earliest study on the resilient properties of cement treated base and subbase materials was undertaken by Rada and Witczak (1981). They evaluated the resilient modulus results of 271 nonlinear tests conducted on aggregates obtained from 10 different research agencies. In another study, five different types of cement treated virgin aggregates which are commonly used by Maryland State Highway Administration were

considered by Lofti and Witczak (1985). Janoo (1994) conducted an experimental setup to evaluate the potential use of RAP materials as the pavement base material. Falling Weight Deflectometer (FWD) and other tests were conducted on test sections of different RAP materials. Layer deflections were then used to back calculate the resilient modulus of a particular layer. Taha et al. (2002) used the correlation of UC strength and resilient modulus to evaluate the resilient modulus response of cement treated RAP-virgin aggregate mixtures. In another study, Gnanendran and Woodburn (2003) conducted resilient modulus, UCS and CBR tests on cement, fly ash and lime stabilized RAP materials. Potturi (2006) determined the resilient properties of RAP and fiber reinforced RAP materials at 3 different cement contents and concluded that fiber reinforcement causes a significant enhancement in moduli values. In all studies discussed above, it has found that resilient modulus increases with the increase of cement content but decreases with the increase of RAP percentage. All the results of the studies discussed above are summarized in Table 2-5.

Table 2-5 Summary of structural layer coefficients obtained from different studies

Reference	Type of Recycled Material Tested	Tests Conducted	Resilient Modulus
Lofti an Witczak (1985)	Cement treated Dense Graded Aggregate	Resilient Modulus (M_r)	1260 MPa (4.5% cement)
Janoo (1994)	Reclaimed Stabilized Base	Back Calculation from Layer Deflections (FWD)	N/A

Table 2.5 - continued

Taha et al., 2002	Cement Stabilized RAP aggregates	Back Calculation from UCS	96 to 3,726 MPa (0% to 7% cement)
Gnanendran and Woodburn (2003)	Cement Stabilized RAP aggregates	Resilient Modulus (M_r), CBR and UCS tests	310 to 590 MPa (0% to 3% cement)
Potturi (2006)	RAP and fiber reinforced RAP Stabilized with cement	Resilient Modulus (M_r)	180 to 570 MPa (0% to 6% cement with fiber)

2.7 Non-destructive Tests of Pavement

As a part of quality control and quality assurance, the use of non-destructive testing (NDT) for the estimation of in-situ strength and stiffness parameters of pavement layers has been accepted as a new technique of pavement evaluation. In recent years, NDT has achieved the importance for the evaluation of an existing pavement in terms of strength and stiffness whereas, destructive tastings would reduce structural integrity, serviceability and also may cause significant economic loss. NDT is used as quality assurance of the pavement during construction and also to ensure the usefulness, integrity and safety after construction. Certain mechanical properties such as modulus of elasticity, unconfined compressive strength, resilient modulus, tensile strength may not be evaluat-

ed directly by non-destructive tests and thus, methods have been developed to measure other properties from which measurement of mechanical properties can be done. Basically, there are two types of non-destructive test methods in which the first type may be termed as semi-destructive as they cause some minor surface damage compared to destructive tests. Penetration resistance, pullout, maturity, brake-off etc. are this type of tests. Stress wave velocity, parallel seismic, stiffness gauge, ground penetration radar etc. falls in the second category and are truly non-destructive in which other properties are measured as an indirect method of measuring mechanical properties. Among these, a brief description of several non-destructive tests has been presented in the following section as a pertinent part of this research study.

2.7.1 Stress Wave Propagation Method

Several non-destructive test methods are developed based on stress wave propagation through the concrete materials. The disturbance generated by a stress such as an impact applied to a solid body propagates as a stress wave. Mainly three primary mood of stress waves propagate through an elastic, isotropic medium: dilatational wave also known as compression wave or P-wave, distortional wave also known as shear wave or S-wave and rayleigh wave also known as surface wave or R-wave (Jones 1962). P-wave and S-wave are differentiated from each other by the direction of wave propagation with respect to the direction of particles movement. In P-wave, both the direction of wave propagation and particles movement are parallel to each other. But in S-wave, particles motion is perpendicular to the direction of wave propagation. R-wave is the surface wave and propagates along the surface of the solid mass as shown in Figure 2-8 (Luo Qixian 1996).

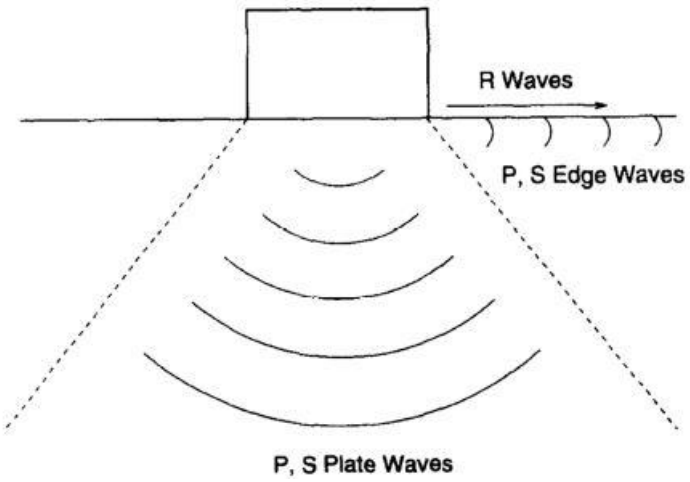

Figure 2-8 Types of waves generated by a P-wave transducer (Luo Qixian 1996).

P-wave travels faster which is followed by S-wave and the R-wave is the slowest one. Both the waves, P and S wave reflect from the interface of significant stiffness difference such as the layered system of a pavement or an anomaly in the structure. The amplitude of the reflected waves depends upon the relative difference of layers acoustic impedance which is defined as the product of wave velocity and the density of corresponding layer (Lin et al., 1994). Also, the energy of stress is reduced with the increase of path length because of absorption and divergence of the wave. However, in pavement applications of stress wave, an impulse impact is made on the pavement surface to generate the stress wave which propagates through the pavement layers. Wave reflects back from the layer interfaces as the layers exhibits significant stiffness difference. By identifying the arrival of reflected wave and by knowing the time difference between the stress wave generation and its arrival, wave velocities can be determined. Previous studies have shown that, the compression wave and shear wave velocities are the function of young's modulus of elasticity, density and poission's ratio by the following equation given in British Standard (BS1881: Part 203):

$$Vp = \sqrt{\frac{E\,(1-\mu)}{(1+\mu)(1-2\mu)\rho}} \quad (2.2)$$

Where,

E = Dynamic modulus of Elasticity

m = Poission's Ration

ρ = Density

And the S-wave velocity is related by the following equation:

$$Vs = \sqrt{\frac{E}{2\,(1+\mu)\rho}} \quad (2.3)$$

Shear modulus of elasticity is often used for the simplicity of the correlation and is given below:

$$G = \frac{E}{2\,(1+\mu)} \quad (2.4)$$

By knowing the P-wave and S-wave velocities, R-wave velocity can also be determined by the following equations:

$$Vr = \frac{0.87+1.12\mu}{(1+\mu)}\,Vs \quad (2.5)$$

Combining equation 1, 2 and 3, gives the relationship between P-wave and R-wave velocities which depends only on the poission's ratio of the test materials.

$$Vr = \frac{0.87+1.12\mu}{(1+\mu)} Vp / \sqrt{\frac{2\,(1-\mu)}{(1-2\mu)}} \quad (2.6)$$

For the convenience of use, equation 2.6 is illustrated in Figure 2-9 (Luo Qixian 1996).

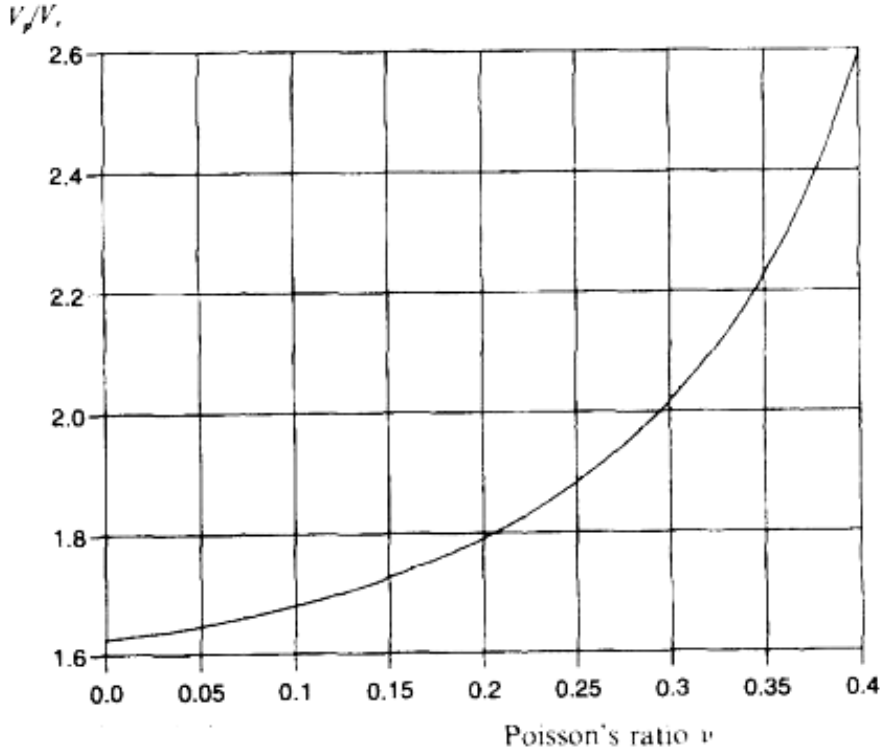

Figure 2-9 Relation between Vp/Vr and Poission's ratio (Luo Qixian 1996)

Thus, strength properties could be determined by using the pre-established strength-velocity correlations. But the relationships are not unique and are affected by many factors including aggregate size, mix proportion, cement content, water-cement ratio, moisture content etc. (Sturrup et al, 1984). Therefore, strength-velocity relationships are needed to be established by testing before going for field application. Thus, considering these drawbacks and immense possibilities of stress wave in strength and stiffness prediction, different methods for the measurement of wave velocities in different materials have been developed. A brief description of different methods of stress wave velocity measurements are given below:

2.7.2 Impact Echo

Carino and Sansalone developed the impact echo method for the testing of thin layer of concrete structure (Sansalone 1991). It's a technique based on stress wave propagation used to identify flaws in concrete structures. Studies have also proven that impact echo technique is effective in measuring materials properties and identifying voids, delamination, honeycombing, surface cracking and member thickness. In recent times, standard method for impact echo testing has been adopted by ASTM and is designated by ASTM C 1383-04 (Standard Test Method for Measuring the P-wave Speed and Thickness of Concrete Plates Using the Impact-Echo Method). Two different test procedures are described in ASTM test standard among which procedure A describes the measurement of P-wave velocity by measuring the travel time between two receivers placed at a known distance. Procedure B describes the technique of thickness calculation of a test member by using the P-wave velocity found by procedure A and the frequency response found by impact echo testing (ASTM C 1383-04). The standard also includes the procedures to estimate systematic errors caused by the digital sampling in both Procedure A and B. Figure 2-10 and Figure 2-11 (ASTM C 1383-04) represents the schematic of standard test method of procedure A and B.

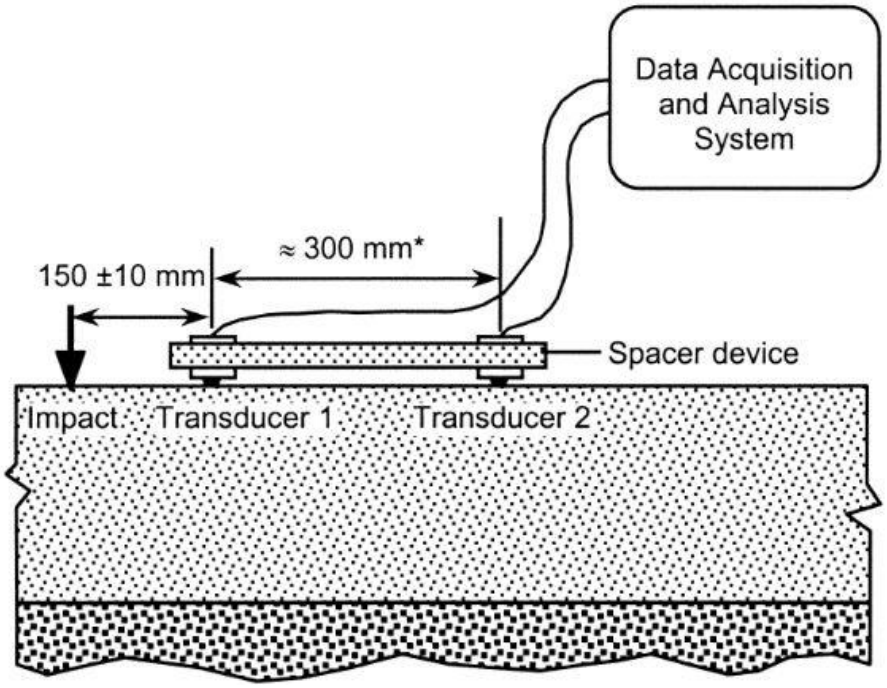

Figure 2-10 Schematic of Testing Configuration for Procedure A (ASTM C 1383-04)

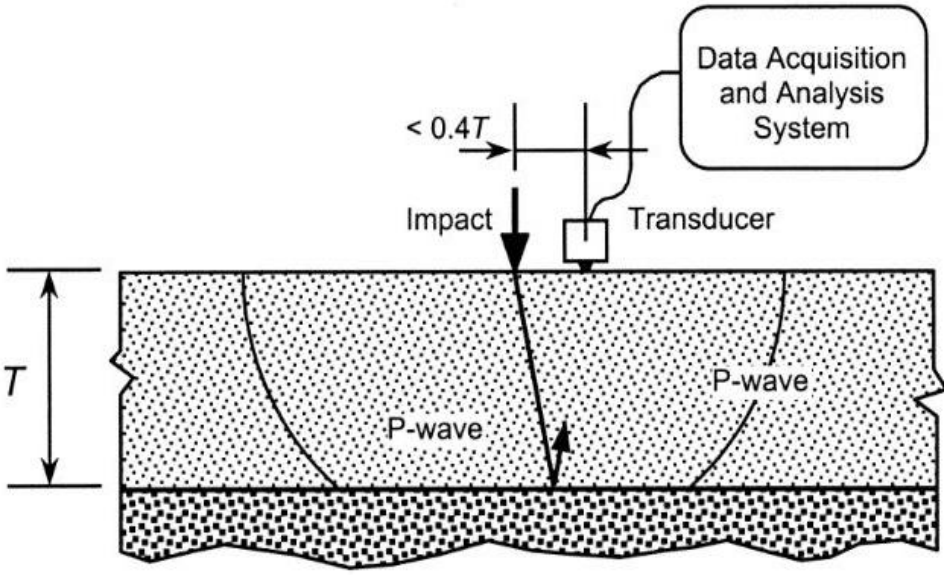

Figure 2-11 Schematic of Testing Configuration for Procedure B (ASTM C 1383-04)

2.7.2.1 Instrumentation

Impact echo test was first commercially manufactured by Cornell University in 1990 which included a laptop computer with special program as a part of data acquisition system, receiving transducers and a series of different size of impactors. Since then this test method comprises of three basic components:

1. An Impactor: A spherical or spherically tipped impact source

2. Displacement Transducer: Transducer capable of identifying the displacement associate with the arrival of P-wave

3. Waveform Analyzer: Hardware and Software assembly to record and analyze the response from transducers

Impactors are typically steel balls of varying diameter attached to a spring rod. The impact force and duration are dependent on ball diameter and impact speed (Graveen 2001). Frequency part of the stress wave is determined by contact time which is also defined as the impact duration (Carino et al., 1986). Wavelength decreases as the impact time decreases causing an increase in frequency range. Thus, to identify the smaller disorders, shorter impact time is implemented though the identification of the arrival of P-wave is difficult with higher frequency ranges (Sansalone et al., 1997a and Sansalone et al., 1988).

The displacement transducers are commonly made of conical piezoelectric elements attached to a brass backing block (proctor et al., 1982). To accurately record the arrival of P-wave, a small contact zone between the concrete surface and the piezoelectric element is required (ASTM C 1383-04). The use of a suitable coupling material is recommended to attach transducers to the concrete.

The data acquisition system is an assembly of hardware and software for acquiring, recording and processing the transducers output. It can be a portable computer with data-

acquisition card or a wave front analyzer. The system needs to be operated by a power source such as battery power that does not generate detectable electric noise.

2.7.2.2 Test Method

In impact echo, a stress pulse is induced on the surface of test structure by a mechanical impact. The generated P and S waves propagate along the test object and the R-wave travels away from the impact point along the surface. The P-wave and the S-wave then reflect back from the external boundary. The arrival of reflected waves are identified and recorded by the transducer place on the test surface where the impact was made. If the transducer is placed close to the impact point than the wave front is dominant by the arrival of P-wave (Sansalone et al., 1988). The arrival of P-wave can easily be identified as it travels faster and therefore is the first to arrive the transducer. So the first notable pick above the threshold amplitude of the wave front is taken as the arrival of P-wave. By knowing the travel time of P-wave through a know thickness the P-wave velocity can be determined. The schematic diagram of Impact echo test is presented in Figure 2-12 (Redrawn after Olson et al., 1998).

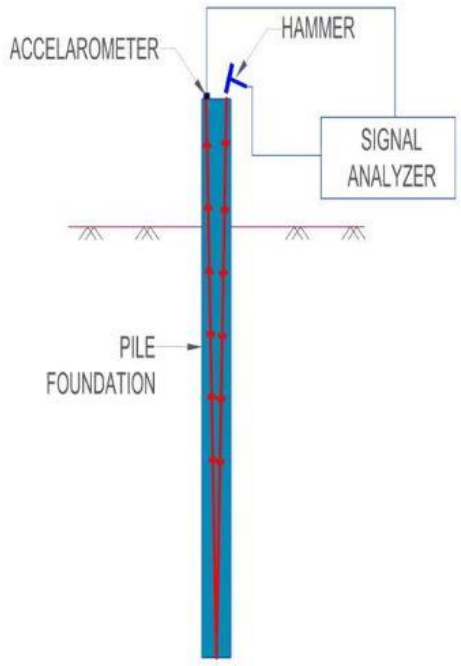

Figure 2-12 Schematic diagram of Impact echo test (Olson et al., 1998)

2.7.2.3 Data Analysis

Between the top and bottom surface of the test object, the stress wave generated by the impact reflects back and forth. Each time it reaches the top, it produces a notable surface displacement which is monitored in time domain by the transducer placed at surface. Within the time period between two successive displacements, the wave travels twice within the test object. By knowing the time period and measuring the travel path, P-wave speed through the test object is calculated. If T is the thickness of the test object and t is the travel time period then the P-wave velocity (Vp) can easily be calculated by the following equation:

$Vp = 2T/t$

During the early development of Impact Echo method, the arrival of P-wave was identified in time domain analysis. But the identification of the arrival of P-wave in time domain

is difficult and time consuming depending upon the geometry of test object (Sansalone et al., 1991, Sansalone et al., 1988, and Carino, 1984a). An alternative approach is frequency analysis which is an efficient and quick technique for data interpretation (Sansalone et al., 1988). Using First Fourier Transform (FFT) which is programmed in wave front analyzer (Sansalone et al., 1988) the wave front is transferred into frequency domain. A typical time domain spectrum and an amplitude spectrum for a concrete pavement with minimal imperfection are shown orderly in Figure 2-13 and Figure 2-14. As the frequency is inversely equal to the time period, product of travel path and the frequency difference between two consecutive peaks will yield the P-wave velocity through that test object. Hence, the velocity calculation equation becomes:

$$Vp = 2Tf$$

Where,

f = frequency difference between two consecutive peaks

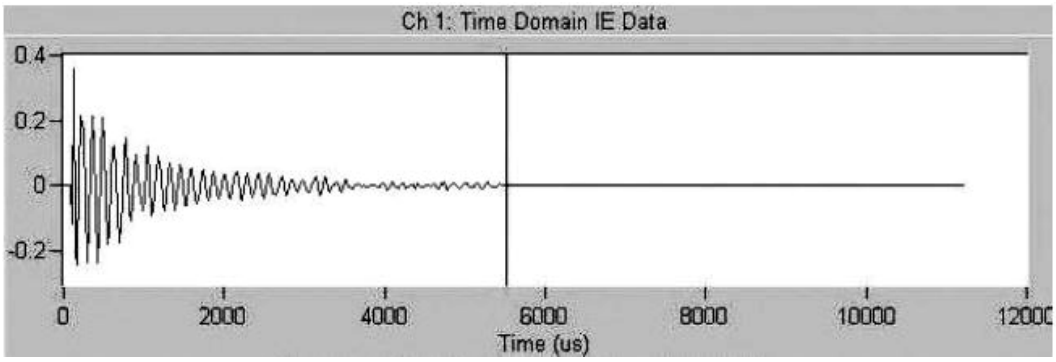

Figure 2-13 Time domain waveform of Impact Echo test

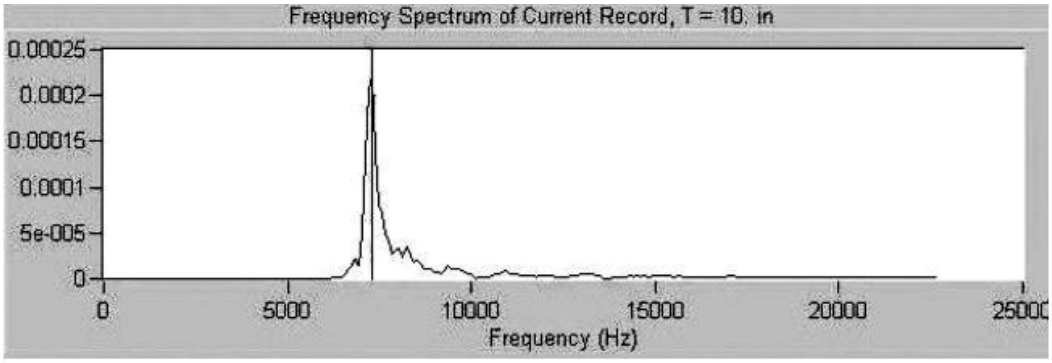

Figure 2-14 Frequency spectrum of Impact Echo test

2.7.2.4 Typical Application

From the very beginning, impact echo method has been used successfully in evaluating materials properties, integrity of concrete piles, slabs, pavements, bridge decks, walls etc. This method can also be used in determining the depth of piers, wall foundations and even shallow footings. The impact can be made on the free end of a pile or even on a pile cap and the reflected echo is monitored by the transducer. If the pile is free from major imperfections, the echo reflects back from the bottom end of the pile which facilitates the accurate measurement of the pile length. Locations of partial and complete discontinuities such as voids, weak zones, soil intrusions and cross sectional changes can also be identified as the wave also reflects back from the significant acoustic impedance difference. The success of this method often depends on the type of surrounding soil. If the pile is too long and the tip is on stiff soil having the same range of acoustic impedance of the pile, then the reflection of wave is too weak which leads to an erroneous estimation of pile length. As a thumb rule, when the length to diameter ratio of a pile exceeds 20:1 to 30:1 ratio, identification of the bottom echo becomes difficult due to excessive damping of the wave energy (Olson et al., 1998; Briaud et al, 2002).

2.7.2.5 Advantages and Disadvantages

The equipments of impact echo method are portable, easy to operate, very light weight and the method requires access only on one side. Test type is completely non-destructive and can locate the flaws in structures without any complicated analysis. The biggest disadvantage is that, experience is required to interpret the frequency data as the waveform is associated with numerous peaks because of the non-homogeneous nature of the concrete. As the method is based on digital sampling and digital signal analysis, inherent systematic error is also common in determining wave speed and plate thickness (ASTM 1983). Electric noise associated with the impact response sometimes makes it difficult to identify the accurate arrival of P-wave.

2.7.2.6 Available Research

Pessiki and Carion (1987 and 1988) studied the feasibility of using the impact echo method in predicting the concrete stiffness and strength properties. It was found that P-wave velocity is a good indicator of strength development at early stage. But at higher maturity, strength development is faster than the increase of P-wave velocity. W/c ratio, curing temperature and aggregate content play a vital role in strength-P-wave relationship though at low maturity, w/c ratio has no effect. Pessiki and Johnson (1996) performed the impact echo test on concrete slab, prepared cylinders and slab cores to develop the relationship between strength and P-wave velocity. Compression tests were conducted on cylinders and cores to determine the compressive strength. Good correlations with high coefficient of determination were found in all cases.

Field and laboratory tests by impact echo method were done by Sansalone et al. (1997a and 1997b) to measure the P-wave velocity using surface method. Mechanical impact was made to generate the stress wave and the response was recorded by the transducer placed on the test surface. He identified the arrival of P-wave by the first disturbance

above the threshold level considering that P-wave is the faster travelling component of stress wave. However, Lin et al. (1997) established that, the P-wave velocity found by the surface method represents the velocity in an infinite medium which is higher than the P-wave velocity in a plate like structure. Impact echo test yields 4 percent lesser velocity than the velocity found in an infinite medium. So as a more accurate practice, P-wave velocity found from surface method is adjusted to get the real velocity magnitude in impact echo test. Thus the apparent P-wave velocity in a plate like structure becomes:

$V_{p(plate)} = 0.96\ V_p$

Where,

$V_{p(plate)}$= Apparent P-wave velocity in a plate

V_p= P-wave velocity found by surface method

Thickness measurement of laboratory samples by impact echo method varied within 0.12 inch of the actual thickness. Pavement sections with two different nominal thicknesses and three different types of sub-bases were also tested. Maximum difference between the impact echo test and actual thickness was 0.35 inch.

Popovics et al. (1998) modified the surface method of measuring P-wave velocity by correcting the arrival time of P-wave for pulse dispersion. He used the corrected arrival time to calculate P-wave velocity and the average reduction of error was found to be around 4%. Popovics et al. (1998) also monitored the strength development of concrete specimens by both surface and direct thickness method and showed that, consistency of P-wave velocity measured by through thickness method is much higher than the P-wave velocity measured by surface method. But in case of R-wave velocity, the consistency of R-wave velocity measured by surface method was found to be better than the of P-wave velocity. This study by Popovics also conclude that, moisture content plays a vital role in wave velocity measurement which increases with the increase of moisture content.

Lin et al. (1994) showed that some part of the stress wave refracts and some part of the wave reflects back from the intersection of two different layers of a pavement system. The ration of reflection and refraction depends on the acoustic impedance difference of the adjacent materials at the interface. The product of P-wave velocity and the density of the material is the acoustic impedance of that material. The surface deflection caused by a reflected P-wave can only be identified when the acoustic impedance of the top layer is at least 24 percent higher than the acoustic impedance of underlying material (Lin and Sansalone, 1996).

2.7.3 Slab Impulse Response

Slab Impulse Response is a non-destructive test for concrete which is based on the use of transient vibrations created by a mechanical impact and monitoring the response of the test element by placing a velocity transducer adjacent to the impact point (ASTM C1740-10). Slab impulse response is generally used for the general condition evaluation of structural elements. It is primarily used to map and identify the voids in subgrade below the pavements and also behind the walls or tunnels. This is an excellent method for the rapid evaluation of pavement support condition and is very helpful in repairing damaged slabs or pavements by comparing before and after repair conditions (Olson et al,. 1990). Slab IR method can be used for a wide range of slab or pavement thicknesses but the most reliable result yields for thinner slabs, slabs with a thickness less the 12 inch (Olson et al,. 1990). The reinforced and non-reinforced slabs as well as asphalt and asphalt coated pavements can be tested by Slab IR method. A Ground Penetration Radar (GPR) is often used along with the Slab IR method for the accurate detection and mapping of subgrade voids. Damages associated with low stiffness such as delamination, honey-combing, voids and cracking can also be identified which enables Slab IR as an effective tool in evaluating the general condition of concrete structures. ASTM has adopted the

standard test procedure of slab impulse response which is designated as ASTM C1740-10 (Standard Practice for Evaluating the Condition of Concrete Plates Using the Impulse-Response Method). Traffic noise and structural vibration may influence the result of Slab IR in highway applications. Engineering judgement is required to determine whether the results are influenced by the noise and vibration (ASTM C1740-10).

2.9.3.1 Instrumentation

This test method comprises of three basic components (ASTM C1740- 10):

1. Impact Hammer: A hammer with cylindrical rubber tip

2. Transducer: A velocity transducer capable of measuring the response of the impact

3. Data acquisition and Analysis System: Hardware and Software assembly to record and analyze the output from load cell and transducer

The hammer is 50 mm in diameter and weight 1 kg. A load cell is provided along with the hammer for measuring the dynamic force up to 20 kN. The rubber tip provides sufficient hardness to produce an impact force associated with an amplitude spectrum of at least 2 kHz. Maximum frequency generated by the hammer impact is inversely related to the impact duration. A typical force-time waveform and a force amplitude spectrum from an impact hammer have been shown in Figure 2-15 (ASTM C1740- 10).

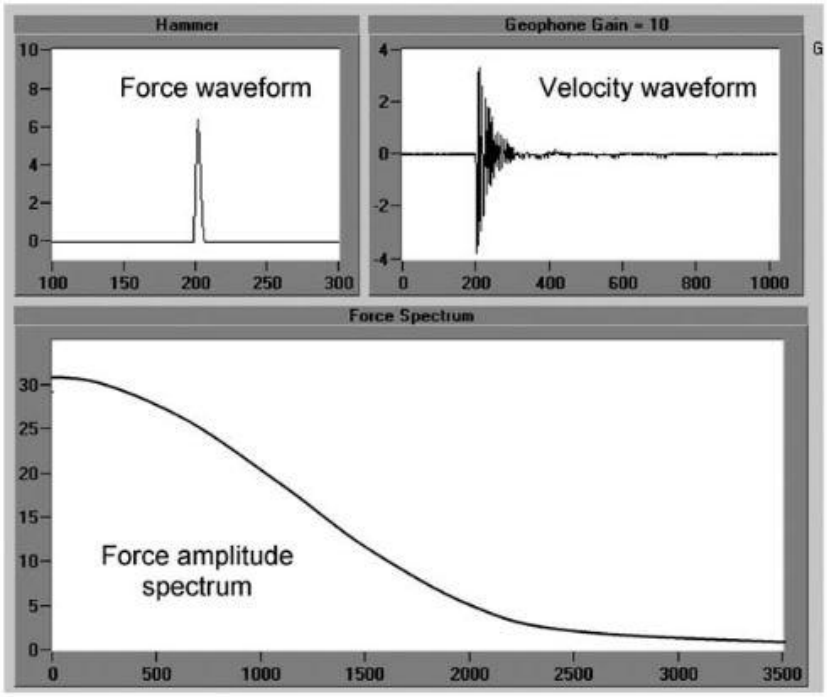

Figure 2-15 Typical Force-Time Waveform and Amplitude Spectrum (ASTM C1740- 10)

2.7.3.2 Test Methodology

For locating the receiver and the hammer hitting, SIR requires the top surface of the test slab to be accessible. The transducer is placed on the top of the slab surface typically 3 to 4 inch away from the hammer impact point. The test surface is then impacted by a load cell hammer and the slab response is monitored by the geophone. The data acquisition system records the hammer input and also the receiver output. Once the data is recorded, Fast Fourier Transform (FFT) operation is performed to transform the time domain signals into frequency domain. In frequency domain, impulse force and the velocity response are integrated as velocity per pound force and plotted with frequency. A coherence curve is also generated which is the indication of data quality with the frequency. The schematic of the field setup for the slab IR method has been shown in following Figure 2-16 (Olson Instruments, 2013).

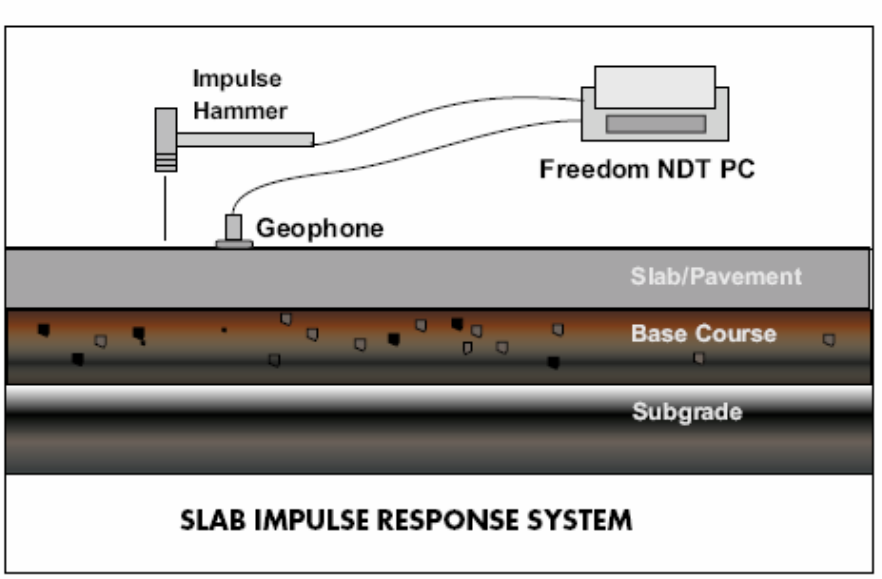

Figure 2-16 Schematic of the field setup for slab IR (Olson Instruments, 2013)

2.7.3.3 Data Analysis

The data analysis of the Slab impulse response is complex as the test results are highly dependent on the geometry and boundary conditions of the test elements. Location on the test slab, material properties, impact duration etc. also play significant role on the velocity response of the test slab (ASTM C1740- 10). The member response as a function of frequency is the mobility spectrum which is the main output of Slab IR test. Mobility at a certain point and given frequency represents the maximum velocity per unit of applied force. Thus, mobility is related with the flexibility of that point. Higher mobility indicates relatively higher velocity resulting by unit applied force. Plate support condition, thickness, modulus of elasticity and voids control the variation of mobility of particular structure. A series of high peaks which are spaced regularly in mobility plot indicates resonant frequency (ASTM C1740-10). For the easiness of data analysis, average mobility of the mobility spectrum, flexibility, mobility slope and the ratio of maximum to average mobility

are considered as the significant parameters of SIR test. A brief description of these controlling parameters is given below:

Average Mobility

The average mobility over the frequency range of 100 to 800 Hz is directly related to the slab thickness, elasticity of the materials and defects in the vicinity of test point. Reduction of plate thickness corresponds to a large increase in average mobility as the flexural rigidity is proportional to the third power of the thickness (Amick et al, 2009). Delamination, cracking and honeycombing reduce the rigidity and cause a significant increase in mobility than for a test on the sound portion of element (Davis et al, 1997). If the top layer is delaminated from the bottom ones then the average mobility increases, as the mobility is higher corresponding to the upper layer. Delamination occurs due to the presence of trapped air and water which should have replaced by particles through the bleeding process. So the variation of average mobility through a slab element of constant thickness indicates the regions of anomalies. Additional testing of the regions of high mobility found from the SIR test confirms the possible variation of concrete quality. An example of mobility plot along with average mobility has been shown in Figure 2-17 (ASTM C1740-10).

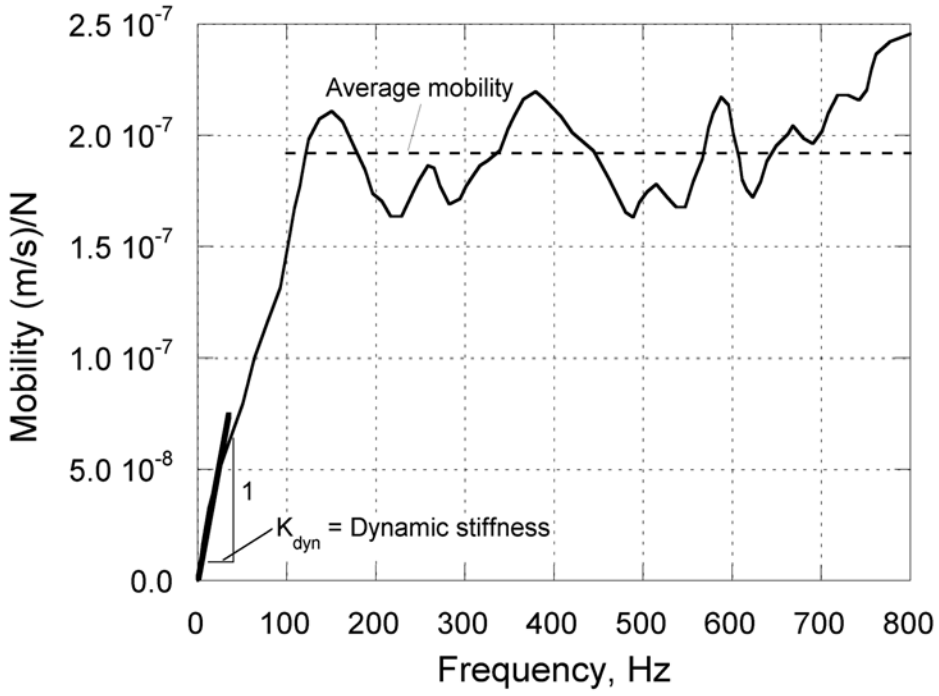

Figure 2-17 Mobility plot with average mobility (ASTM C1740-10)

Mobility Slope

Mobility slope is determined by the best fit line to the mobility plot for the frequency range of 100 to 800 Hz (ASTM C1740-10). The high value of mobility slope indicates the honeycombing in the concrete. Honeycombing occurs because of poor compaction and also because of lower amount of fines present in the mix. Hollows and cavities in structural elements where cement or finer materials could not reach are the location of honeycombing. Close grid spacing may be required to detect the locations of honeycombing as this happens in discrete pockets in concrete elements. Figure 2-18. shows a mobility plot with higher and irregular mobility slopes indicating the possible presence of honeycombing.

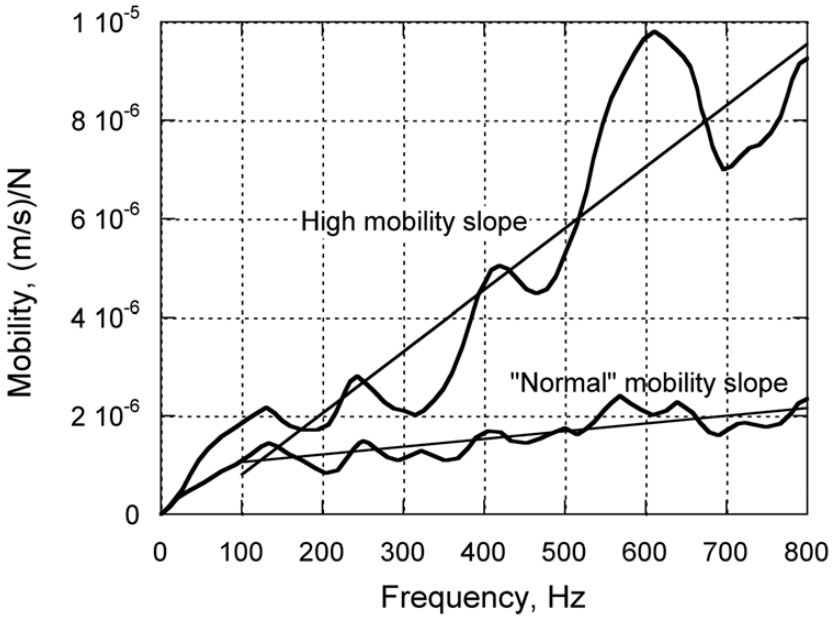

Figure 2-18 Mobility slope at poor consolidation and sound concrete (ASTM C1740-10)

Flexibility

Flexibility also known as dynamic compliance around a test point is determined by the slope of the initial portion of the mobility plot, basically up to 40 Hz. If the initial portion of the mobility plot is steep then the element is more flexible and hence less stiff. The inverse of flexibility is the dynamic stiffness in unit of force/distance which is the function of modulus of elasticity, voids and support condition.

Peak to Mean Mobility Ratio

High ratio of peak to mean mobility indicates poor support condition and deboning of elements within the concrete. If the support condition is poor or there are possible locations of delamination then the upper most layers dominates the response and shows higher mobility then the average value found within first 100 Hz frequency. Experience showed that, loss of support is likely to happen when the peak to mean ration exceed the value 2.5 (ASTM C1740-10). So the presence of higher peaks at low frequency is the indication

of poor support condition and voids in the concrete. Typical signals with poor and good support conditions have been shown in Figure 2-19 (ASTM C1740-10).

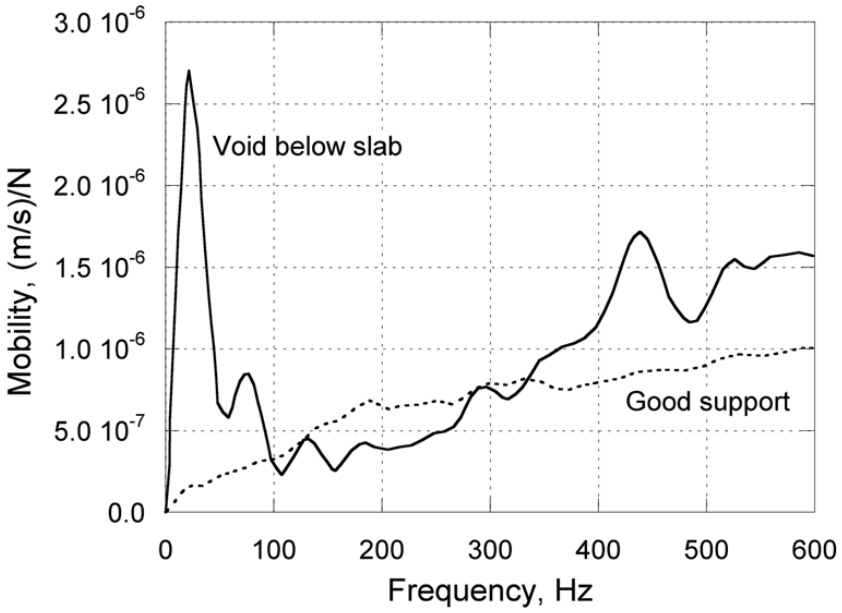

Figure 2-19 Signals with poor and good support conditions (ASTM C1740-10)

2.7.3.4 Advantages and Disadvantage

The use of Slab IR is not applicable on the locations subjected with vibration created by mechanical equipments. Electric noise such as noise generated from a generator heavily influences the data acquisition and the use of Slab IR is not applicable. By altering the frequency and the shape of mobility plot, heavy load on suspended slab may also influence the result. Debris on the test surface might have influence on test result as a sharp hammer impact is disturbed. Test conducted on stiffen materials overlying on low stiff material may not represent the internal condition as the mobility represents the response of upper stiffer plate. The Slab IR method is used to determine the support conditions of the slab and to map out the areal extent of any void or poor supported zones, but the method cannot determine the thickness of voids. Collecting Slab IR data at multiple,

densely-spaced locations can improve the conclusions by mapping relative areas of higher and lower mobility. However, relatively low mobility does not indicate the absence of a subgrade void, but qualitatively indicates an area appears to be more solidly supported than an area with relatively high mobility. For thick slabs (thickness > 2 ft), the interpretation of the Slab IR data becomes difficult because the stiffness of the system is controlled by the slab itself and not by the support condition under the slab.

2.7.4 Pulse Echo Test

In pulse velocity test a longitudinal stress pulse is introduced by a vibrating transducer on the surface of the test object. After traveling through the test object the pulse is received by another transducer and is converted to electric signal (ASTM C 597- 02). By indentifying the arrival of the pulse, the pulse travel time through the test object is determined from which pulse velocity can be determined simply by knowing the thickness of the test object. The test can be performed in direct, semi-direct or surface transmission depending on the accessibility of the test surface. Figure 2-20 presents the three different mode of transmission according to Naik and Malhotra (1991). Direct transmission method yields most accurate measurement whereas, surface transmission method is highly prone to errors as the receiving signal amplitude is least in this mode (Naik and Malhotra, 1991). But the surface transmission method is the only option when a single surface of the structure is accessible such as in pavements. Moreover, It requires a series of transient time recording for incrementally increasing distance between the pulse generating and receiving transducers (Graveen, 2001).

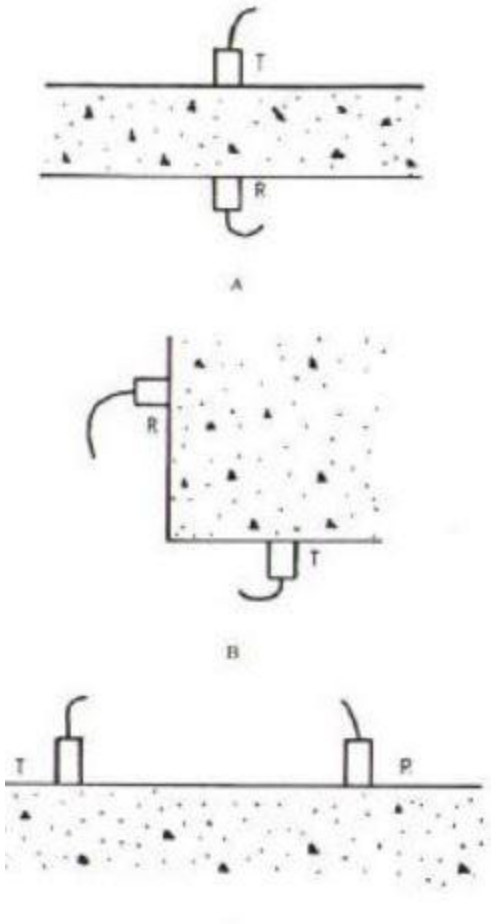

Figure 2-20 Different mode of pulse transmission (Naik and Malhotra, 1991)

2.7.4.1 Instrumentation

According to ASTM C 597– 02, the test method is comprised of the following three basic components:

Pulse Generator and Transmitting Transducer: Pulse generator is consist of circuitry to generate pulses and the transmitting transducer is required to transform the electric pulses into wave bursts of resonant frequency in the range from 20 to 100 kHz (ASTM C 597-02). According to ASTM, It is recommended to use a pulse generator which generates at least 3 pulse per second.

Receiving Transducer and Amplifier: Similar type of transducer is used for receiving the pulse as that was used for transmitting the pulse into the test object. An amplifier is also used along with the receiving transducer to produce triggering amplitude for the time measuring circuit.

Time-Measuring Circuit: The time measuring circuit provides output when the pulse is detectable. The received pulse is amplified to achieve the triggering voltage which initiate the time measurement.

Display Unit: In older system a cathode ray tube (CRT) was used in which the pulse transmission and the receiving were displayed as the deflections of the traces established to a time scale. In modern units direct reading is displayed as the interval of time.

Connecting Cables and Coupling Agent: Shielded, low capacitance and coaxial cables are recommended for the use of interconnections. For the efficient transfer of energy and for the proper connection between the transducers and the test surface, use of viscous material such as grease, oil, water soluble jelly, petroleum jelly, moldable rubber etc. are recommended.

2.7.4.2 Test methodology

ASTM has adopted the standard method for pulse velocity test through concrete and is designated by ASTM C 597– 02 (Standard Test Method for Pulse Velocity through Concrete). Direct transmission method is adopted for the measuring of the pulse velocity as it holds the maximum sensitivity and accuracy level. Sufficient coupling agent and pressure are recommended to apply to the transducers for the stable transient time. Using inadequate coupling will result in incorrect and unstable time measurements which will reduce the effectiveness of the instrument significantly. A zero time adjustment and the functionality of the equipment are also verified before the test. A reference bar with known transient time is used for the zero-time adjustment. It is recommended to check the zero ad-

justment on hourly basis if the instrument is used continuously. Standard test method adopted by ASTM C 597– 02 has been represent by Figure 2-21.

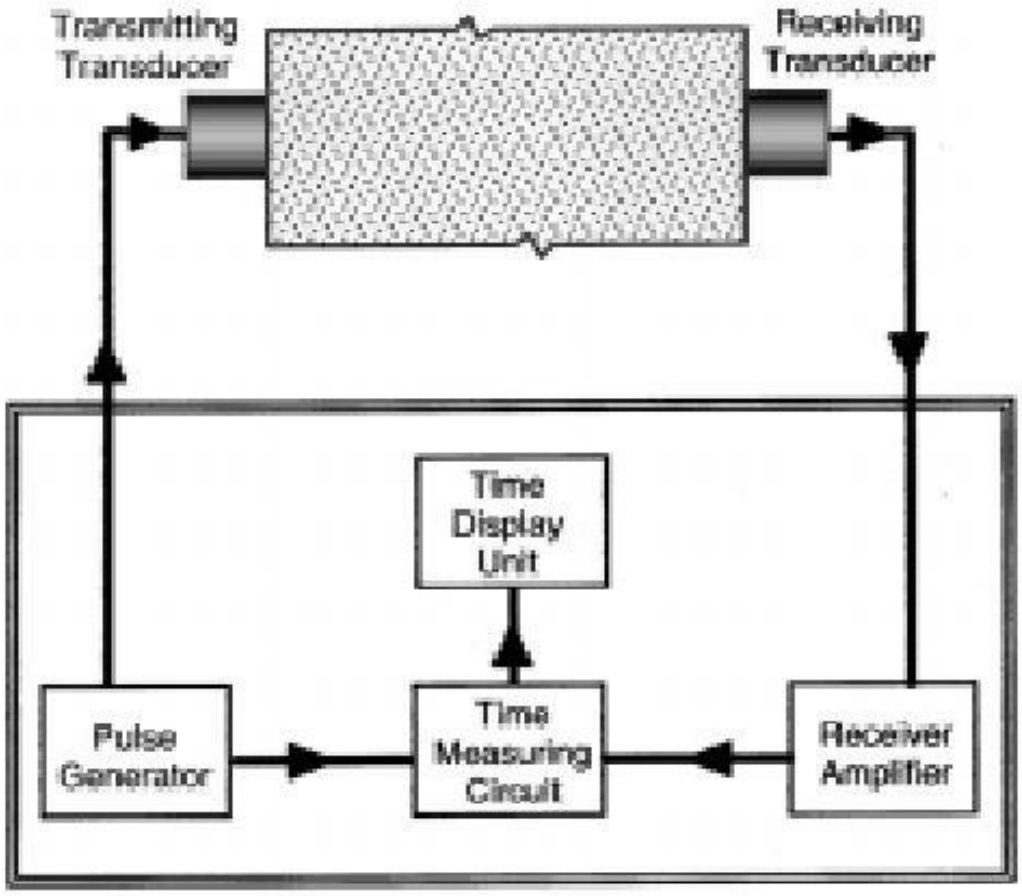

Figure 2-21 Standard test method for pulse echo test (ASTM C 597– 02)

2.7.4.3 Advantages and Disadvantages

The main advantage of pulse velocity method is that, this method is independent of the dimensions of the test object and hence the boundary conditions do not interrupt the determination of the arrival time of the transmitted pulse. This method is applicable in both laboratory and in-situ testing depending on the available pulse-generating source. The main disadvantage is that, this method is not suitable for pavement application as the

surface transmission method is needed to follow which makes the result erroneous. The accuracy is also dependent on the operator's ability to determine the distance between the transducers and to identify the arrival of the pulse accurately. Presence of cracking and the degree of cracking in the test structure effect the travel path and hence the pulse velocity.

Chapter 3

EXPERIMENTAL PROGRAM

3.1 Introduction

Depending on three different types of aggregates commonly used in Texas as the pavement base and subbase materials, this experimental test program was designed and conducted to assess the potential applicability of non-destructive tests in pavement evaluation. Reclaimed Asphalt Pavement (RAP), Recycled Grade-1 and Grade-2 materials were considered for the designated test program. Materials were collected from the site of Big City Crushed Concrete located at Dallas, Texas. This company is one of the Texas Department of Transportation (TxDOT) approved companies which supplies recycled flex base materials in Dallas – Fort Worth (DFW) area in accordance with TxDOT specifications.

3.2 Basic Properties of Test Materials

Basic engineering tests were conducted on all three test materials which included sieve analysis, proctor compaction test and specific gravity test. Sieve Analysis was performed to determine particle size distribution of the materials following standard test method specified in TxDOT guidelines (Tex- 110E), as shown in Figure 3-1. Sieve analysis shows that about 99 percent of the materials are retained on No. 200 sieve. According to TxDOT specification Item 276, no hydrometer analysis is required if percent passing on No. 200 sieve is less than 1% and hence; no Hydrometer analysis was performed. Atterberg limits were also not determined because of the same reason.

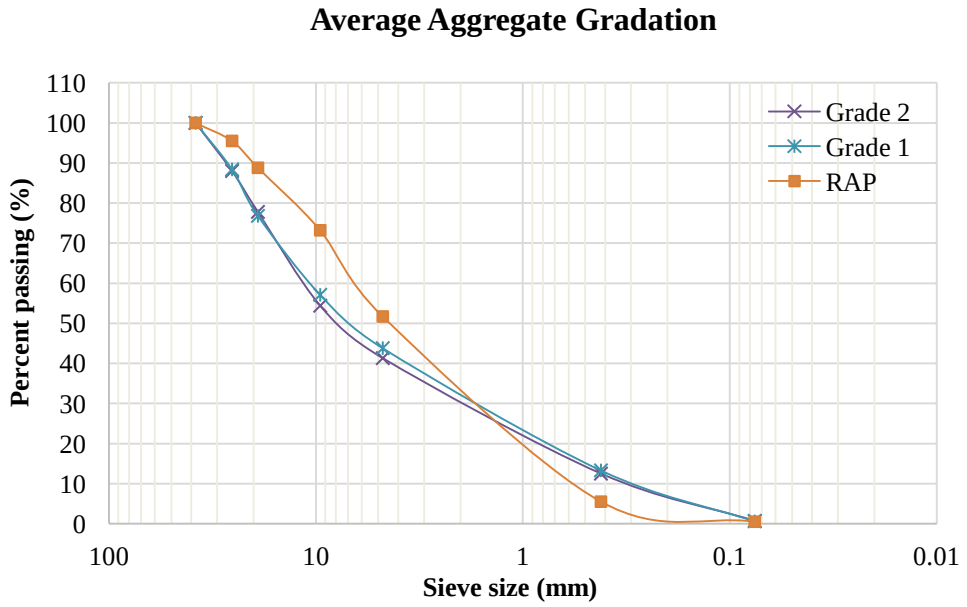

Figure 3-1 Sieve Analysis

Coefficient of Curvature and Uniformity coefficient calculated from the gradation curves, along with Bulk Specific Gravity of all the materials are reported in Table 3-1. Bulk Specific Gravity for all the materials was also determined and is reported in the same table. Maximum size of the aggregate was limited to 1.25 inches (32 mm) throughout the test program to ascertain proper compaction and homogeneity of the test samples. Portland Type II cement was used as the binder in this study, which has 28 days compressive strength greater than 7252 psi (50 MPa).

Table 3-1 Material Properties

	RAP	Grade 2	Grade 1
Coefficient of Curvature	1.33	2.28	2.51
Coefficient of Uniformity	7.84	34.09	23.21
Moisture Content (%)	0.23	0.93	1.12
Dry Bulk Specific Gravity	1.90	1.92	1.88

3.3 Experimental Setup

For the experimental program of this study, seven different combinations of RAP, Grade-1 and Grade-2 materials were considered for unconfined compressive strength test and four different combinations were selected for resilient modulus test. Test samples for each combination were prepared using 0, 2, 4 and 6% cement contents, as the cement treated base layer typically consists of 3-10 percent cement of the total dry weight of the mix. For each combination, three samples were prepared at a certain cement content for unconfined compressive strength and resilient modulus test separately, to check the repeatability of the test results. Optimum moisture content (OMC) and maximum dry density (MMD) were also determined for each combination at four different cement contents. Again, three samples were prepared to check the repeatability of the test results. A list of all the combinations and total number of samples prepared for this study has been shown in Table 3-2.

Table 3-2 Experimental Program

Mix ID	Material Combination For UCS Test			Number of Samples (For OMC, UCS and M_R Test)			
	Grade-1/2 (%)	RAP (%)	OMC & MDD (0, 2, 4 & 6%) cement contents	0%	2%	4%	6%
$M1^{[M_R]}$	G2- 100	0		3	3	3	3
M2	G2- 90	10		3	3	3	3
M3	G2- 70	30		3	3	3	3
$M4^{[M_R]}$	G2- 50	50		3	3	3	3
$M5^{[M_R]}$	G2- 30	70		3	3	3	3
M6	G2- 0	100		3	3	3	3
$M7^{[M_R]}$	G1-100	0		3	3	3	3

Each sample prepared for unconfined compressive strength and resilient modulus test was subjected to stress wave velocity (sonic echo/ impact echo test) method. Table 3-3 provides the total number of tests performed for this experimental study. As a very high number of tests were executed, all the analysis are done based on the average values of obtained parameters. A summary of all the test variables with each phase of the test program is given by Figure 3-2.

Table 3-3 Total number of tests performed

	Combinations	Cement Content	Test Variables	No. of Samples per test variable	Total number of test	Parameters obtained
UC strength test	7	4	7X4= 28	3	28X3= 84	Compressive strength
						Modulus of elasticity
Resilient modulus test	4	4	4X4= 16	3	16X3= 48	Resilient modulus
Stress wave velocity test					84+48= 132	P-wave velocity

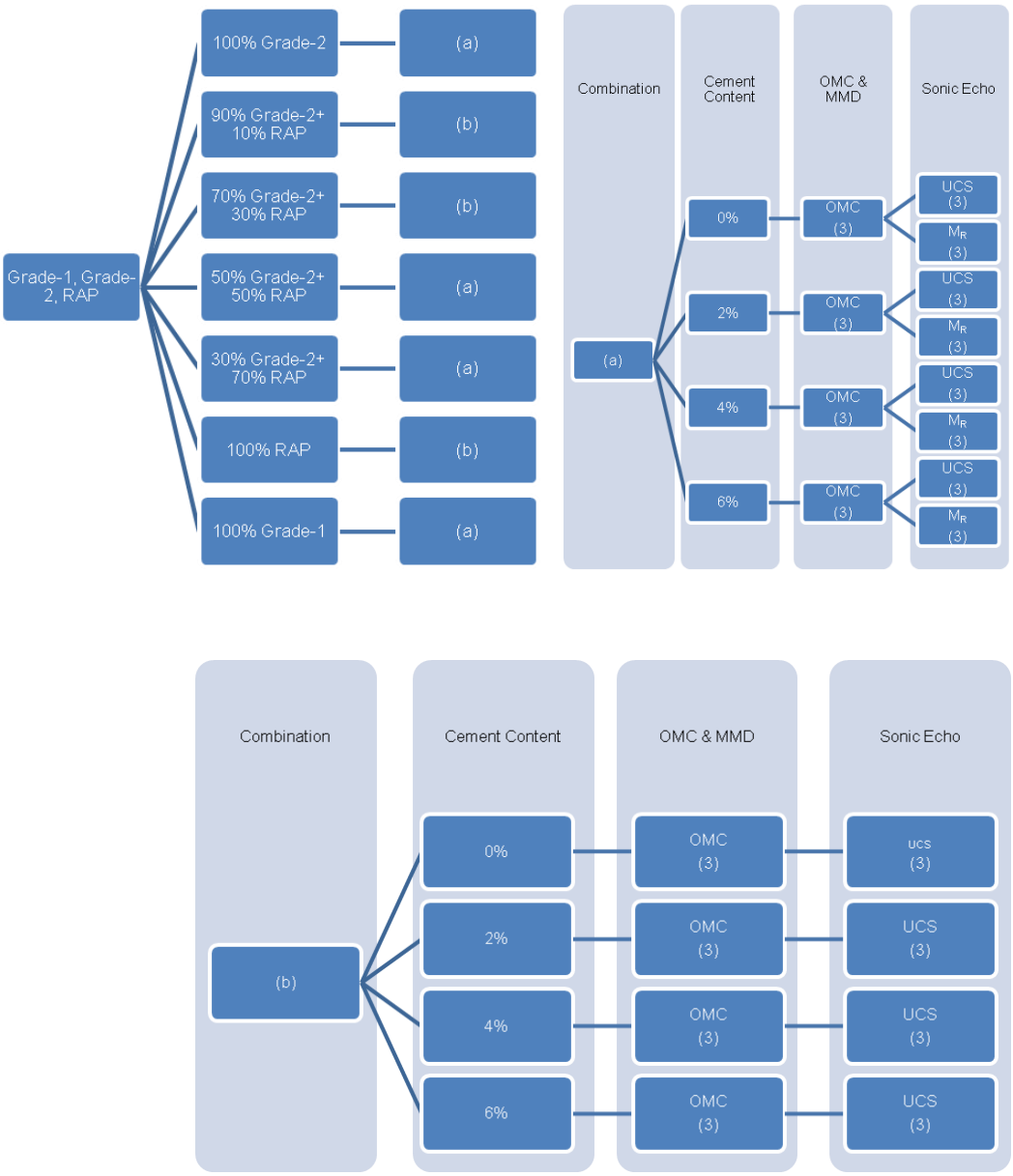

Figure 3-2 Summary of the test variables at different phase of the experimental program

3.4 Optimum Moisture Content & Maximum Dry Density

Optimum Moisture Content (OMC) & Maximum Dry Density (MDD) were determined in accordance with Tex-113-E (Texas Department of Transportation 1999b); Laboratory Compaction Characteristics and Moisture-Density Relationship of Base Materials. The dimensions of the mold were 4 inch (101.6 mm) in diameter and 6 inch (152.4 mm) in height. The aggregates were mixed thoroughly with water and cement. Each sample was compacted in three lifts delivering 17 blows to each lift which render the required compaction energy of 13.25 ft-lb/in^3 (1097.4 m-kN/m^3). The required energy was obtained by selecting the parameters included in Table 3-4. The compaction tests were done for at least 4 different moisture contents and the maximum dry density was determined from moisture content vs. dry density plots. Moisture content corresponding to maximum dry density is the optimum moisture content. The summary of OMC and MDD shown in Figure 3-3, 3.4 and 3.5, indicating that the addition of cement dosage does not influence the moisture-density relation of a particular aggregate mixture. But, the increase of RAP percentage causes a gradual decrease of OMC and MDD as the water absorption capacity and unit weight of RAP is less than Grade-2 and Grade-1 materials. Optimum moisture content for all cement doses and aggregate mixes vary within the range of 6.5-11% whereas; maximum dry density ranges between 120-131 pcf. If the mold diameter increases from 4 inch (101.6 mm) to 6 inch (152.4 mm), the maximum dry unit weight changes $\pm$0.5 pcf (0.0786 kN/m^3) and optimum moisture content changes $\pm$0.75% (Hoyos et al. 2011). This small variation is acceptable for further testing.

Table 3-4 Obtained compaction parameters (Tex-113E)

Parameter	Values
Weight of Hammer	10 lb (4.50 kg)
Height of Drop	18 inch (457 mm)
Specimen Diameter	4 inch (101.6 mm)
Specimen Height	6 inch (152.4 mm)
Volume of prepared sample	75.36 $inch^3$ (1234929 mm^3)
Drop per layer	17
Number of layer	3
Compaction effort	13.25 ft-lb / in^3 (1097.4 m- kN/m^3)

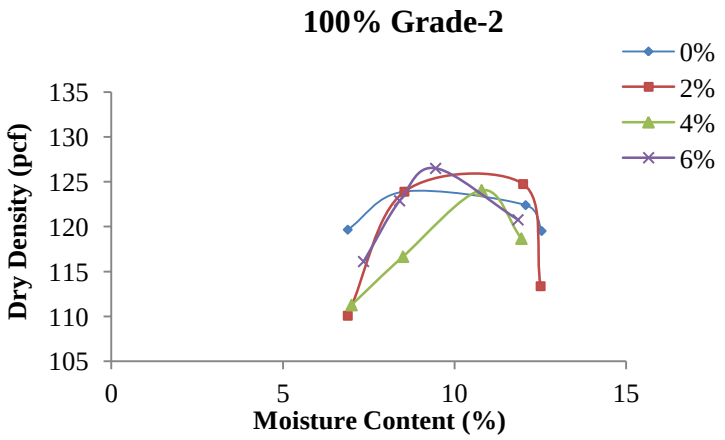

Figure 3-3 Moisture-Density relationship of cement treated mixtures of Grade-2 materials

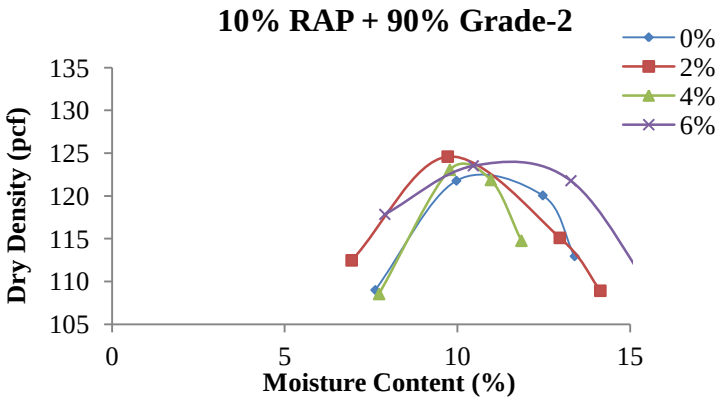

(a)

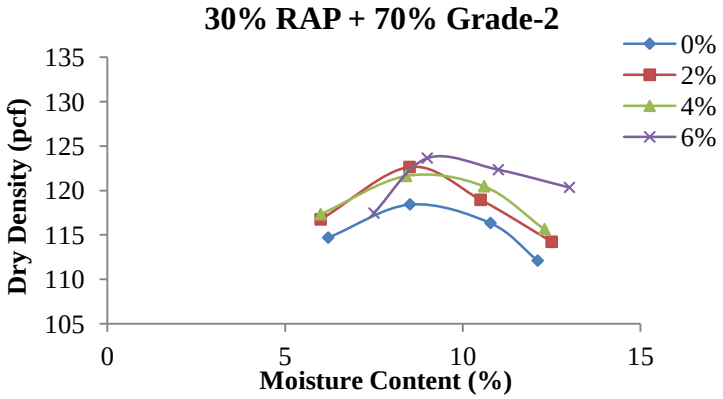

(b)

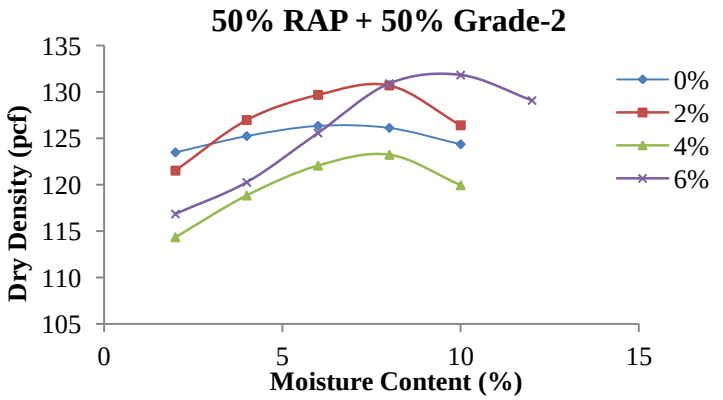

(c)

Figure 3-4 Moisture-Density relationship of cement treated mixtures

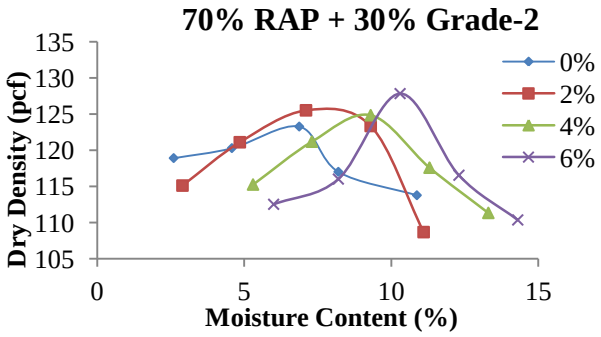

(a)

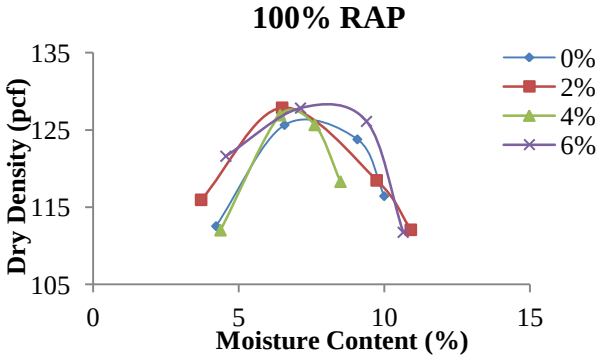

(b)

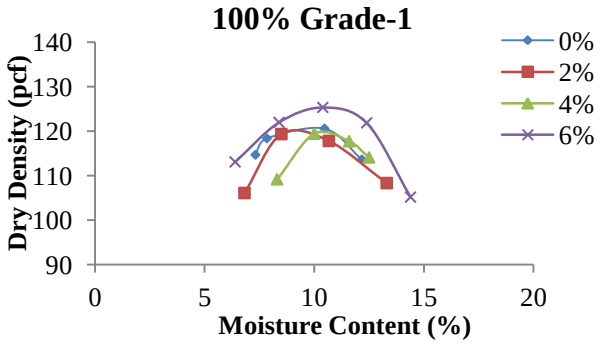

(c)

Figure 3-5 Moisture-Density relationship of cement treated mixtures of RAP, Grade-1 and Grade-2 materials

3.5 Specimen Preparation

For each combination of mixes which are labeled from M1 to M7 as shown in Table 3-2, each sample was prepared at optimum moisture content in order to attain maximum dry density. Mix M1 contains 100% Grade-2 materials, while Mix M6 is of 100% RAP. Specimens were prepared as per TxDOT guidelines. The mold used to prepare the UCS samples was 6 in. (152.4 mm) in diameter and 8 in. (203.2 mm) in height, but for the resilient modulus test the mold height was 12 in. (254 mm). Samples for UCS test were prepared in 4 lifts, compacted by 50 blows to achieve the required compaction level at optimum moisture content. For the resilient modulus test, 6 lifts were implemented each having a thickness of 2 in. An automated mechanical compactor was used which meets the TxDOT specifications as shown in Figure 3-6 and 3-7. Prepared specimens were kept for 7 days in the 100% moist room in accordance with Soil-Cement testing procedure (Tex-120 E) specified by TxDOT before testing.

(a) (b)

Figure 3-6 (a) 2 different types materials (b) Mixing of the materials

(a)

(b)

(c)

(d)

Figure 3-7 (a) Prepared materials (b) Sample compaction (c) Sample extruding (d) Prepared sample

3.6 Stress Wave Velocity Measurement

For the stress wave velocity measurement, standard test method for concrete designated by ASTM C 1383-04 (Standard Test Method for Measuring the P-Wave Speed and the Thickness of Concrete Plates Using the Impact-Echo Method) was followed. Two procedures designated as Procedure-A and Procedure-B are described in this standard test method, where Procedure-A details the process of P-wave velocity measurement and Procedure-B depicts the process of thickness measurement of plate like structure by implementing impact echo method. In Procedure-A, an impact on the selected concrete surface is made by an impulse hammer. The wave generated by the impact propagates along the surface of the test concrete. Two transducers are placed on the test surface at a known distance and the arrival of the P-wave in both transducers is identified. By knowing the time difference between the arrival of P-wave at each transducer, travel time of the P-wave for the known distance is calculated. Once the travel time is known, measurement of the P-wave velocity is possible by simply dividing the distance between the transducers with the travel time.

In Procedure-B, process of determining the thickness of an unknown concrete structure is described using the P-wave velocity, which is found in Procedure-A. The P-wave generated by the impact propagates into the concrete structure and reflects back from the opposite side. A transducer placed adjacent to the impact point records the surface deflection in time domain caused by the reflected wave. First Fourier Transformation (FFT) technique is then applied to transfer the time domain response into the frequency domain. Thus an amplitude spectrum is obtained where the arrival of the reflected wave can easily be identified by a dominant peak in the spectrum. The frequency corresponding to this peak and eventually the P-wave velocity are then used to determine the thickness of the concrete plate.

For this test study, a combination of procedure-A and B has been adopted for the stress wave velocity measurement. Test was performed on each mold by direct transmission method as both ends of the samples were accessible. Hammer impact was made on one end and the Geophone was placed on the other end. Height of each sample was determined at the very beginning of the test. By knowing the sample height and the travel time of the wave, corresponding P-wave velocity was calculated. Figure 3-8 and Figure 3-9 shows the test procedure for the stress wave velocity measurement.

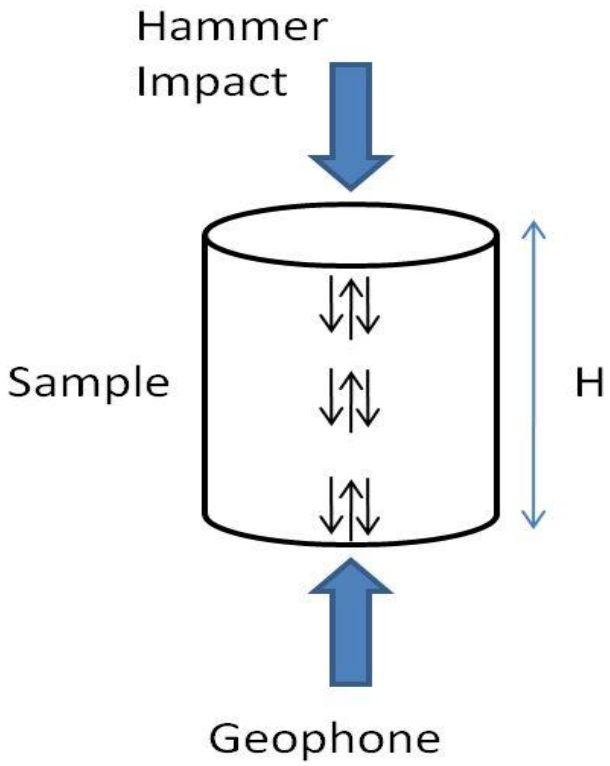

Figure 3-8 Test methodology for wave velocity measurement

Figure 3-9 Test Setup for wave velocity measurement

P-wave generated by the impact propagates into the sample and when it reaches the geophone it produces a significant peak in the amplitude spectrum. This wave then reflects back to the top and from the top, another reflection takes place and the wave travels back to the bottom. When it reaches the bottom surface for the second time, another significant peak in the amplitude spectrum can be noticed. The frequency difference between these two peaks is associated with the travel time of the P-wave, in which the wave travels twice along the test sample. If the height of the sample is H, and the frequency difference between two consecutive peaks is $\triangle f$, then the P-wave velocity can be calculated by the following equation.

$$V_p = 2H \times \triangle f \qquad (3.1)$$

3.6.1 Description of the Test Apparatus

For the stress wave velocity measurement, Sonic Echo/ Impulse Response (SE/IR) test with the NDE-360 system manufactured by Olson Instruments was used. Basic components include a 4 channel NDE-360 for data collection, analysis and display, an instru-

mented hammer, a geophone, grease and connection cables. NDE-360 platform is a powerful, small and easy to handle system which allows fast data collection by a single operator. Windows software WinTFS with a number of analysis tools were used for post data analysis. Figure 3-10 represents the different components of the test apparatus used for the stress wave velocity measurement.

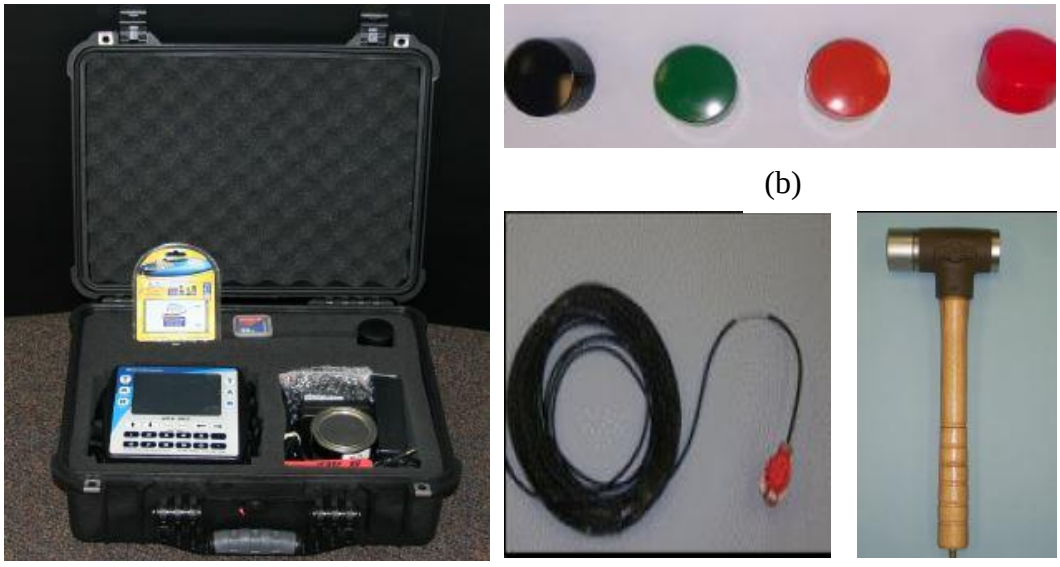

(a) (b) (c) (d)

Figure 3-10 Test apparatus for the P-wave velocity measurement (a) Total components (b) Hammer heads (c) Geophone (d) Hammer

The hammer weighed 3 lbs and a black head was screwed with the hammer. There were four types of hammer head with different hardness, but the black one was used as the sample height was small. A BNC cable was connected at the end of the hammer and the other end of the cable was connected to the NDE-360. The Geophone was also connected to the NDE-360 by a 4 pin adaptor. Small amount of coupling grease was used with

the Geophone for the proper contact between the Geophone and the test sample. Figure 3-11 shows the complete setup of the hardware for the test.

Figure 3-11 Complete setup of the hardware for the P-wave velocity measurement

3.6.2 Data Acquisition Parameters

Sampling Rate:

Sampling rate, also termed as sampling interval is the time interval between two recorded data points within a data trace. It indicates how frequently the system will acquire data in the time domain. According to ASTM C 1383-04, the sampling rate should be in between 2 to 4 microseconds or less. But for this study to match the sensitivity of the transducer with the voltage range, sampling rate was taken as 7 microseconds (142 Hz), which means that the system acquired data at 7 microsecond intervals.

Point Per Record:

According to ASTM C 1383-04, typical number of data points in a record is to be 1024 or 2048 depending on the lateral dimension of the test sample. But in this study, data were taken by the direct transmission method, rejecting the influence of lateral extension of the

samples. Due to the acceptance of higher sampling interval, 1024 data points were considered for stress wave velocity tests.

Sampling Period:

Sampling period is the product of sampling rate and the number of points per record. The sampling period for this study was 7168 microseconds.

Pre- Trigger:

Pre-trigger is the number of points before the starting of data collection. In this study, 100 points were taken as the pre-trigger.

Trigger Level:

Trigger lever is the minimum signal amplitude exceeding which, the system starts the data acquisition. For this case the trigger level was set to 6% indicating that the system starts to acquire data when the absolute value of signal amplitude exceeds 0.6 volt.

Number of Records:

Number of records for this study was set to 3 which means that the system takes three impact data to generate the surface displacement spectrum caused by the stress wave.

3.7 Unconfined Compressive Strength (UCS) Testing

Unconfined Compressive Strength (UCS) is the index property of cement stabilized flex base materials in pavement design. Unconfined compressive strength (UCS) test results were used as the measurement of compressive strength of the samples and also to measure the modulus of elasticity. Variations of strength and stiffness of different cement treated mixtures were analyzed on the basis of UCS test. ASTM D 2166 standard test procedure was followed for the unconfined compressive strength test and the samples were loaded at the strain rate of 0.25%. After 7 days of curing period, test samples were placed on the compressive test platform and were loaded at a constant rate. A data acquisition system was attached to the testing machine to measure the lateral and axial

deformations. Maximum axial load at which the sample failed was taken as the ultimate load bearing capacity of that sample. A servo controlled tensile/compression testing machine (Figure 3-12) was used for the UCS test on the specimens. The stress vs. strain curves obtained from the test were used to determine the tangent modulus of elasticity for different specimens.

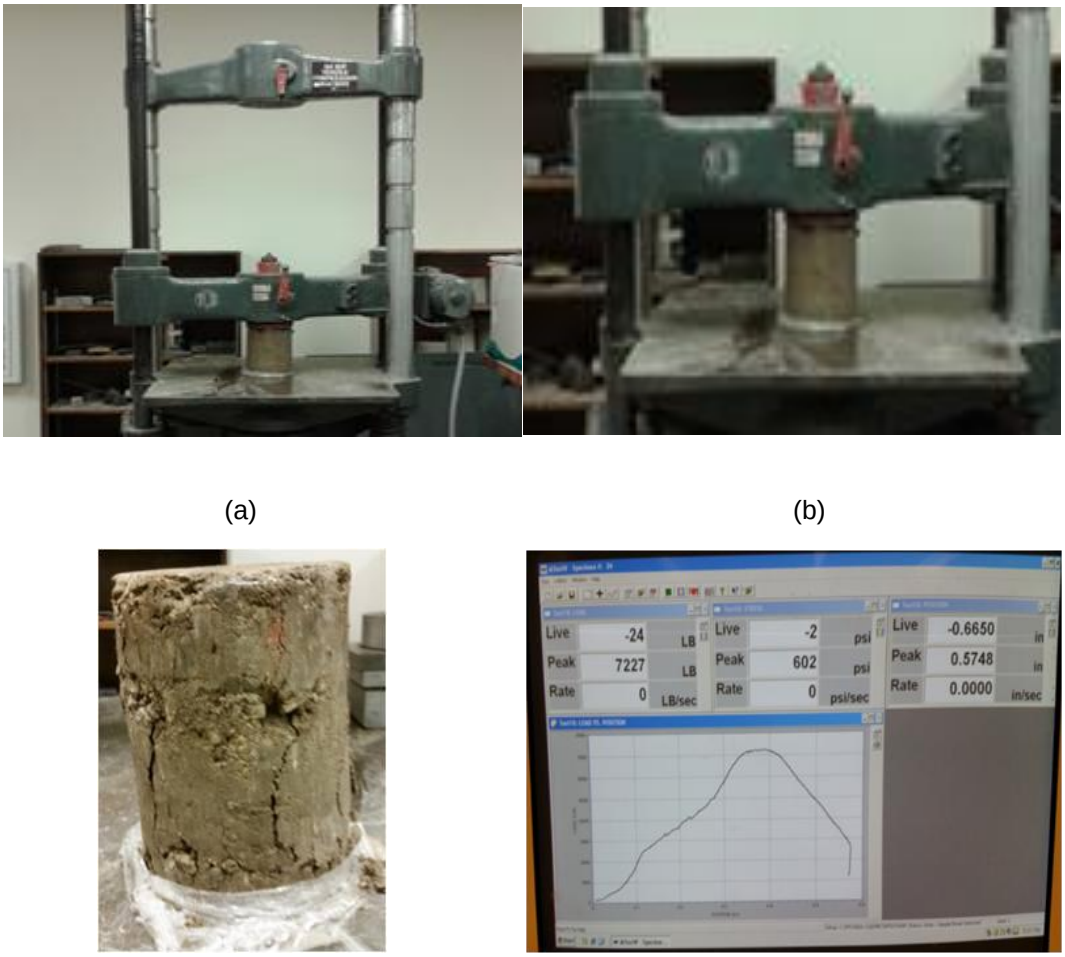

(a) (b)

(c) (d)

Figure 3-12 (a) Servo controlled tensile/compression testing machine (b) testing of a sample (c) sample after testing (d) machine output

3.8 Resilient Modulus Testing

Standard test method designated by AASHTO T307-99 was adopted for the determination of resilient modulus. MR-cyclic machine was used for the simulation of traffic load by applying a sequence of cyclic load on the specimens. Cyclic load sequences used for the resilient modulus test were standardized by AASHTO on the basis of the location within the pavement section. Test sequences adopted in this test program are presented in Table 3-5. Confining stresses around the test specimens represent the overburden pressure whereas; deviator stresses represent the wheel load. The loading period for the testing was 0.1 sec and the relaxation period was 0.9 sec, as mentioned in AASHTO T 307-99 procedure. Samples were tested after 7 days of curing period in the moist room. The average total vertical deformation of the samples was monitored during the test by two Linear Variable Displacement Transducers (LVDTs) placed on the top of the test cell. Figure 3-13 shows the test arrangement for resilient modulus test and Figure 3-14 shows the output of the test.

Table 3-5 Load sequence for resilient modulus test

No.	Confining Stress (psi)	Max. Deviator Stress (psi)	Cyclic Stress (psi)	Constant Stress (psi)	No. of Load Cycles
0	15	15	13.5	1.5	500-1000
1	3	3	2.7	0.3	100
2	3	6	5.4	0.6	100
3	3	9	8.1	0.9	100
4	5	5	4.5	0.5	100
5	5	10	9	1	100
6	5	15	13.5	1.5	100
7	10	10	9	1	100
8	10	20	18	2	100
9	10	30	27	3	100
10	15	10	9	1	100
11	15	15	13.5	1.5	100
12	15	30	27	3	100
13	20	15	13.5	1.5	100
14	20	20	18	2	100
15	20	40	36	4	100

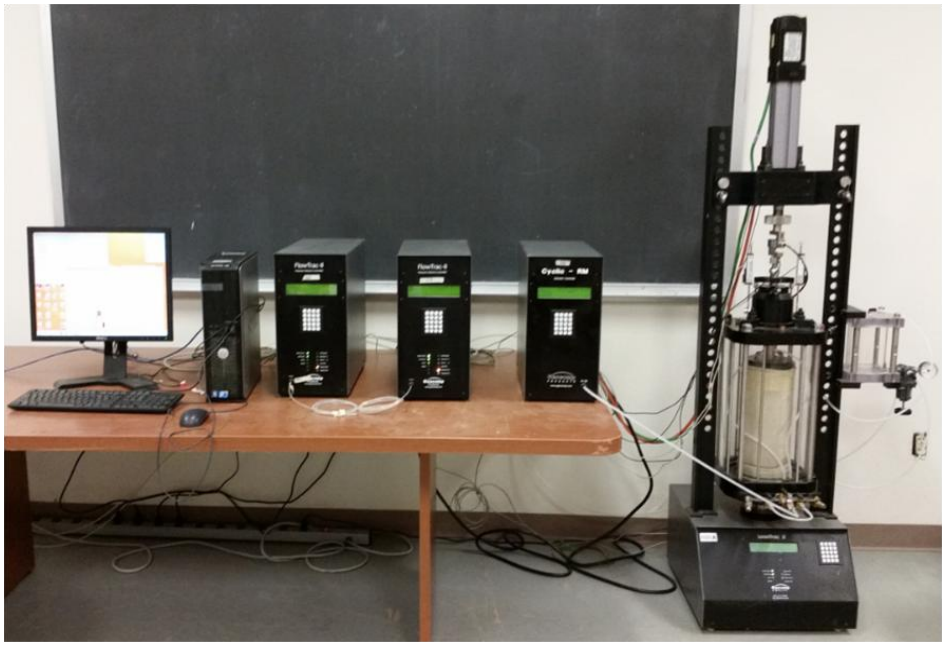

Figure 3-13 Experimental setup for Resilient Modulus test

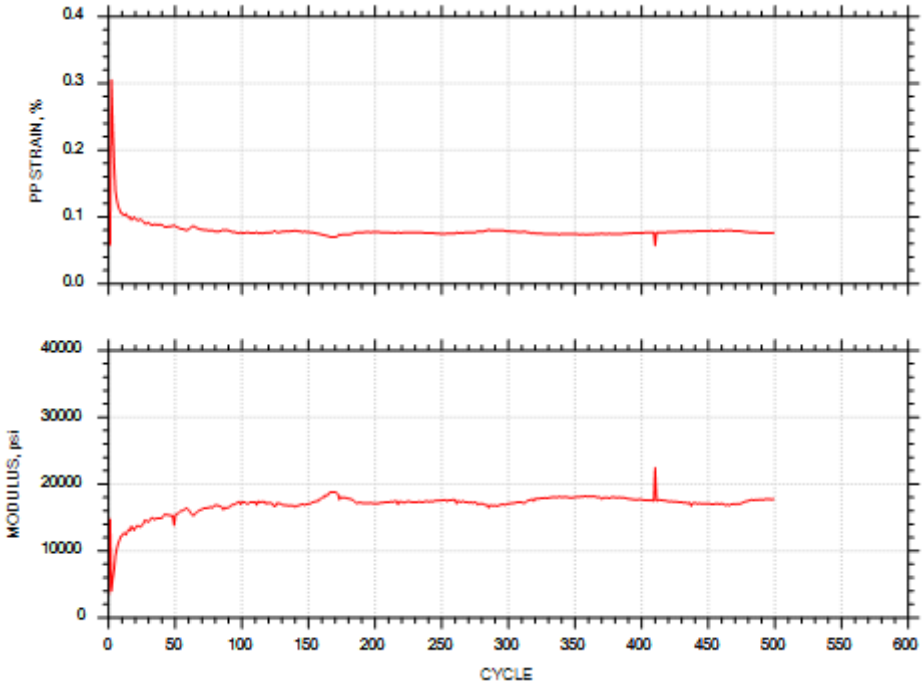

Figure 3-14 Test output of Resilient Modulus test

Chapter 4

DATA ANALYSIS

4.1 Introduction

This chapter focuses on the test results and analyses of three different tests conducted on 7 different aggregate mixes at 4 different cement contents. Results are discussed and analyzed with respect to P-wave velocity, poission's ratio, aggregate ratio and cement content. Devoting the main objective of this study, the analyses are mainly based on P-wave velocity measurements, whereas; unconfined compressive strength (UCS) and resilient modulus (M_R) tests are mostly used as response variables. Common trends found from unconfined compressive strength and resilient modulus tests are discussed and compared with previous studies to validate the experimental data. All the correlations and explanations of this study are based on the trends found from test results.

4.2 Wave Velocity Test Results

Standard test method designated by ASTM C 1383-04 (Standard Test Method for Measuring the P-Wave Speed and the Thickness of Concrete Plates Using the Impact-Echo Method) was followed for the P-wave velocity measurement through each of the samples. Hammer impact was made on the top of the sample to generate the stress wave and a Geophone was placed at the bottom. As the P-wave reaches the bottom, it causes a notable peak in geophone response and bounces back to the top. From the top it rebounds back to the bottom and again creates a peak. The frequency difference between these two peaks is associated with the travel time of the P-wave within which the wave travels twice along the test sample. P-wave velocity is then calculated by measuring the height of the sample.

4.2.1 Equations and Parameters

Once the P-wave velocity through each of the samples is determined, existing empirical correlations are used for the prediction of strength and stiffness parameters. Dynamic modulus of elasticity was predicted from P-wave velocity, density and poission's ratio using the following equation given in British Standard (BS1881: Part 203):

$$V_p = \sqrt{\frac{E\,(1-\mu)}{(1+\mu)(1-2\mu)\rho}} \qquad (4.1)$$

Where,

E= Dynamic modulus of elasticity

m= Poission's Ration

ρ = Density

For the prediction of dynamic modulus of elasticity from P-wave velocity, maximum dry density found by Optimum Moisture Content (OMC) test was taken as the density of each sample. The value of poission's ratio had to be assumed as no test was conducted for the accurate estimation of this parameter. According to the study conducted by Popovics (1998), the value of poission's ratio for concrete varies within the range of 0.2 to 0.33. But for the unbound granular materials poission's ratio varies from 0.3 to 0.4.

For the approximation of poission's ratio for this study; dynamic modulus of elasticity at 0% cement content and 6% cement contents were determined for a wide range of poission's ratio as shown in Figure 4-1. Poission's ratio at which the dynamic modulus of elasticity matched the modulus of elasticity found from UCS test was taken as the poission's ratio for that combination. For Grade-2 material, poission's ratio was found to be 0.395 at 0% cement content and 0.342 at 6% cement content. Assuming linear variation of poission's ratio with cement content, a line joining the dynamic modulus of elasticity allowed to estimate the poission's ratio at 2% and 4% cement content. It was observed

that, addition of 2% cement does not have any significant effect on poission's ratio. At 2% cement, poission's ratio was a bit lower than the poission's ratio found at 0% cement content. Also at 4% cement, poission's ratio was not that significantly different from the poission's ratio at 6% cement content. At 2% cement, poission's ratio was found to be 0.386 and at 4% cement content estimated poission's ratio was 0.355.

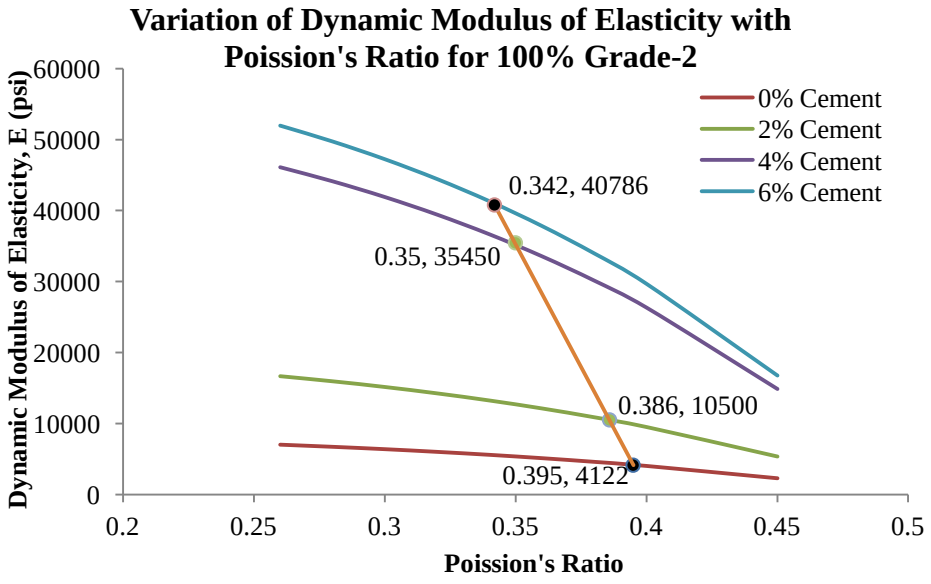

Figure 4-1 Variation of Dynamic Modulus with Poission's Ratio for 100% Grade-2

Same procedure as shown in Figure 4-2 was followed to estimate the Poission's ratio for 100% RAP. No variation of poission's ratio was observed between Grade-2 and RAP materials at 0% cement content though; higher value was found for 100% RAP at 6% cement content. At 6% cement content, poission's ratio was found to be 0.359. For 2% and 4% cement content the value of poission's ratio were found to be 0.393 and 0.370 respectively.

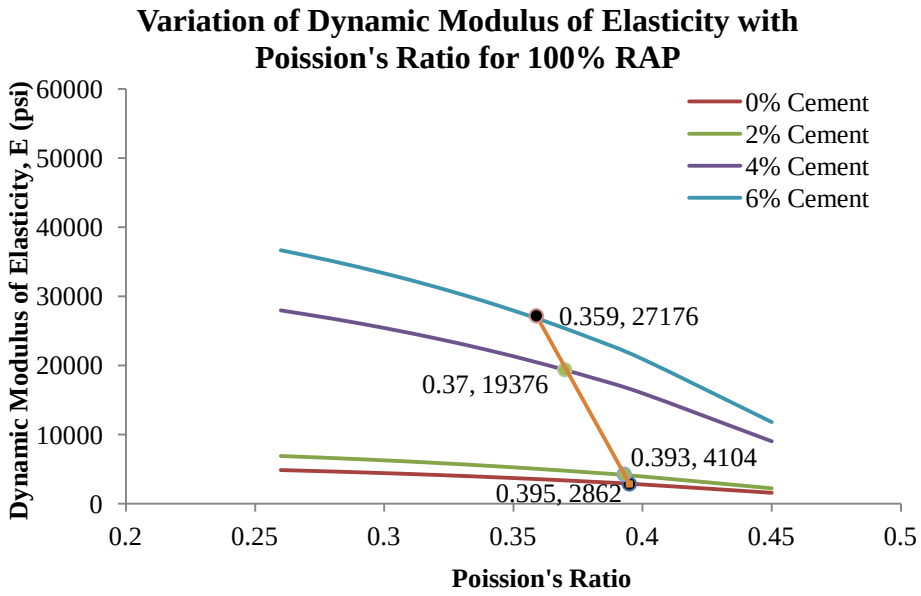

Figure 4-2 Variation of Dynamic Modulus with Poission's Ratio for 100% RAP

Figure 4-3 shows the variation of poission's ratio with cement content. Poission's ratio at 0% cement content was same both for 100% Grade-2 and RAP materials. It was observed that, both for Grade-2 and RAP, Poission's ratio tends to decrease with the increase of cement content. Minimum poission's ratio was found to be 0.342 for Grade-2 material which is higher than the typical values of cement treated granular materials. This might have happened due to the bigger aggregate size and relatively lower cement content to fill the voids in the aggregate blends.

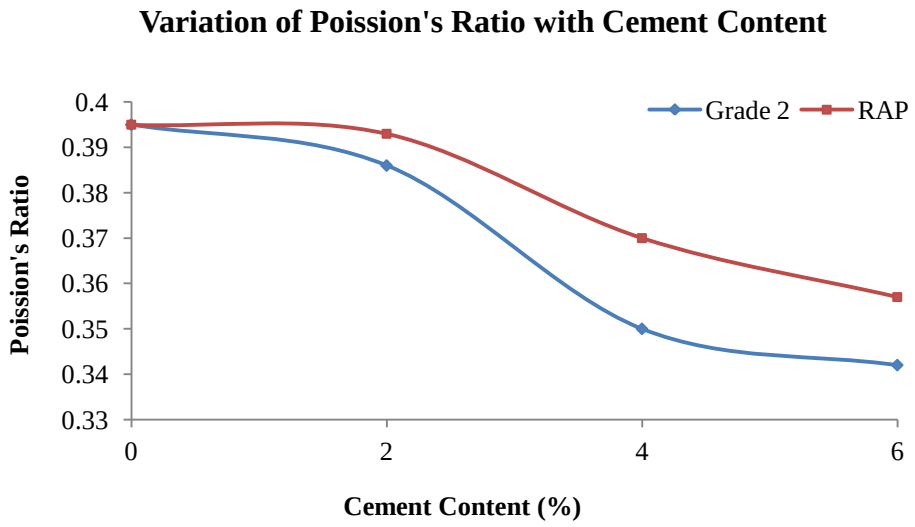

Figure 4-3 Variation of Poission's Ratio with Cement Content

Similar type of analysis for poission's ratio was also done for Grade-1 materials and is shown in Figure 4-4. It was found that, Poission's ratio values for Grade-1 materials were slightly higher than Grade-2 materials.

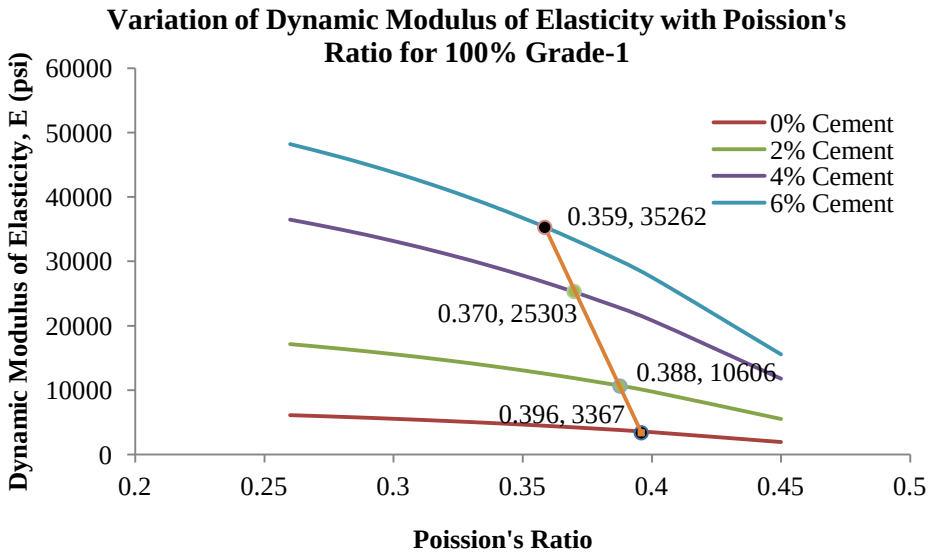

Figure 4-4 Variation of Dynamic Modulus with Poission's Ratio for 100% Grade-1

Based on the above analysis, Poission's ratio for all the combinations at 4 different cement contents were determined and is represented in Table 4-1. From the table it can be observed that, poission's ratio at a particular cement content varies within a very narrow range. Hence; for the simplicity of the analysis, the average values of the Poission's ratio at four different cement contents were used, regardless the proportion of different materials in the aggregate blend.

Table 4-1 Poission's ratio for different combinations

Cement (%)	100% G-2 (M1)	90% G-2 + 10% RAP (M2)	70% G-2 + 30% RAP (M3)	50% G-2 + 50% RAP (M4)	30% G-2 + 70% RAP (M5)	100% RAP (M6)	100 % G-1 (M7)	Poission's Ratio Taken for Analysis
0	0.395	0.395	0.395	0.395	0.395	0.395	0.396	0.395
2	0.386	0.387	0.388	0.390	0.391	0.393	0.388	0.39
4	0.350	0.352	0.356	0.360	0.363	0.369	0.370	0.36
6	0.342	0.344	0.347	0.351	0.354	0.359	0.359	0.35

4.2.2 Test Results

4.2.2.1 P-wave Velocity Results

P-wave velocity increases with the increasing amount of cement content at every combination of the mixes. Figure 4-5 shows the variation of P-wave velocity with the increasing amount of cement content for all seven different combinations used in this study. Cement makes the samples denser by filling the voids which eventually increases the wave velocity. Percent increase in P-wave velocity with the addition of cement has been shown in Figure 4-6, taking the strength of untreated samples (0% cement) as the base line. From

this graph it can be seen that, addition on 2% cement in 100% RAP materials has increased the velocity only by 19% than that was found from untreated RAP materials. This indicates that 2% cement is too inadequate to create adhesion between the asphalt coated aggregates. In other cases, addition of 2% cement has increased the velocity significantly ranging from 63% to 97%. Addition of 4% cement has more significant effect on the increase of wave velocity. P-wave velocity increases within the range of 139% to 187% with the inclusion of 4% cement. With 6% cement, the increase in velocity is more significant. But the increases are not that high compared to the increases found by 4% cement indicating the proximity of optimum cement content.

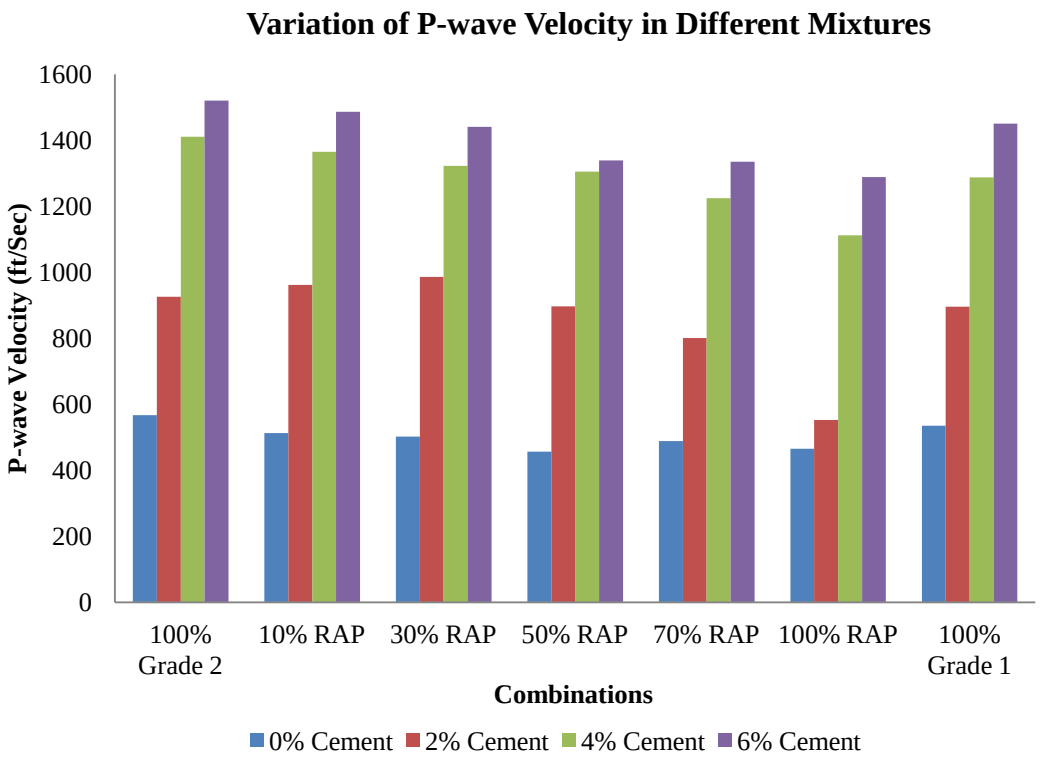

Figure 4-5 Variation of P-wave velocity in different aggregate blends

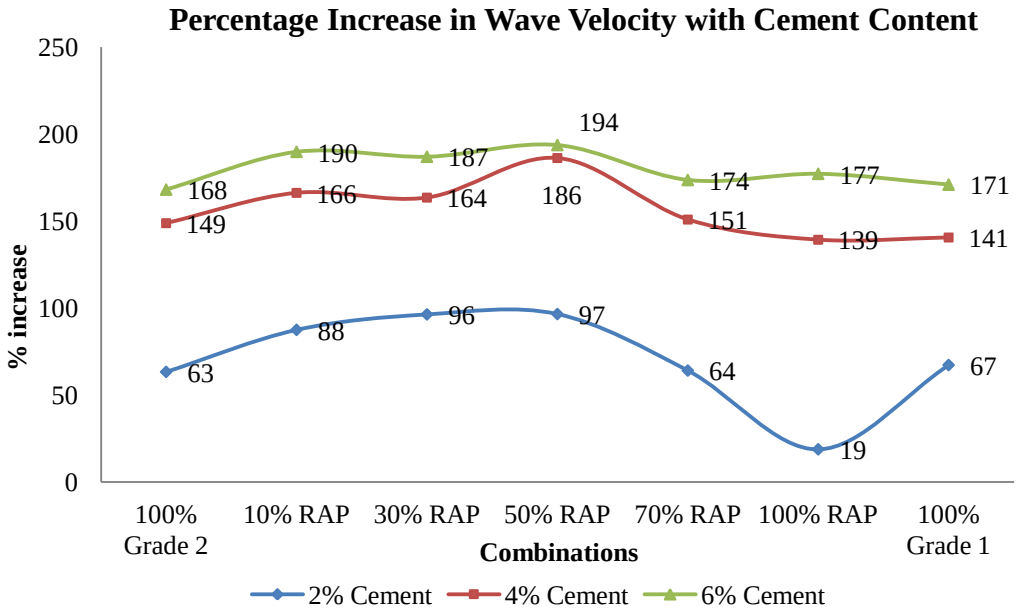

Figure 4-6 Percent increase of P-wave velocity with cement content from taking untreated mixtures as the base line

The influence of RAP content on P-wave velocity can easily be seen in Figure 4-7. For 0% cement, P-wave velocities found from different combinations are almost similar. This might have happened because of the identical values of poission's ratio found for Grade-1, RAP and Grade-2 materials as tabulated in Table 4-1. At 2% cement content, no mentionable trend was found yielding the maximum wave velocity for the mix containing 30% RAP materials. But the influence of RAP percentage on P-wave velocity can clearly be seen at 4% cement content. P-wave velocity decreases with the increasing percentage of RAP materials. At 6% cement content, no significant decrease in P-wave velocity was observed, if RAP materials are used up to 30% in the mix. This signifies the fact that, RAP can be used in pavement base construction without impairing the strength requirements by keeping RAP percentage within 30% of the mixture.

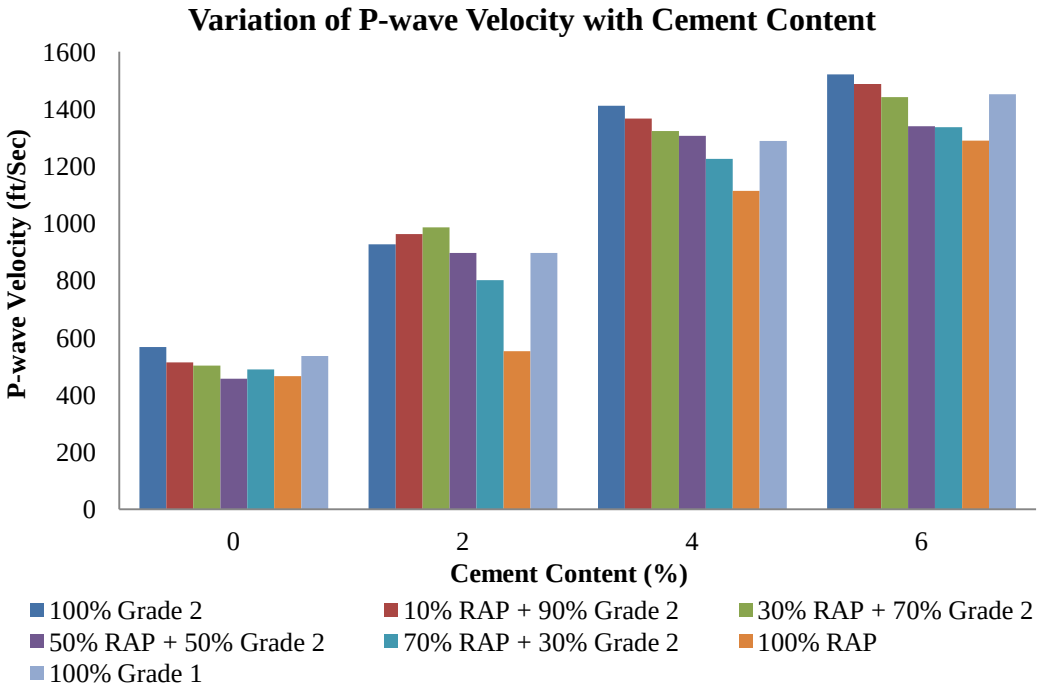

Figure 4-7 Variation of P-wave velocity with cement content

4.2.2.2 Dynamic Modulus of Elasticity Results

Modulus of elasticity from P-wave velocity has been calculated by using the correlation (Equation 4.1) given in British Standard (BS1881: Part 203). Figure 4-8 shows the variation of average dynamic modulus of elasticity for 7 different aggregate blends at 0% cement content. Moduli values decrease with the increase of RAP percentage yielding maximum dynamic modulus for mix M1 and minimum for mix M6. This trend remains same in every cement content which indicates that, RAP are relatively weaker materials than the Grade-2. Poor interlocking between the RAP aggregates might be the reason of lower stiffness. RAP aggregates are coated with asphalt which generates slip surface in the specimen and reduces the strength of transition zone. Grade-1 showed higher moduli values than all other mixes, except 100% Grade-2.

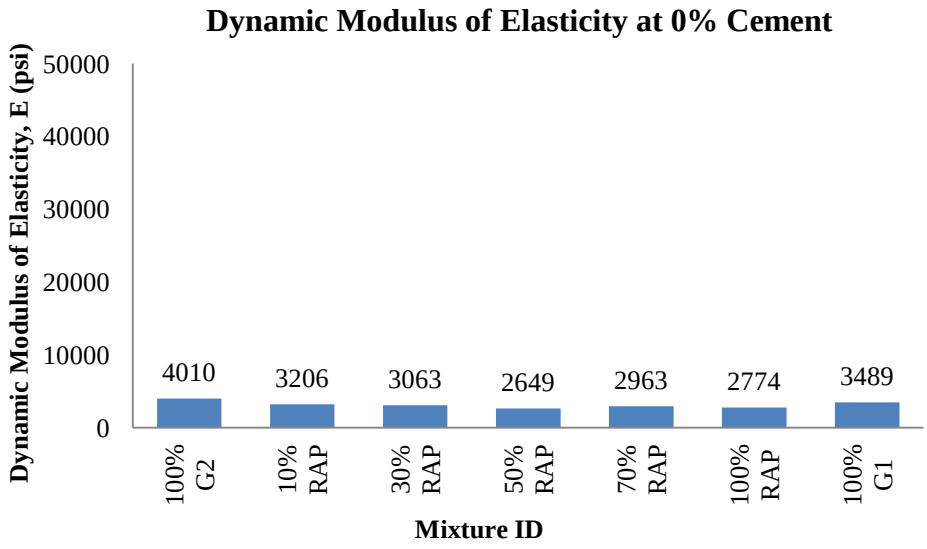

Figure 4-8 Dynamic Modulus of Elasticity at 0% Cement

Moduli values increase significantly with the addition of cement for every composition of aggregate blends. The addition of 2% cement increases modulus around 1.5 times than the modulus obtained at 0% cement content. But for 100% RAP, inclusion of 2% cement does not increase the modulus significantly as that was observed for other combinations. This indicates that, 2% cement is inadequate for 100% RAP materials to create proper adhesion between the asphalt coated aggregates. Addition of 4% and 6% cement are significant in terms of stiffness as the addition of 4% cement increases the modulus of elasticity around 6 to 9 times and the addition of 6% cement increases the modulus of elasticity around 8 to 12 times than that was found at 0% cement content. Variations of dynamic modulus of elasticity at three other cement contents are shown in Figure 4-9 and Figure 4-10.

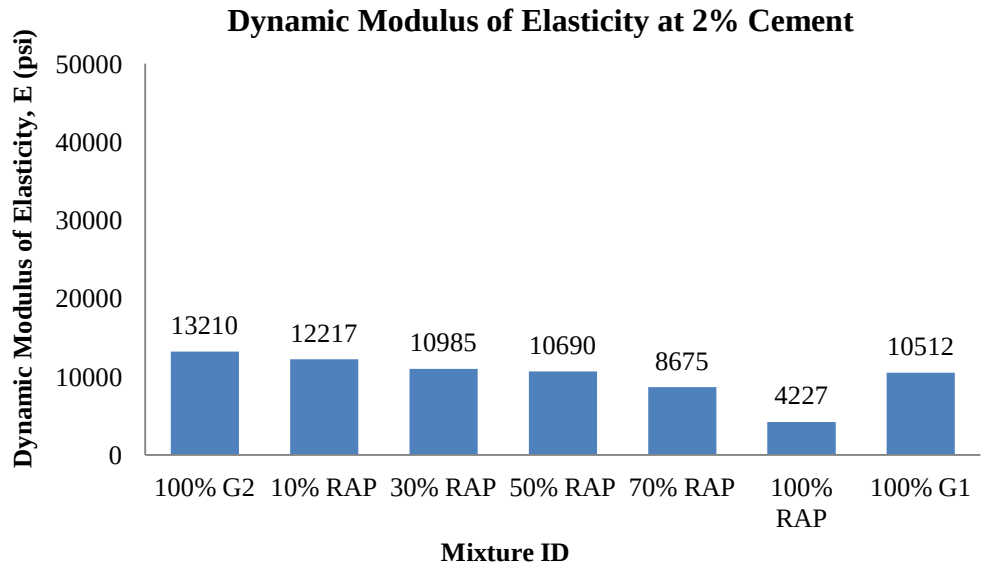

(a)

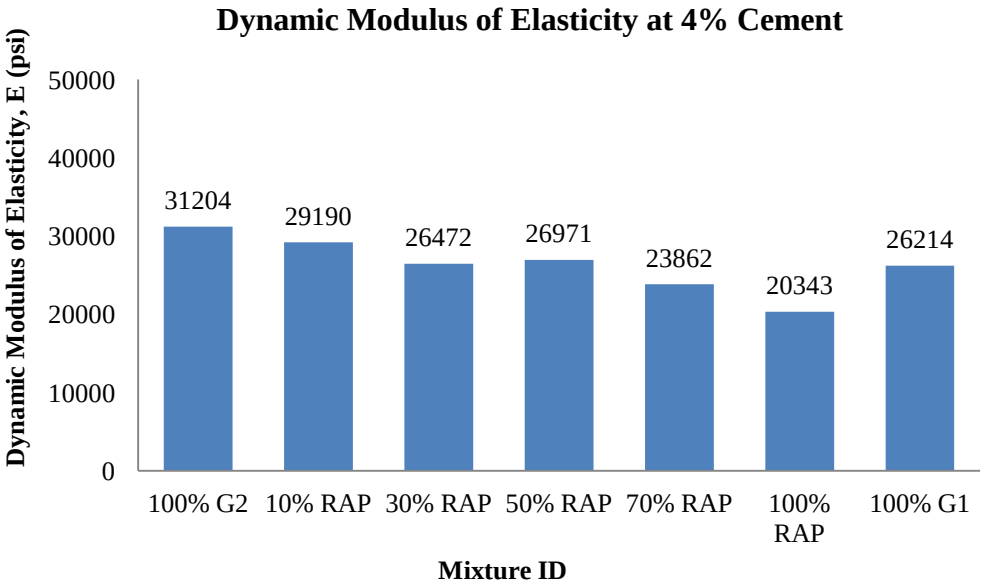

(b)

Figure 4-9 Dynamic Modulus at (a) 2% Cement (b) 4% Cement

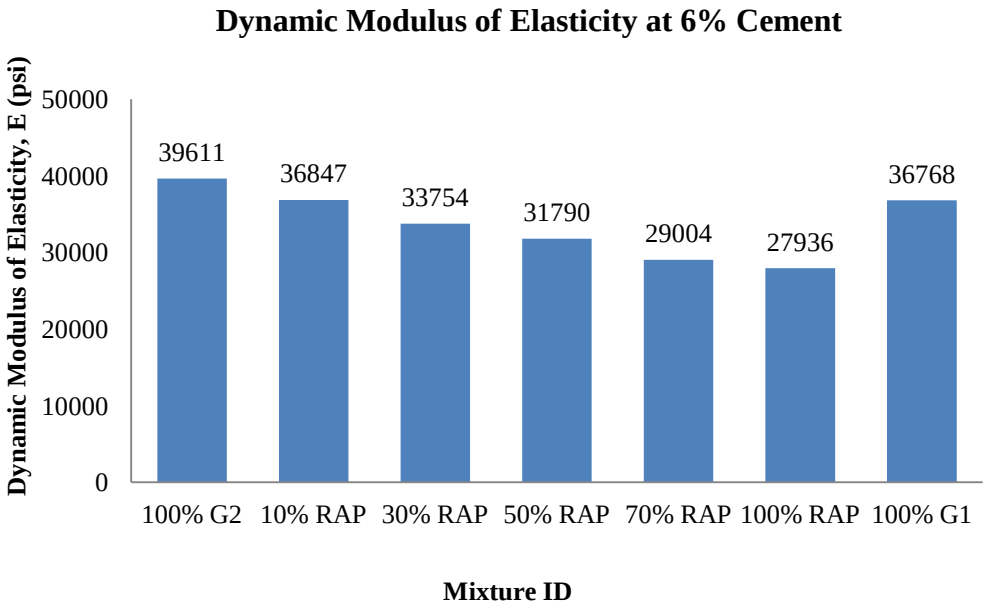

Figure 4-10 Dynamic Modulus at 6% Cement

Figure 4-11 shows the variation of dynamic modulus of elasticity with cement content for 7 different aggregate blends, focusing the fact that the dynamic modulus of elasticity increases significantly with the increase of cement content. No significant difference in modulus was observed at 4% cement content. Dynamic modulus remains within the range of 26000 to 31000 psi at 4% cement content for every mixture, except for mixture M1 (100% Grade 2) and M6 (100% RAP).

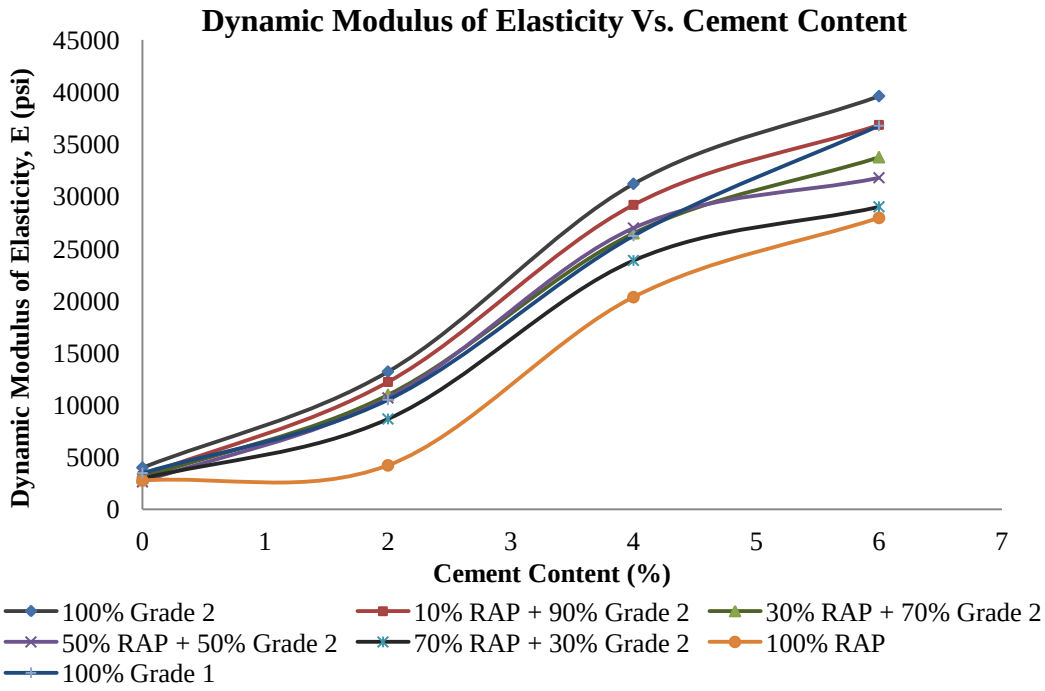

Figure 4-11 Variation of dynamic modulus of elasticity with cement content

4.3 Unconfined Compressive Strength (UCS) Test Results

Figure 4-8 shows the variation of unconfined compressive strength (UCS) with the cement content for different aggregate blends. The trend indicates that, compressive strength increases significantly with the increase of cement content for every mixture of RAP-Grade-2 aggregates. At a fixed cement content, compressive strength tends to decrease with the increase of RAP percentage. This trend can be more clearly observed in Figure 4-9 where compressive strength is expressed with the increasing ratio of Grade-2 and RAP for 4 different cement contents. Guidelines for construction of a pavement base course are specified by TxDOT under Item 276 “Cement Treatment (Plant Mixed)” in which minimum strength requirements are shown for class specified on the plans. For Class-L listed minimum 7 days unconfined compressive strength is 300 psi and for Class-M the minimum strength value is 175 psi. Figure 4-12 shows that strength requirement for

Class-L can never be achieved by cement treated RAP when cement is added up to 6%. Figure 4-13 also shows that, minimum UC strength requirements can easily be achieved by adding 6% cement to a mixture where minimum Grade-2-RAP ratio is 0.25. This signifies that, strength requirements will be satisfied for any combination of RAP and Grade-2 materials in which RAP can be used up to 80%, if 6% cement is added.

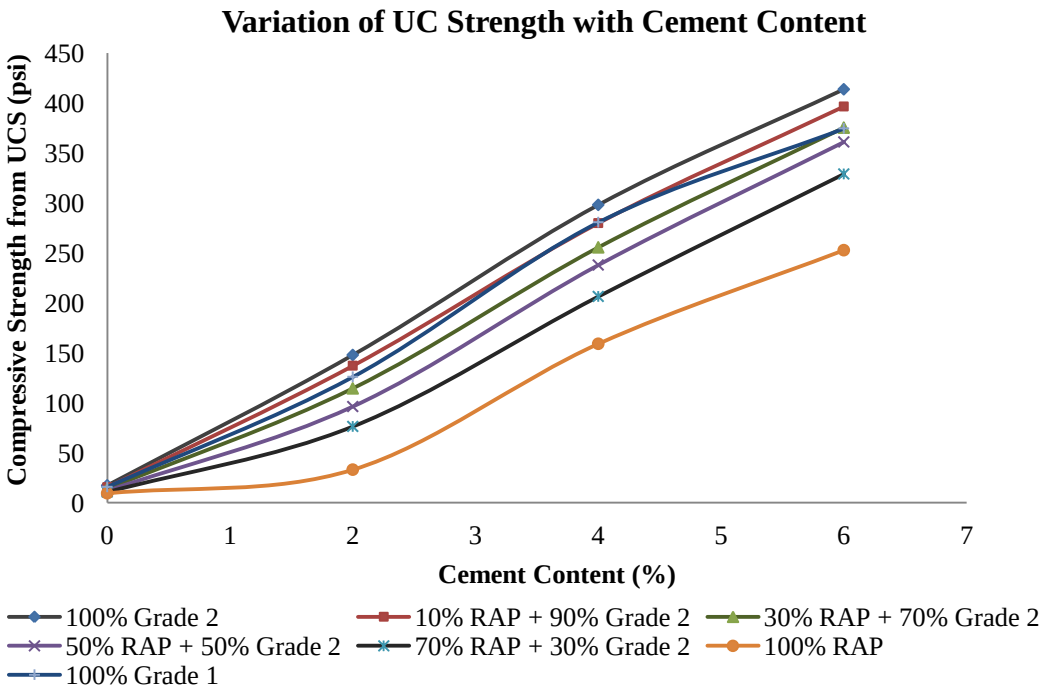

Figure 4-12 Variation of Unconfined Compressive Strength

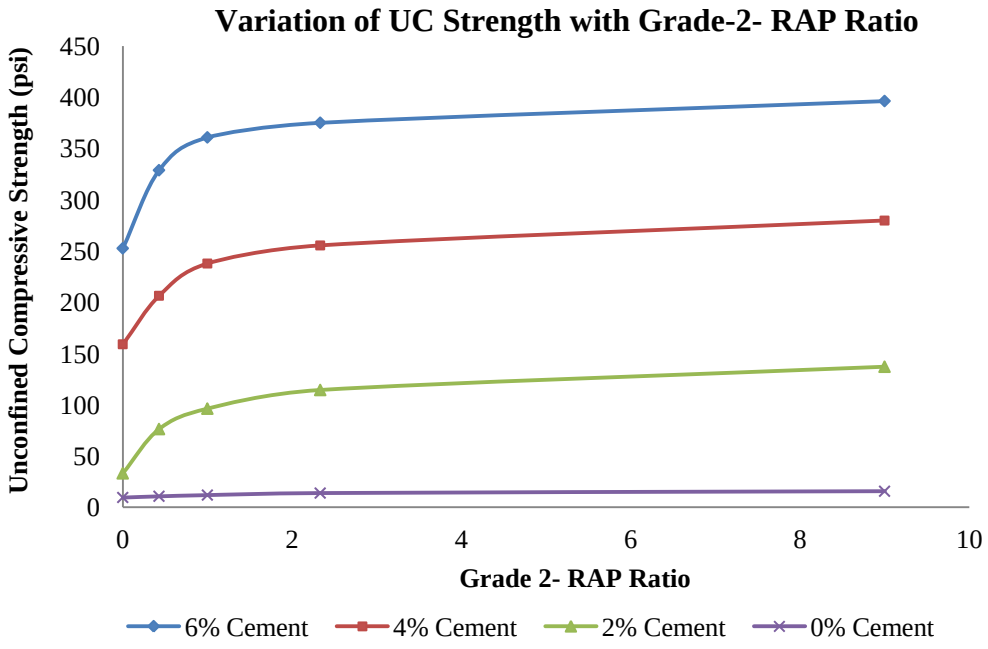

Figure 4-13 Variation of UC Strength with Grade-2- RAP Ratio

4.3.1 Tangent Modulus

The stress-strain relationships were used to investigate the elasticity of cement stabilized RAP-Grade-2 blends. A typical stress-strain curve from the unconfined compressive strength test is presented in Figure 4-14 which indicates the non-brittle response of RAP-Grade-2 aggregate mix. The modulus of elasticity was determined as the offset tangent modulus of the stress-strain curve. Figure 4-15 shows the variation of elastic modulus with different cement dosages and Figure 4-16 shows the influence of aggregate mix ratio on moduli response. Little variation of elastic modulus was observed for unbound mixes, whereas; inclusion of cement causes a dramatic increase of moduli values. Modulus of elasticity also tends to increase with the increasing ratio of Grade-2 and RAP. The trend is flatter at higher ratio and equals asymptotically to the moduli values of 100% Grade-2.

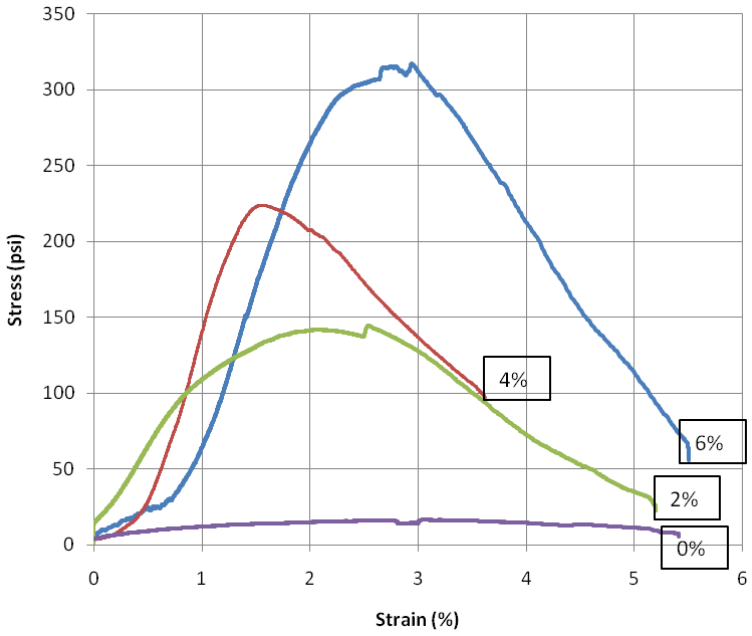

Figure 4-14 Typical stress-strain graph

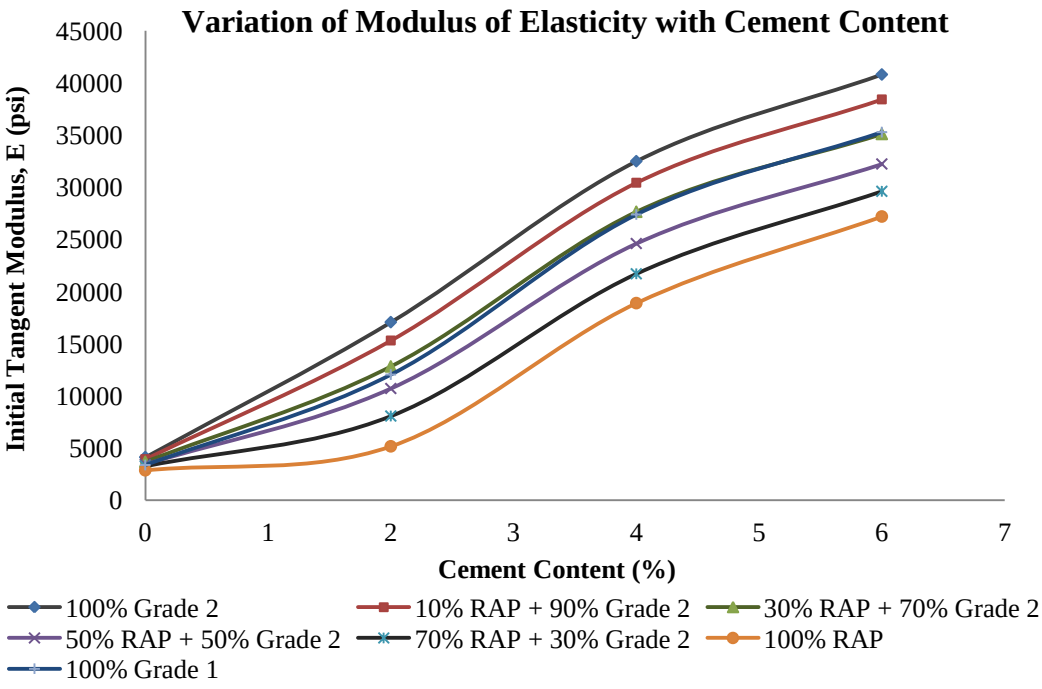

Figure 4-15 Variation of Modulus of Elasticity with Cement Content

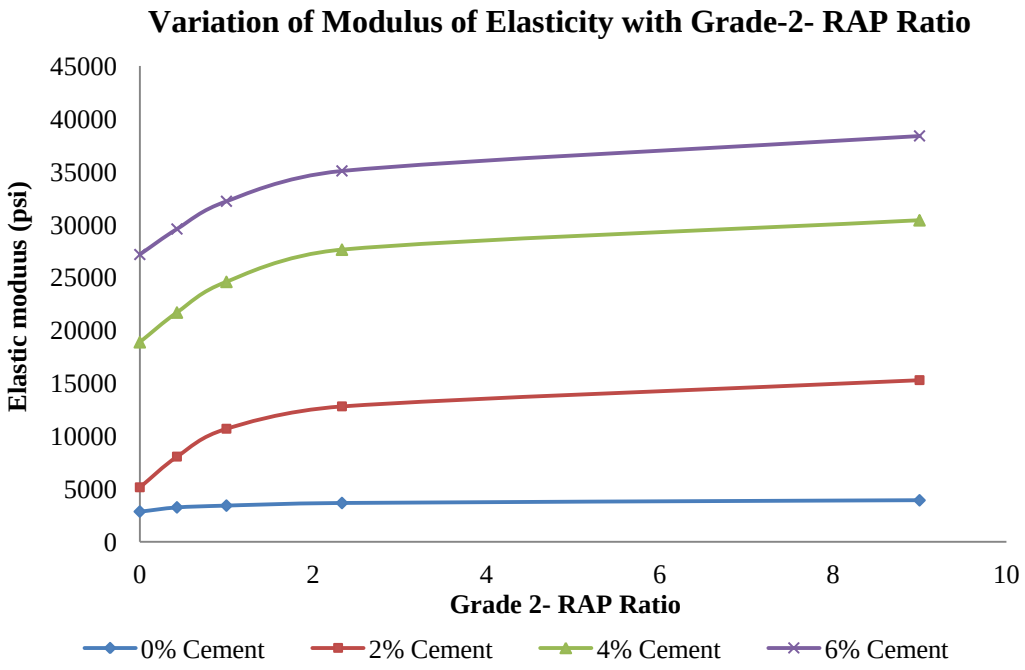

Figure 4-16 Variation of elastic modulus with Grade 2- RAP ratio

4.4 Resilient Modulus Test Results

For the resilient modulus test, samples were subjected to five different confining stresses each with three different deviator stresses to simulate the wheel load condition as presented in chapter 3. Three identical samples of each combination at a particular cement content were tested with similar conditions to check the repeatability. Figure 4-17 shows the resilient modulus response of Grade-2 materials at 0% cement contents. From the figure it is clear that both the confining and deviator stresses have noteworthy effects on resilient modulus response. Resilient Modulus increases with the increase in confinement as at higher confinements, samples tend to get denser and hence stronger. Resilient modulus also increases with the increase of deviator stress at a constant confining pressure because of stress hardening.

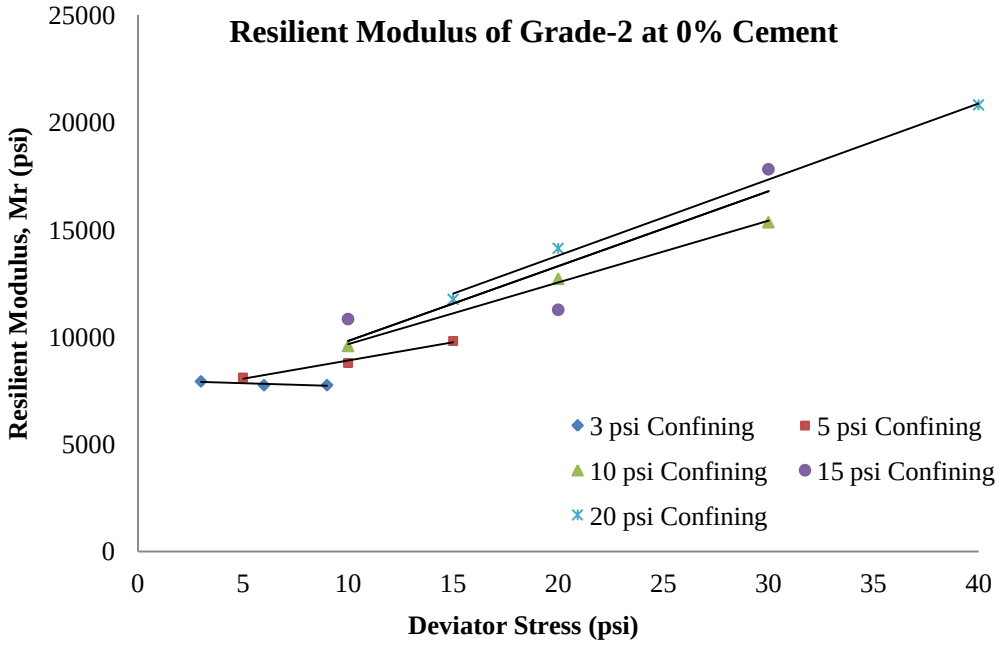

Figure 4-17 Resilient Modulus response of Grade-2 at 0% Cement

Resilient modulus response of Grade-2 materials treated with 6% cement is present by Figure 4-18. Resilient modulus followed the same trend with confining and deviator stresses as it did for the untreated condition except the fact that; M_R values were found higher for every confinement when treated with cement. The effect of confinement was less pronounced at higher cement contents as the samples were stiff enough to be influenced by confinements. All the resilient moduli values found from this experimental setup are tabulated in Appendix A.

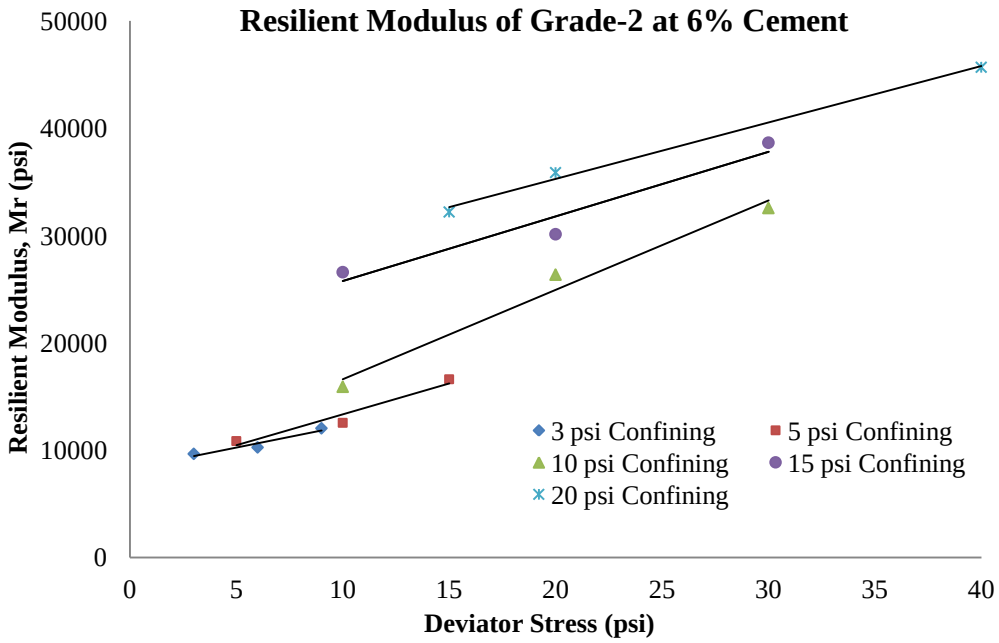

Figure 4-18 Resilient Modulus response of Grade-2 at 6% Cement

4.5 Comparison of Stress Wave Velocity & UCS Test Results

4.5.1 Qualitative Comparison

P-wave velocity found from stress wave velocity method and unconfined compressive strength from UCS testing both increase with the increasing amount of cement content. Minimum values of wave velocity and compressive strength were found for 0% cement content. At 0% cement content, no significant difference in P-wave velocities were observed. Difference in compressive strength was also not significant at 0% cement content. Maximum compressive strength was found when the samples were treated with 6% cement. Similarly, samples treated with 6% cement yielded the maximum wave velocity. Addition of cement increases the density of aggregate blends which eventually increases both the strength and wave velocity through the samples. RAP percentage in the aggregate blends also has similar type of influence on P-wave velocity and compressive

strength. P-wave velocity and compressive strength both decrease with the increasing amount of RAP content. Minimum strength and wave velocity were found for 100% RAP materials at every cement content indicating that RAP are the weakest materials. Also, the specific gravity of RAP materials is 1.90 (Table 3-1) that is the lowest of all three types of materials used in this study. The similar trends of P-wave velocity and compressive strength of all the aggregate blends at four different cement contents are illustrated in Figure 4-19.

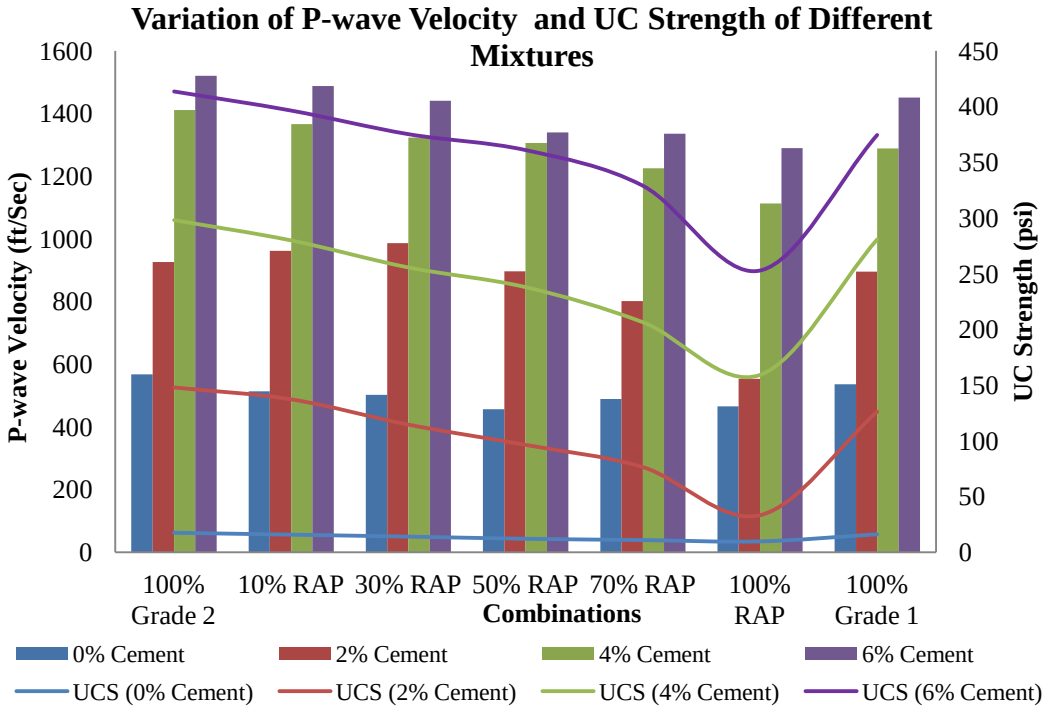

Figure 4-19 Variation of P-wave velocity and UC strength of different aggregate blends

Similar tends between P-wave velocity and modulus of elasticity were also found for all the aggregate blends which are presented by Figure 4-20. Modulus of elasticity and P-wave velocity both increase with the increasing amount of cement content but decrease with the increase of RAP percentage. Based on these analogies it is anticipated that,

strength and stiffness parameters could be predicted from the estimation of P-wave velocity, which led to the further analysis of these relationships.

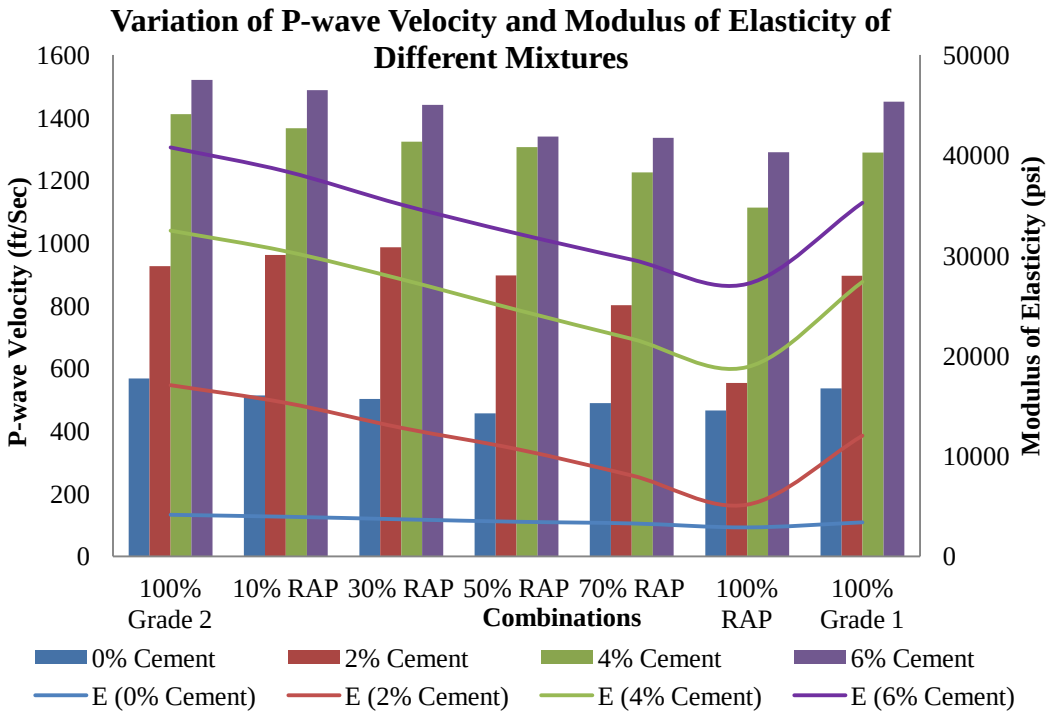

Figure 4-20 Variation of P-wave velocity and modulus of elasticity of different mixtures

4.5.2 Quantitative Comparison

Figure 4-21, 22, 23 and 24 show the comparison of modulus of elasticity found from P-wave velocity measurement and UCS testing for 7 different aggregate mixes at four different cement contents. At 4% and 6% cement contents, dynamic modulus of elasticity falls within 10% range of the modulus of elasticity determined by the UCS test. But at lower cement content such as 0% and 2% cement, the variation of modulus of elasticity was higher compared to the variation found at 4% and 6% cement content. This trend holds true for all 7 different combinations, but the deviations are still not that significant. Inadequate fines to fill the voids might be the reason of lower P-wave velocity at 0% and 2% cement content which eventually predicted lower values of elastic modulus.

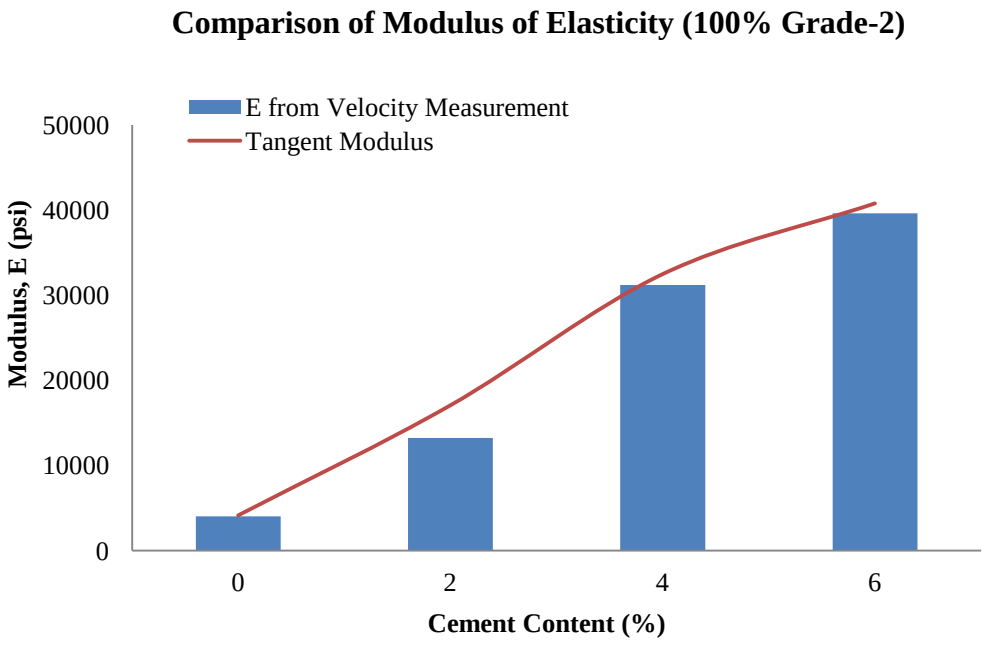

(a)

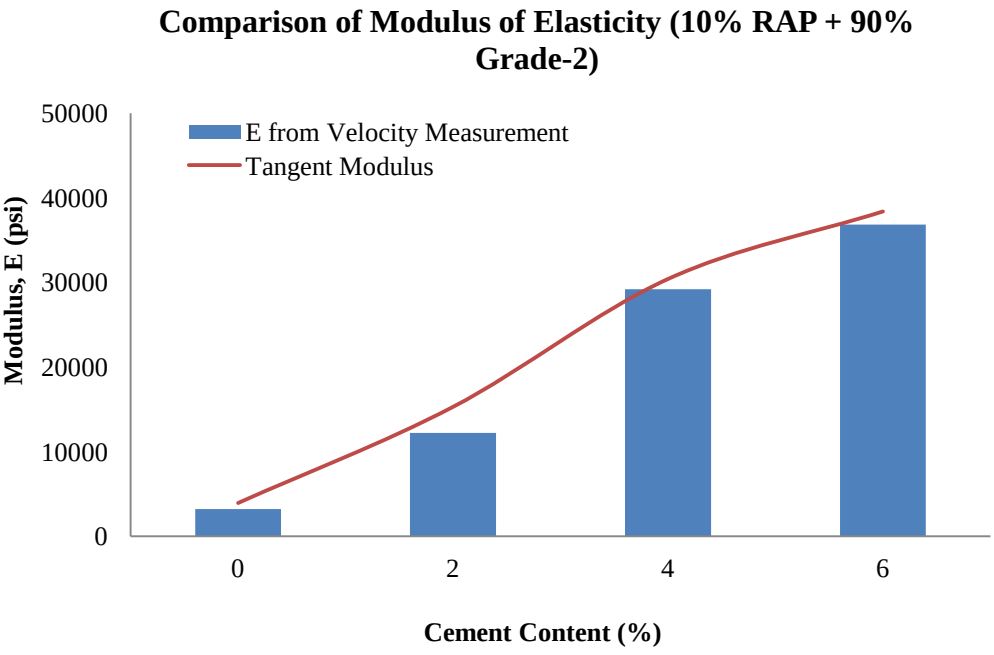

(b)

Figure 4-21 Comparison of Modulus of Elasticity (a) 100% Grade-2 (b) 10% RAP+ 90%

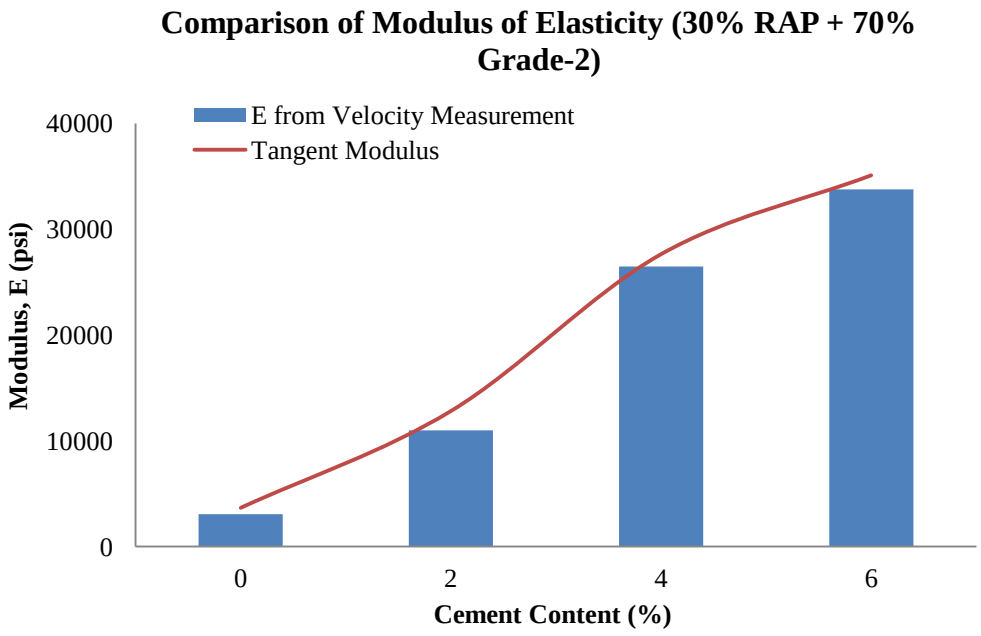

(a)

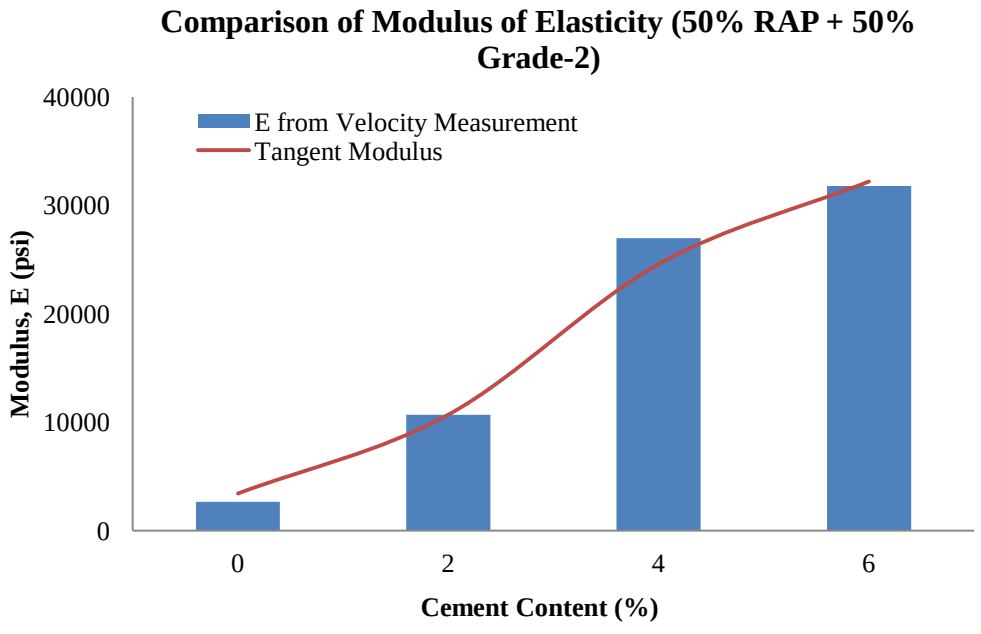

(b)

Figure 4-22 Comparison of Modulus of Elasticity (a) 30- 70 mix (b) 50-50 mix

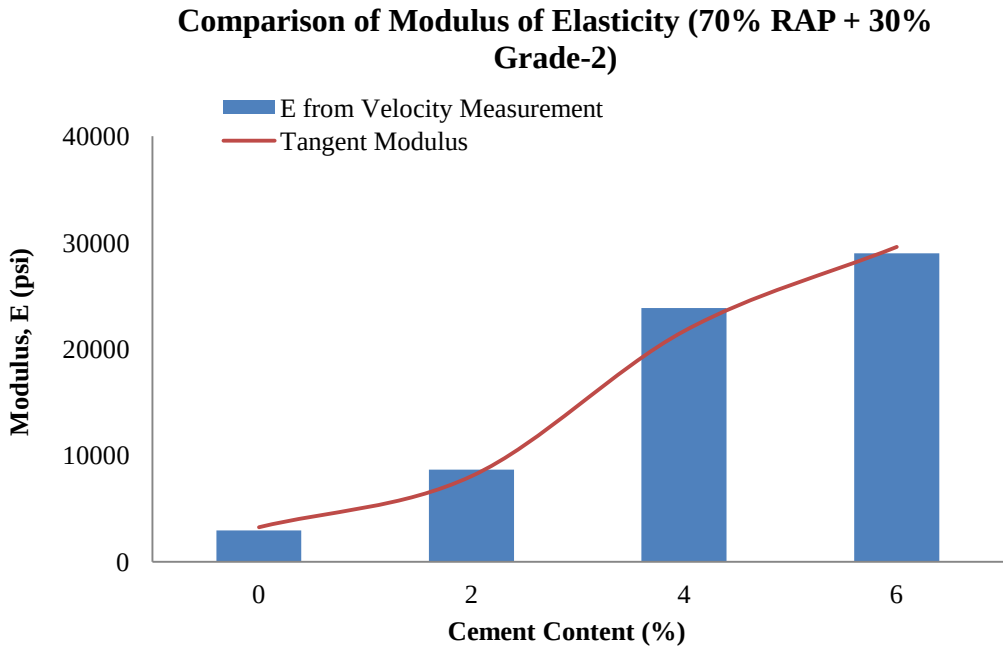

(a)

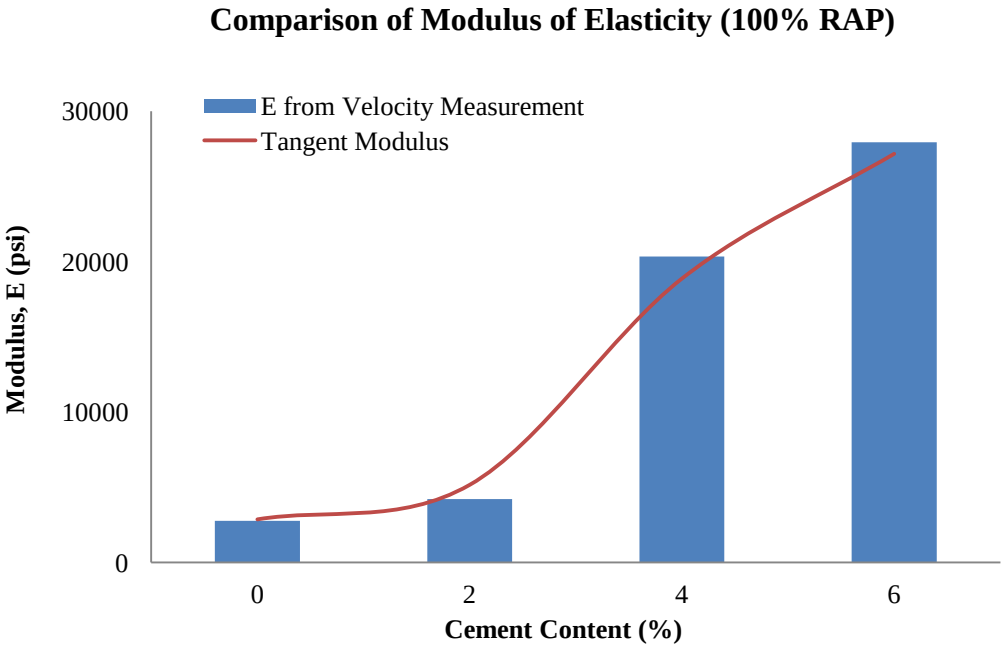

(b)

Figure 4-23 Comparison of Modulus of Elasticity (a) 70- 30 mix (b) 100% RAP

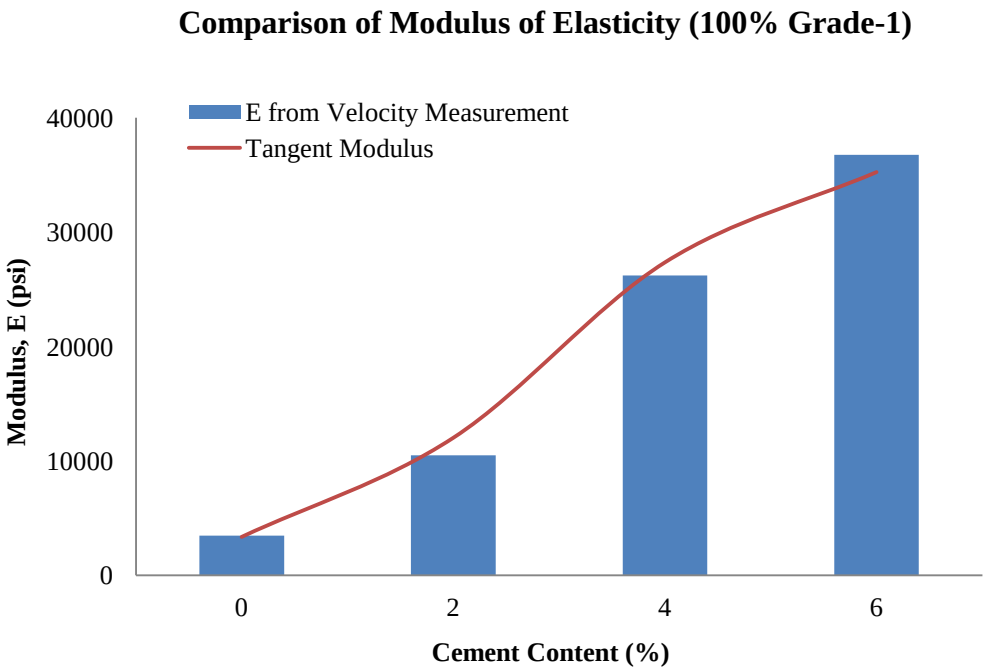

Figure 4-24 Comparison of Modulus of Elasticity 100% Grade-1

4.6 Analytical Modeling

4.6.1 Elastic Model

As the variations between dynamic modulus and the tangent modulus were insignificant, linear regression analysis between the P-wave velocity and the modulus of elasticity found from UCS test was performed using Minitab Student Version; regardless the amount of cement used to stabilize the mixes. Higher value of coefficient of determination (adjusted R^2= 95.6%) was associated with this linear regression analysis indicating that, data points are very closely distributed around the regression line. Figure 4-25 shows the best fit line of the linear regression along with 95% confidence and prediction intervals.

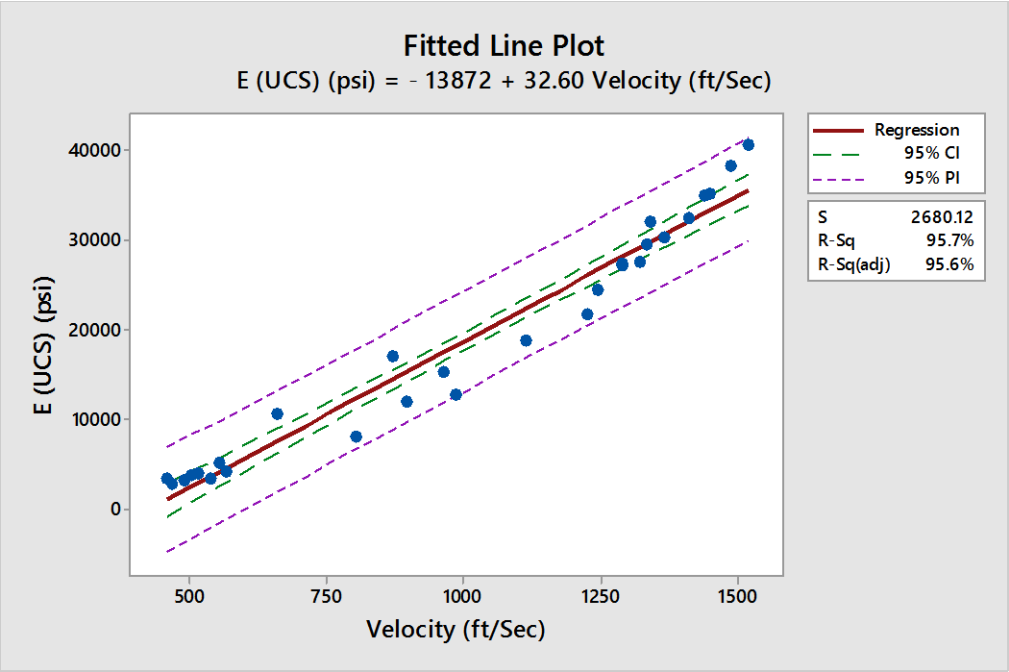

Figure 4-25 Linear regression between P-wave velocity and Modulus of Elasticity

But the residual plot of this regression as shown in Figure 4-26 indicates model inadequacy as a nonlinear trend can clearly be observed. Higher order terms such as quadratic and cube were added but still the trend keeps persisting which yielded the necessity for variable transformation.

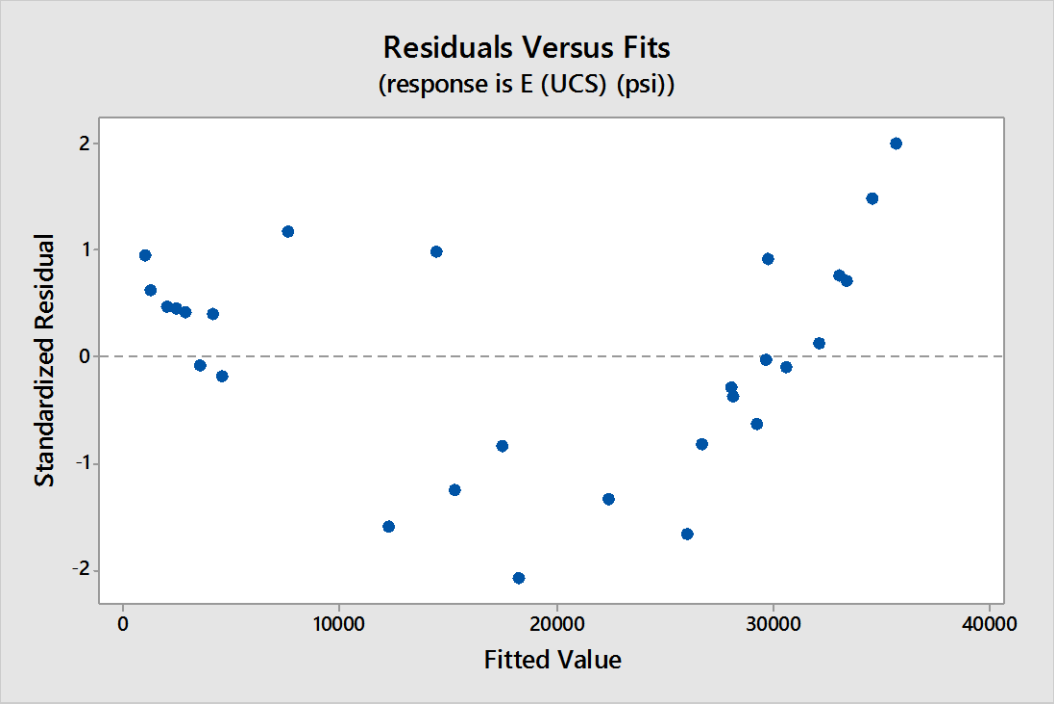

Figure 4-26 Residual plot of the linear regression between P-wave velocity and Modulus of Elasticity

Log-function was considered for the transformation of x and y axis. Good trend with symmetric distribution of residuals was observed when both the x and y axis were transformed. This indicates the inevitability of nonlinear power regression of these two parameters. Power regression is also supported by the initial empirical formula that was used for the estimation of dynamic modulus of elasticity from P-wave velocity. The theoretical form of the equation initially used can be expressed by the following equation:

$$E = a \times V^{b} \quad (4.2)$$

Where,

a, b = Regression Coefficients

After taking logarithmic function on both sides, the equation takes the following form:

$$\log(E) = \log(a) + b \log(V) \quad (4.3)$$

Based on this theoretical form, regression analysis was performed to find the trend of elastic modulus with P-wave velocity. Figure 4-27 shows the results of the regression modeling with very closer distribution of data points around the fitted line. Model outputs are also given in Table 4-2. Coefficient of determination of the regression increases to 98.6% and also the standard deviation decreases. Both the intercept and the variable coefficient of the model were found to be significant in terms of P-values. P-values were found to be very small that those were considered as zero in the regression output. This indicates the rejection of null hypothesis, suggesting that the coefficients are significant in terms of statistical judgments. Listed F-values in the ANOVA table for each coefficient were well above zero which also supports the reliability of these accepted coefficients.

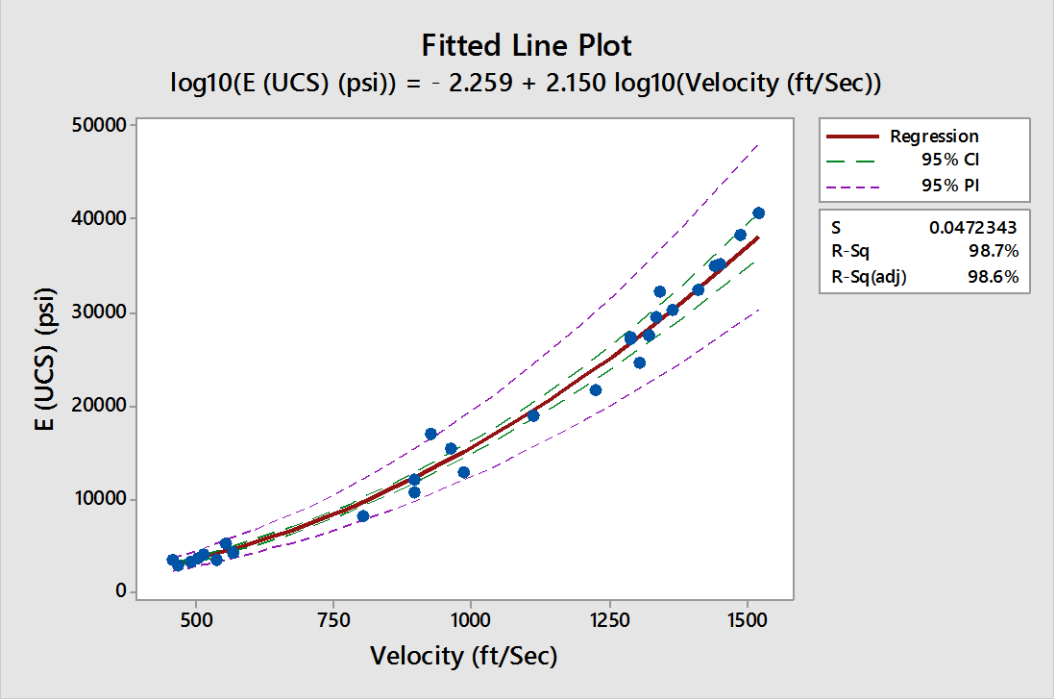

Figure 4-27 Non-linear regression between P-wave velocity and Modulus of Elasticity

Table 4-2 Model output of non-linear regression between P-wave velocity and Modulus of Elasticity

```
Regression Analysis: log10(E) versus log10(V)

Analysis of Variance

Source      DF   Adj SS   AdjMS   F-Value  P-Value
Regression   1  4.34456  4.34456  1947.30    0.000
log10(V)     1  4.34456  4.34456  1947.30    0.000
Error       26  0.05801  0.00223
Total       27  4.40257


Model Summary

        S    R-sq  R-sq(adj)  R-sq(pred)
0.0472343  98.68%     98.63%      98.48%


Coefficients

Term        Coef   SECoef  T-Value  P-Value   VIF
Constant  -2.259    0.145   -15.57    0.000
log10(V)  2.1499   0.0487    44.13    0.000  1.00


Regression Equation

log10(E) = -2.259 + 2.1499 log10(V)


Fits and Diagnostics for Unusual Observations

Std
Obs  log10(E)     Fit   Resid  Resid
  2    4.2319  4.1192  0.1127   2.43  R

R  Large residual
```

Standardized residuals as indicated in Figure 4-28, are also well distributed within ± 2 standard deviation around the mean, except only in 1 case. Normal probability plot follows the straight line pattern indicating the Gaussian distribution of data points around the mean which is also supported by the bell shaped histogram. Considering all these, the model seems satisfactory in terms of statistical definitions. So it is anticipated that the regression equation can be useful in estimating the stiffness response of cement treated

base materials. After converting to the theoretical format by transforming the logarithmic function, the regression equation for predicting elastic modulus can be represented by the following equation:

$$E = 10^{-2.259} V^{2.15} \quad (4.4)$$

Where,

E = Modulus of Elasticity measured in psi

V = P-wave velocity measurement in ft/sec

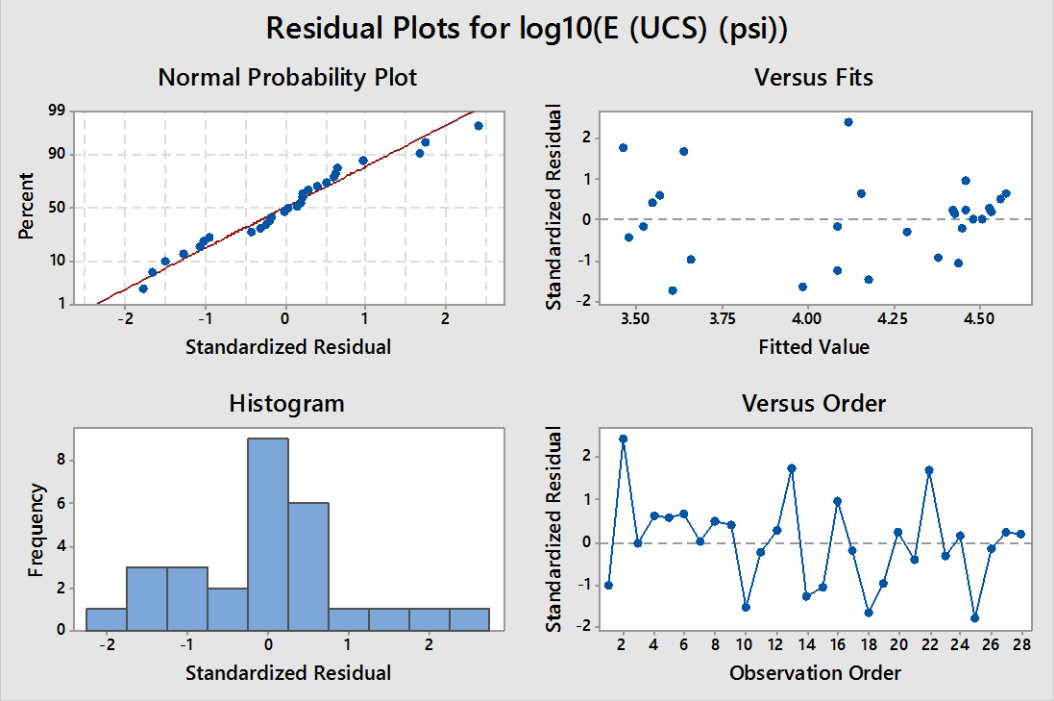

Figure 4-28 Normal probability plot, Residual plot, Histogram, Order plot of the non-linear regression between P-wave velocity and Modulus of Elasticity

4.6.2 Strength Model

Since; the elasticity was determined as the tangent of the stress-strain curve found from UCS test, it is anticipated that the relationship between the compressive strength and P-wave velocity will also be nonlinear, following the same theoretical model. Similar trend

has also been reported for concrete by Cho et al. 2011. So the theoretical correlation between the strength and P-wave velocity can be expressed by the following equation:

$$\text{UC Strength} = c \times V^{d} \quad (4.5)$$

Again; after applying logarithmic function on both sides the equation takes the following form:

$$\text{UC Strength} = \log(c) + d \log(V) \quad (4.6)$$

Where,

c, d = Regression Coefficients

Linear regression was then performed based on this transformed theoretical equation to find the trend of UC strength with P-wave velocity. Figure 4-29 shows the results of the regression modeling for different aggregate mixtures, regardless the amount of cement used. Model outputs are given in Table 4-3. Standardized residual plot, normal probability plot, histogram and the order plot are also given separately in Figure 4-30. Considering all of these it is concluded that, from statistical point of view the regression is valid and can be expressed by the following equation when transferred back in original theoretical form:

$$\text{UC Strength (psi)} = 10^{-7.061} \times V^{3.052} \quad (4.7)$$

Where,

UC Strength = Unconfined Compressive Strength in psi

V = P-wave velocity measurement in ft/sec

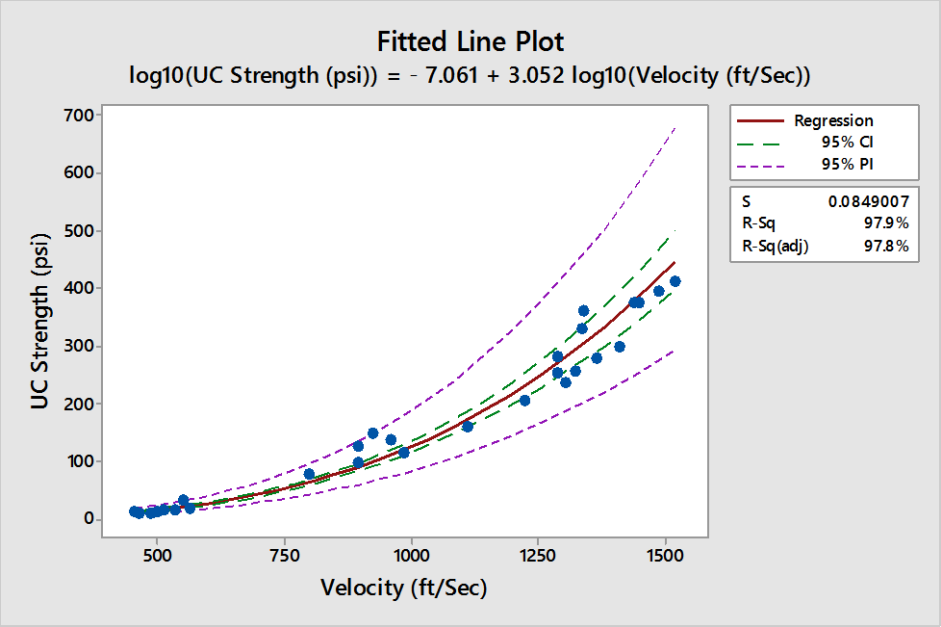

Figure 4-29 Non-linear regression between P-wave velocity and UC Strength

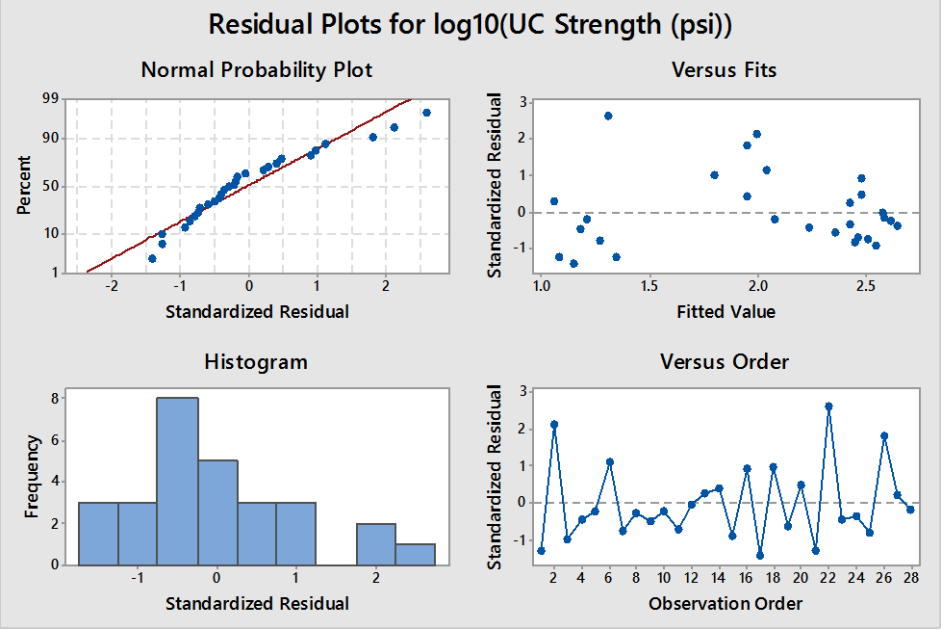

Figure 4-30 Normal probability plot, Residual plot, Histogram, Order plot of the non-linear regression between P-wave velocity and UC Strength

Table 4-3 Model output of non-linear regression between P-wave velocity and Unconfined Compressive Strength

```
Regression Analysis: log10(UCS) versus log10(V)

Analysis of Variance

Source      DF  Adj SS  Adj MS   F-Value    P-Value
Regression   1  8.7542  8.75416  1214.48    0.000
log10(V)     1  8.7542  8.75416  1214.48    0.000
Error       26  0.1874  0.00721
Total       27  8.9416


Model Summary

        S    R-sq   R-sq(adj)  R-sq(pred)
0.0849007  97.90%     97.82%      97.57%


Coefficients

Term        Coef  SECoef   T-Value  P-Value   VIF
Constant  -7.061   0.261   -27.08    0.000
log10(V)  3.0517  0.0876    34.85    0.000  1.00


Regression Equation

log10(UCS) = -7.061 + 3.0517 log10(V)


Fits and Diagnostics for Unusual Observations

                          Std
Obs   log10(UCS)   Fit   Resid   Resid
  2      2.1697  1.9931  0.1766   2.12  R
 22      1.5205  1.3086  0.2119   2.62  R

R  Large residual
```

4.6.3 Model Verification

4.6.3.1 Introduction

To verify the regression models, 2 different combinations of Grade-2 (from source-2) and RAP materials, designated as V1 and V2 were prepared at four different cement contents. Table 4-4 shows the details of these two combinations used for the verification

purpose. Samples were prepared according to the standard procedure as before and unconfined compressive strength tests were performed after 7 days of curing period. This time, the gradation curve for Grade-2 materials was a bit different as the materials were collected from another source. But still the materials can be classified as Grade-2 according to gradation specifications. Figure 4-31 shows the gradation curve of Grade-2 materials used for the model verification along with the gradation curves of the materials used for initial testing. Comparison of basic properties of Grade-2 materials collected from these two different sources is also shown in Table 4-5. From the table, no basic difference can be observed except the fact that, the coefficient of uniformity was lower for source-2 indicating higher uniformity of particle size. Other basic properties such as coefficient of curvature, moisture content and dry bulk specific gravity were almost same for both sources.

Table 4-4 Combinations used for model verification

Mix ID	Material Combination		OMC & MDD (0, 2, 4 & 6%) cement content	UCS Test at Different Cement Content			
	Grade-2 (%) Source-2	RAP (%)		0%	2%	4%	6%
V1[MR]	100	0		3	3	3	3
V2	70	30		-	3	3	3

Table 4-5 Comparison of basic properties used in this test study

	RAP	Grade 2	Grade 1	Grade 2 (Source 2)
Coefficient of Curvature	1.33	2.28	2.51	2.33
Coefficient of Uniformity	7.84	34.09	23.21	24.85
Moisture Content (%)	0.23	0.93	1.12	0.87
Dry Bulk Specific Gravity	1.90	1.92	1.88	1.91

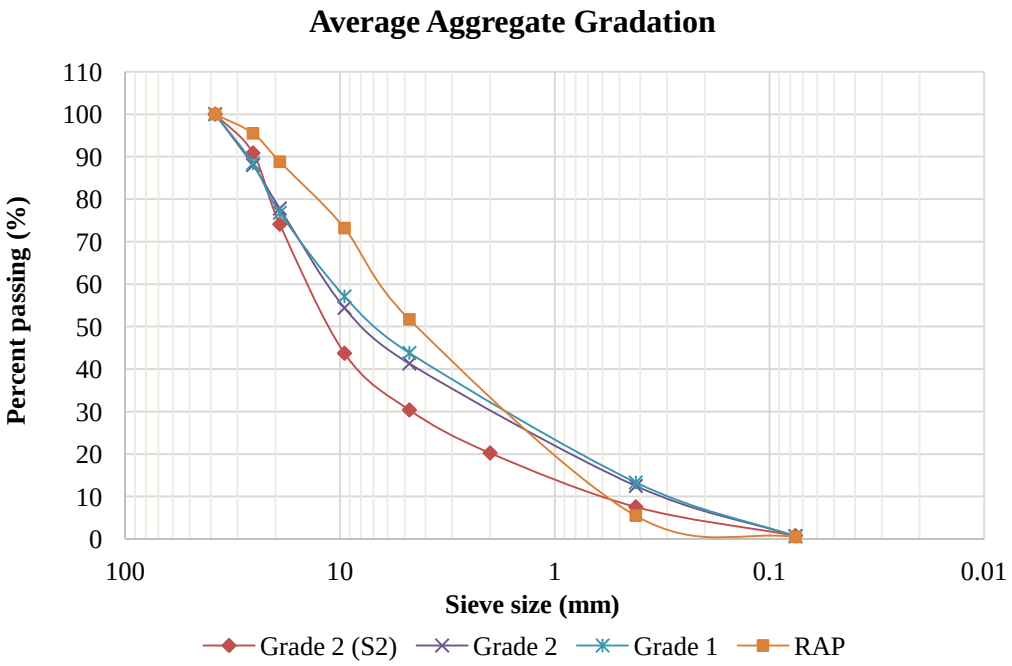

Figure 4-31 Gradation curve of Grade-2 (Source 1 and 2), Grade-1 and RAP

4.6.3.2 Elastic Model Verification

Figure 4-32 shows the comparison between the predicted and actual test values of modulus of elasticity at four different cement contents. Predicted values are within 9-13% range of the actual values for Mix- V1 (100% Grade-2). Higher variations are observed

for Mix- V2 (30% RAP + 70% Grade-2) which might have caused due to the presence of asphalt content. Table 4-6 shows the percent difference between the actual and predicted modulus of these two different combinations.

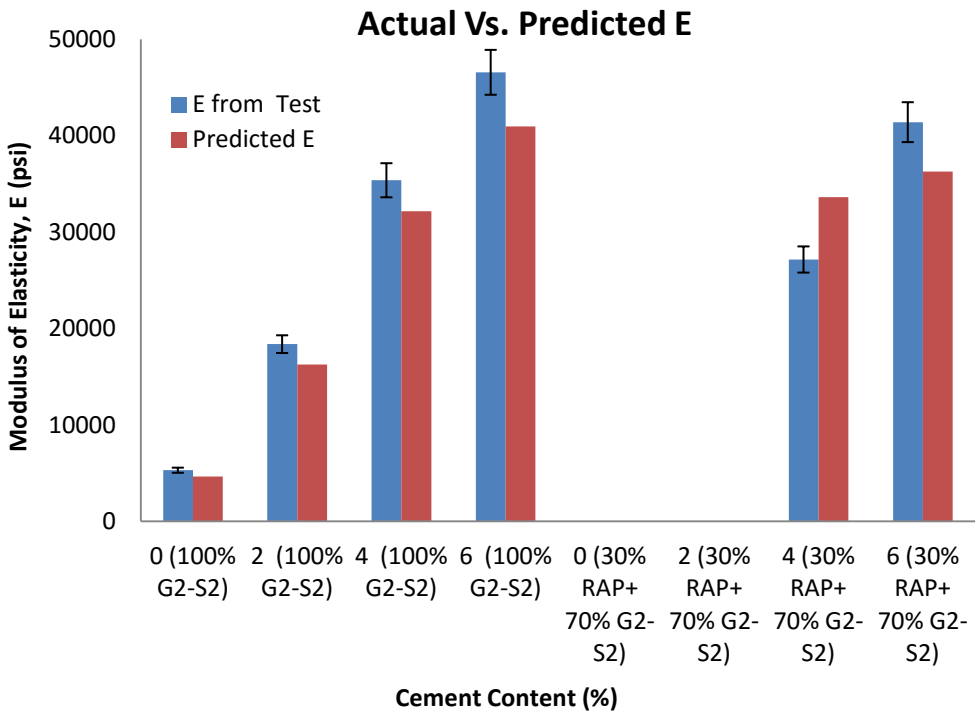

Figure 4-32 Comparison between predicted and actual Modulus of Elasticity

4.6.3.3 Strength Model Verification

Strength comparison between the actual and predicted values has been shown in Figure 4-33. Higher deviations from actual values are observed at 0% and 2% cement contents for both mixtures. But for the case of 4% and 6% cement contents, the deviations are insignificant as the predicted values are closer to the actual test values. Very high variation is observed at 4% cement content for Mix- V2 (30% RAP + 70% Grade-2) which might have occurred due to improper capping of the test specimens. Table 4-6 shows the percent difference between the actual and predicted strength of these two different combinations.

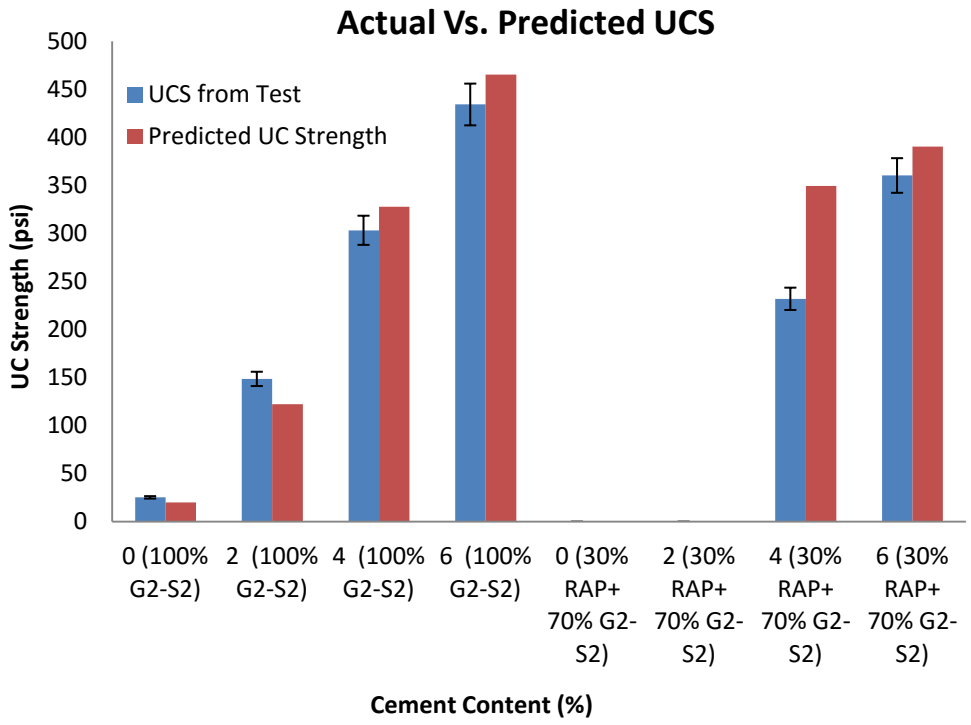

Figure 4-33 Comparison between predicted and actual UC Strength

Table 4-6 Percent variation of predicted and actual values

Cement Content	100% Grade-2 (Source 2)				30% RAP + 70% Grade-2 (Source 2)			
	0%	2%	4%	6%	0%	2%	4%	6%
% Difference in Strength	20.98	17.63	8.07	7.16	-		50.68	8.34
% Difference in Modulus	12.05	11.4	9.09	12.02	-		23.79	12.34

4.7 Stress Wave Velocity and Resilient Modulus Relationships

4.7.1 At A Fixed Confining and Deviator Stress

As a definite correlation was observed between the P-wave velocity and the modulus of elasticity, it is projected that there should also be some relationships between the resilient

modulus and the P-wave velocity. It was anticipated that the variation of resilient modulus with P-wave velocity follows the same theoretical relationship as it does on the elastic modulus model.

$$M_R = k_1 \times V^{k2} \quad (4.8)$$

Where,

M_R (psi) = Resilient Modulus in psi

V = P-wave velocity measurement in ft/sec

k_1, k_2 = Regression Coefficients

After applying logarithmic function in both sides the equation becomes:

$$\log (M_R) = \log(K_1) + K_2 \log(V) \quad (4.9)$$

Now the linear regression analysis of resilient modulus and P-wave velocity can be performed. But resilient modulus tests were performed for a series of pressure combinations, whereas; stress wave velocity tests were performed without applying any external pressure. For room temperature and ambient pressure conditions, bulk stress around a sample was calculated to be 55 psi, which provides a guideline of using a specific value of resilient modulus. For 10 psi confining stress and 30 psi deviator stress calculated bulk stress on the sample is 60 psi, which is close to the bulk atmospheric pressure at room temperature. Figure 4.34 shows the relationship between the resilient modulus at 10 psi confining and 30 psi deviator stresses and the P-wave velocity. Regardless the amount of cement was used, a weak correlation was found between the P-wave velocity and the resilient modulus response. This equation can be used for the initial approximation of resilient modulus at 10 psi confining and 30 psi deviator stress.

$$M_R \text{ (psi)} = 1135.012 \, V^{0.4767} \quad (4.10)$$

Where, V = P-wave velocity measurement in ft/sec

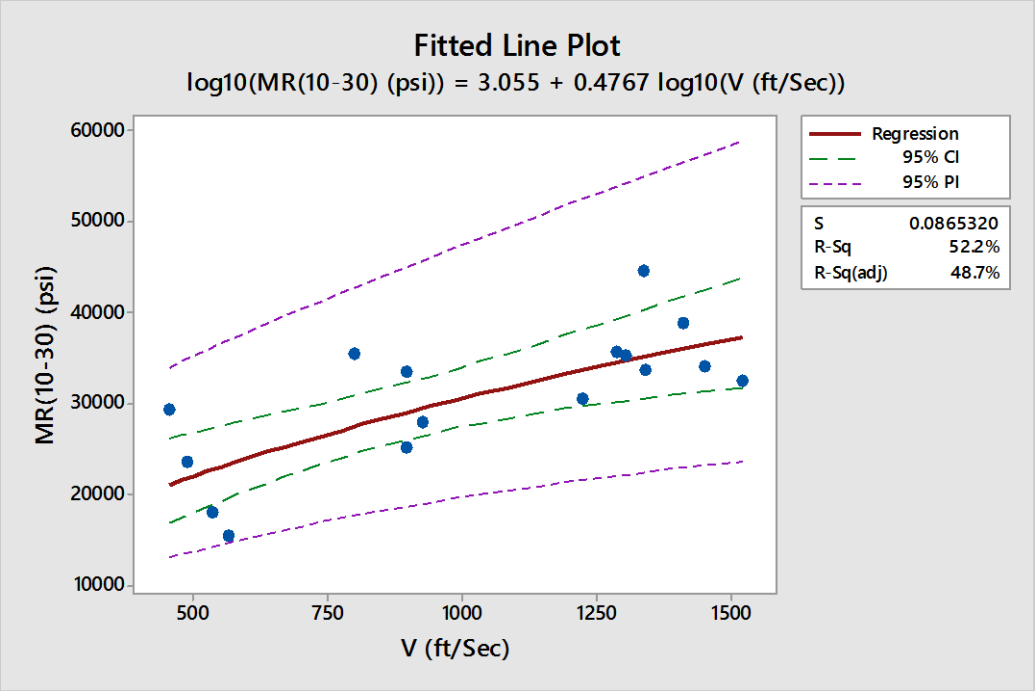

Figure 4-34 Non-linear regression between P-wave velocity and Resilient Modulus at 10 psi confining and 30 psi deviator stresses

4.7.1.1 Check for the Prediction Model

For the testing purpose of the prediction model, average M_R values at 10 psi confining stress and 30 psi deviator stress of Grade-2 materials from source-2 were used. Higher variations were found between the actual and predicted conditions, especially at lowest and highest cement contents. In other cases, predicted values were within 10% range of the actual test values as shown in Figure 4-35.

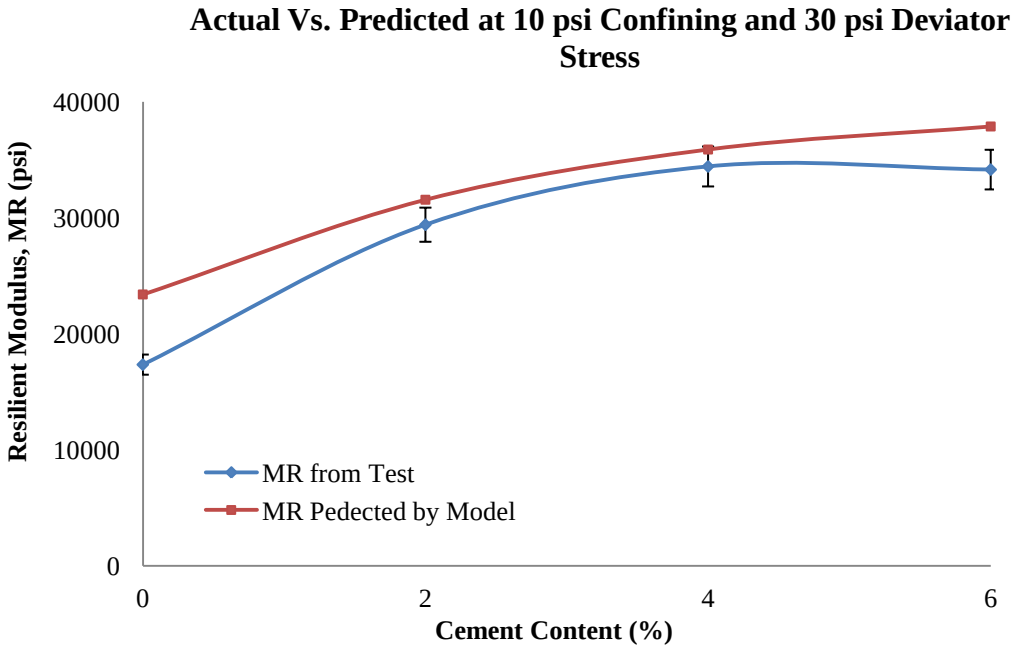

Figure 4-35 Comparison between predicted and actual Resilient Modulus at 10 psi confining and 30 psi deviator stresses

4.7.2 Bulk Stress Modeling

In M_R test, resilient modulus is determined at 5 different confining stresses each with 3 different deviator stresses. At different pressure sequences, to estimate the resilient modulus from P-wave velocity measurement, the bulk stress for each combination was calculated. Regression model based on bulk stress has been studied previously and can be represented by the following equation:

$$M_R = K_3 \times \theta^{K4} \quad (4.11)$$

Where, θ is the bulk stress

By combining Equation 4.8 and Equation 4.11, the expected theoretical model for resilient modulus prediction from P-wave velocity has taken the following form:

$$M_R = K_5 \times V^{k6} \times \theta^{k7} \quad (4.12)$$

Again, after applying the logarithmic function in both sides the equation becomes:

$$\log (M_R) = \log(K_5) + K_6 \log(V) + K_6 \log(\theta) \quad (4.13)$$

Based on this form, linear regression was conducted to find the trend of resilient modulus with P-wave velocity measurements. But the correlation as shown in Table 4-6 was weak with low value of coefficient of determination (adjusted R^2 = 57.12%). This laid the necessity to check the correlation at four different cement contents separately which is presented in Table 4-7 to Table 4-10.

Table 4-7 Regression analysis between P-wave velocity, Bulk Stress and Resilient Modulus regardless the amount of cement was used

```
Regression Analysis: log10MR(0-6%) versus log10(θ), log10(V)


Model Summary

       S    R-sq  R-sq(adj)  R-sq(pred)
0.139971  58.22%     57.87%      57.12%


Coefficients

Term         Coef  SECoef   T-Value  P-Value   VIF
Constant    4.060   0.168    24.15    0.000
log10(θ)   0.6202  0.0350    17.74    0.000  1.22
log10(V)  -0.2387  0.0596    -4.01    0.000  1.22


Regression Equation

log10MR(0-6%) = 4.060 + 0.6202 log10(θ) - 0.2387 log10(V)
```

Table 4-8 Regression analysis between P-wave velocity, Bulk Stress and Resilient Modulus at 0% cement content

```
Regression Analysis: log10MR(0%) versus log10(V), log10(θ)


Model Summary

        S    R-sq  R-sq(adj)  R-sq(pred)
0.0818624  85.31%     84.77%      83.63%


Coefficients

Term        Coef  SECoef  T-Value  P-Value   VIF
Constant  14.113   0.807    17.48    0.000
log10(θ)  0.4465  0.0384    11.63    0.000  1.00
log10(V)  -3.901   0.296   -13.16    0.000  1.00


Regression Equation

log10MR(0%) = 14.113 + 0.4465 log10(θ) - 3.901 log10(V)
```

Table 4-9 Regression analysis between P-wave velocity, Bulk Stress and Resilient Modulus at 2% cement content

```
Regression Analysis: log10MR(2%) versus log10(V), log10(θ)


Model Summary

        S    R-sq  R-sq(adj)  R-sq(pred)
0.0672684  86.22%     85.73%      84.08%


Coefficients

Term        Coef  SECoef  T-Value  P-Value   VIF
Constant    9.34    1.07     8.72    0.000
log10(V)  -1.983   0.363    -5.46    0.000  1.00
log10(θ)  0.5493  0.0304    18.08    0.000  1.00


Regression Equation

log10MR(2%) = 9.34 - 1.983 log10(V) + 0.5493 log10(θ)
```

Table 4-10 Regression analysis between P-wave velocity, Bulk Stress and Resilient Modulus at 4% cement content

```
Regression Analysis: log10MR(4%) versus log10(V), log10(θ)

Model Summary


       S    R-sq  R-sq(adj)  R-sq(pred)
0.154120  54.41%     52.75%      49.78%

Coefficients


Term        Coef   SECoef  T-Value  P-Value   VIF
Constant   -4.36     2.82    -1.54    0.128
log10(V)   2.488    0.904     2.75    0.008  1.00
log10(θ)  0.5471   0.0718     7.62    0.000  1.00

Regression Equation


log10MR(4%) = -4.36 + 2.488 log10(V) + 0.5471 log10(θ)
```

Table 4-11 Regression analysis between P-wave velocity, Bulk Stress and Resilient Modulus at 6% cement content

```
Regression Analysis: log10MR(6%) versus log10(V), log10(θ)

Model Summary


        S    R-sq  R-sq(adj)  R-sq(pred)
0.0826390  83.07%     82.47%      81.29%

Coefficients


Term        Coef   SECoef  T-Value  P-Value   VIF
Constant    6.57     1.41     4.66    0.000
log10(V)  -1.017    0.447    -2.27    0.027  1.00
log10(θ)  0.6185   0.0373    16.57    0.000  1.00

Regression Equation


log10MR(6%) = 6.57 - 1.017 log10(V) + 0.6185 log10(θ)
```

Good trends were observed in all cases except for 4% cement. Higher value of P-test and lower value of t-test indicates the rejection of regression constant at 4% cement. Hence another regression was performed by taking the regression constant as zero and is presented in Table 4-11.

Table 4-12 Revised regression analysis between P-wave velocity, Bulk Stress and Resilient Modulus at 4% cement content

```
Regression Analysis: log10MR (4%) versus log10(V), log10(θ)

Model Summary

       S    R-sq  R-sq(adj)  R-sq(pred)
0.169133  99.85%     99.84%      99.84%


Coefficients

Term        Coef  SECoef  T-Value  P-Value    VIF
log10(V)  1.0698   0.0398    26.89    0.000  32.23
log10(θ)  0.5782   0.0764     7.57    0.000  32.23


Regression Equation

log10(MR (psi)) = 1.0698 log10(V) + 0.5782 log10(θ)
```

After satisfying all the regression criteria, good trends were observed with better reliability. But still the equations are not satisfactory as the contribution of deviator stress and confining pressure in bulk stress cannot be identified separately. The regression equations between bulk stress, P-wave velocity and resilient modulus at four different cement contents can be presented by the following Equations:

At 0% cement content,

M_R (psi) = $10^{14.113}$ $V^{-3.901}$ $\theta^{.4465}$ (Adjusted R^2= 84.77%) (4.14)

At 2% cement content,

M_R (psi) = $10^{9.34}$ $V^{-1.983}\theta^{0.5493}$ (Adjusted R^2= 85.73%) (4.15)

At 4% cement content,

M_R (psi) = $V^{1.0698}\,\theta^{0.5782}$ (Adjusted R^2= 99.84%) (4.16)

At 6% cement content,

M_R (psi) = $10^{6.57}\,V^{-1.017}\,\theta^{0.6185}$ (Adjusted R^2= 82.47%) (4.17)

Where, θ = Bulk stress in psi

V = P-wave velocity in ft/Sec

4.7.2.1 Validation of the Prediction Model

As the statistical correlations between the resilient modulus, P-wave velocity and bulk stress were found to be quite satisfactory, it was intended to test the prediction models. Average resilient modulus values at 15 different bulk stresses found by the testing of cement treated Grade-2 materials from Source-2 were used again. Deviation of the predicted values from the actual test results were found to be higher, especially at higher bulk stresses as shown in Figure 4-36, 37. This indicates the necessity of multiple regression with another new independent variable such as confining stress or deviator stress that addresses the contribution of confinement and deviatoric pressure in bulk stress.

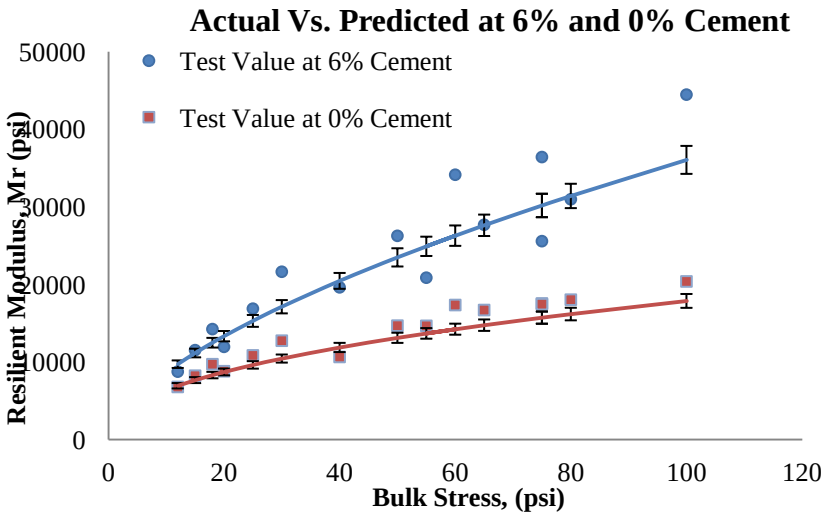

Figure 4-36 Comparison between predicted and actual Resilient Modulus by bulk stress modeling at 0% and 6% cement

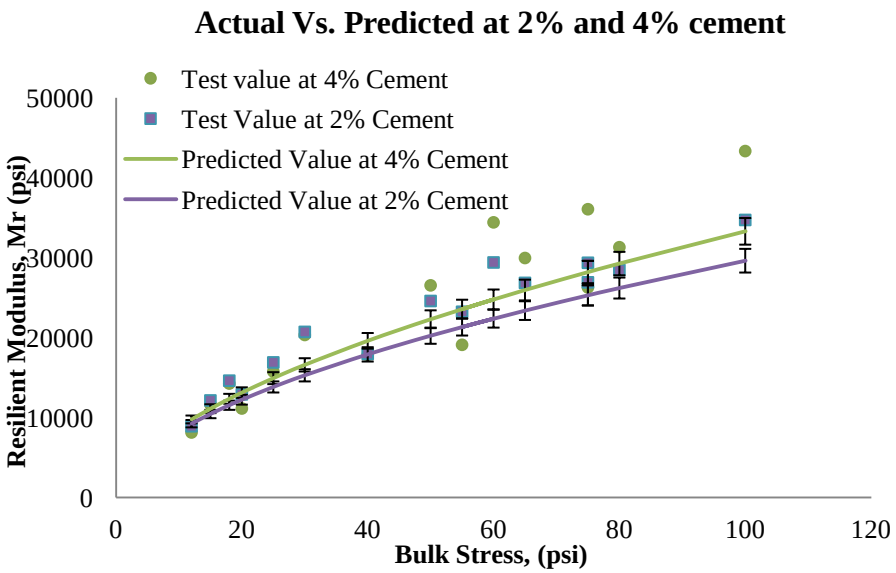

Figure 4-37 Comparison between predicted and actual Resilient Modulus by bulk stress modeling at 2% and 4% cement content

4.7.3 Four Parameter Modeling

In conducting four parameter regression modeling, the first challenge that rised is the selection of third variable that has the most significant effect on resilient modulus response. Initially, other options such as confining stress, deviator stress and bulk stress were considered in the modeling process. Previously available models such as deviatoric stress model and bulk stress model were followed for the theoretical modeling of the intended regression. Puppala et al. 1997 provided three parameter model based on both confining and deviatoric stress that is presented by the following equation:

$$(M_R/\sigma_{atm})=K_8 \times (\sigma_c/\sigma_{atm})^{K9} \times (\sigma_d/\sigma_{atm})^{K10} \quad (4.18)$$

Where, σ_c is the confining stress

σ_d is the deviatoric stress and

σ_{atm} is the atmospheric pressure

Both models as shown by Equation 4.12 and Equation 4.18 are based on the stress conditions. So it is concluded that, if another modeling is done considering all these parameters, it will also take the same theoretical form. Thus, by combining Equation 4.12 and Equation 4.18, initial theoretical model for multiple regression analysis was derived and is presented by the following equation:

$$M_R = K_{11} \times V^{K12} \times \sigma_c^{K13} \times \sigma_d^{K14} \times \theta^{K15} \quad (4.19)$$

After taking the logarithmic function in both sides the equation becomes:

$$\log (M_R) = \log(k_{11}) + k_{12} \log(V) + k_{13} \log(\sigma_c) + k_{14} \log(\sigma_d) + k_{15} \log(\theta) \quad (4.20)$$

Based on this theoretical form, best subsets regression was conducted taking these four parameters as the independent variable to compare between all the possible models. Table 4-12 shows the outcome of the best subsets regression analysis for 6% cement content. Among these possible 14 different models, from the table it is clear that 4 models as marked yellow have the highest possible value of coefficient of determination (R^2) and lowest value of standard deviation (S). The PRESS values for all these 4 possible models are same and the standard deviations do not vary that much. The mallows C_p for model 1 and 2 is less than the number of model coefficient (model coefficient = K+1 = 4) but for model 3, mallows C_p is higher than the model coefficient. For model 4, mallows C_p becomes equal to model coefficient indicating the acceptance of the model. But the acceptance of the parameters cannot be decided based on mallows C_p only, as other three models also seemed quite promising in terms of coefficient of determination (R^2), standard deviation (S) and mallows C_p. So it was decided that further analysis is needed in this regard.

Further analysis for model selection was based on Akaike Information Criterion (AIC). AIC for all the four possible models were calculated and is presented in Table 4-13. Minimum AIC value was associated with model 1 indicating the acceptance of this mode.

Moreover, model 1 yielded minimum standard deviation (S) and maximum coefficient of determination (R^2). So it can be concluded that, the most significant model for 6% cement content will be the one that considers deviator stress, bulk stress and P-wave velocity as the independent variable.

Table 4-13 Best subsets regression analysis for 6% cement

Best Subsets Regression: log10(MR6% (psi)) versus log10(σc), log10(σd), ...

Response is log10(MR6% (psi))

Vars	R-Sq	R-Sq (adj)	PRESS	R-Sq (pred)	Mallows Cp	S	log10(σc)	log10(σd)	log10(V)	log10(θ)	
1	85.2	84.9	0.4	84.1	27.3	0.076712		X			
1	81.5	81.2	0.5	80.3	47.6	0.085558				X	
1	66.4	65.8	0.8	64.2	132.4	0.11538	X				
1	1.5	0.0	2.4	0.0	496.4	0.19755			X		
2	88.7	88.3	0.3	87.4	9.6	0.067637		X		X	
2	88.6	88.2	0.3	87.3	9.8	0.067729	X	X			
2	88.4	88.0	0.3	87.0	10.9	0.068304	X			X	
2	86.7	86.2	0.3	85.0	20.7	0.073270		X	X		
2	83.1	82.5	0.4	81.3	41.0	0.082639			X	X	
3	90.2	89.7	0.3	88.6	3.0	0.063450		X	X	X	(1)
3	90.2	89.6	0.3	88.6	3.2	0.063550	X	X	X		(2)
3	90.0	89.4	0.3	88.3	4.3	0.064173	X		X	X	(3)
3	88.7	88.1	0.3	86.9	11.6	0.068230	X	X	X		
4	90.2	89.5	0.3	88.2	5.0	0.064016	X	X	X	X	(4)

Table 4-14 Akaike Information Criterion (AIC) for possible models

Model ID	Independent Variables	AIC Value
1	V,σ_d, θ	-327.0400862
2	V, σ_c, σ_d	-326.8514277
3	V, σ_c, θ	-325.6797104
4	V, σ_c, σ_d, θ	-325.0560564

The modeling outputs for 6% cement have been shown in Table 4-14. Adjusted coefficient of determination increases significantly to 95.44% and also the standard deviation decreases due to data filtering, which was done by the identification of the outliers from the normal probability curve. All the three variables considered in the modeling were found to be significant in terms of P-values. P-values were found to be very small that those were considered as zero in the regression output indicating the rejection of the null hypothesis. Listed F-values in the ANOVA table for each coefficient were also well above zero. Residuals as indicated in Figure 4-38 are also well distributed within ±2 standard deviation of the mean, except only in one case. Considering all these, the model seemed satisfactory in terms of statistical definitions.

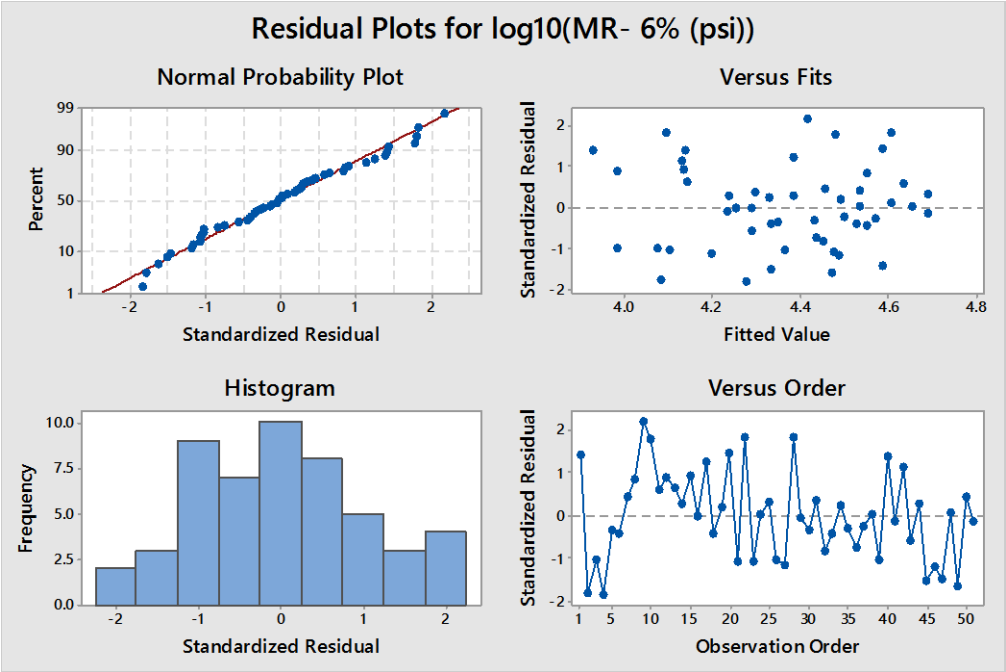

Figure 4-38 Normal probability plot, Residual plot, Histogram, Order plot of the regression analysis between P-wave velocity, Deviator pressure, Bulk stress and Resilient Modulus at 6% cement

Table 4-15 Model output of the regression analysis between P-wave velocity, Deviator pressure, Bulk stress and Resilient Modulus at 6% cement

```
Regression Analysis: log10(MR-6% (psi)) versus log10(σd), log10(V),
log10(θ)


Stepwise Selection of Terms

α to enter = 0.05, α to remove = 0.05


Analysis of Variance

Source       DF   Adj SS    AdjMS  F-Value  P-Value
Regression    3  1.99451  0.664838   349.72    0.000
log10(σd)     1  0.19568  0.195678   102.93    0.000
log10(V)      1  0.02947  0.029472    15.50    0.000
log10(θ)      1  0.04334  0.043336    22.80    0.000
Error        47  0.08935  0.001901
Total        50  2.08386


Model Summary

        S    R-sq  R-sq(adj)  R-sq(pred)
0.0436009  95.71%     95.44%      94.85%


Coefficients

Term         Coef  SECoef  T-Value  P-Value   VIF
Constant    6.772   0.825     8.21    0.000
log10(σd)  0.4450  0.0439    10.15    0.000  4.95
log10(V)   -1.037   0.263    -3.94    0.000  1.01
log10(θ)   0.2247  0.0471     4.77    0.000  4.98


Regression Equation

log10(MR (psi)) = 6.772 + 0.4450 log10(σd) - 1.037 log10(V)
+ 0.2247 log10(θ)


Fits and Diagnostics for Unusual Observations

log10(MR                    Std
Obs    (psi))     Fit   ResidResid
  9    4.5078  4.4182  0.0896   2.19  R

R  Large residual
```

After converting to the theoretical format by removing the logarithmic function, the regression equation for predicting resilient modulus at 6% cement content can be represented by the following equation:

M_R at 6% (psi) = $10^{6.772} \sigma_d^{0.445} V^{-1.037} \theta^{0.2247}$ (Adjusted R^2= 95.44%) (4.21)

Similarly, regression analysis for other three cement content has been done and is presented in following Table 4-15, Table 4-16 and Table 4-17. Regression equations are also presented by Equation 4.22, 4.23 and 4.24.

Table 4-16 Model output of the regression analysis between P-wave velocity, Deviator pressure, Bulk stress and Resilient Modulus at 4% cement

```
Regression Analysis: log10(MR-4% (psi)) versus log10(σd), log10(V),
log10(θ)


Model Summary

       S    R-sq   R-sq(adj)  R-sq(pred)
0.108964  78.93%     77.71%      75.91%


Coefficients

Term          Coef   SECoef  T-Value  P-Value   VIF
Constant    -4.91     2.00    -2.46    0.017
log10(σd)   0.750    0.103     7.29    0.000  3.84
log10(V)    2.699    0.641     4.21    0.000  1.00
log10(θ)   -0.056    0.106    -0.52    0.030  3.84


Regression Equation

log10(MR (psi)) = -4.91 + 0.750 log10(σd) + 2.699 log10(V) -
 0.056 log10(θ)
```

Table 4-17 Model output of the regression analysis at 2% cement

```
Regression Analysis: log10(MR-2% (psi)) versus log10(σd), log10(V),
log10(θ)


Model Summary

        S    R-sq  R-sq(adj)  R-sq(pred)
0.0451998  92.89%     92.47%      91.33%


Coefficients

Term         Coef   SECoef  T-Value  P-Value   VIF
Constant    7.561    0.818     9.24    0.000
log10(σd)  0.2193   0.0428     5.12    0.000  4.37
log10(V)   -1.353    0.278    -4.87    0.000  1.02
log10(θ)   0.3411   0.0444     7.68    0.000  4.33


Regression Equation

log10(MR (psi)) = 7.561 + 0.2193 log10(σd) - 1.353 log10(V)
+ 0.3411 log10(θ)
```

Table 4-18 Model output of the regression analysis at 0% cement

```
Regression Analysis: log10(MR-0% (psi)) versus log10(σc), log10(θ),
log10(V)


Model Summary

        S    R-sq  R-sq(adj)  R-sq(pred)
0.0741857  87.96%     87.26%      85.92%


Coefficients

Term         Coef   SECoef  T-Value  P-Value    VIF
Constant   13.779    0.743    18.54    0.000
log10(θ)    0.845    0.148     5.71    0.000  17.37
log10(σc)  -0.381    0.137    -2.78    0.008  17.37
log10(V)   -3.884    0.270   -14.39    0.000   1.00


Regression Equation

log10(MR-0% (psi)) = 13.779 + 0.845 log10(θ) - 0.381 log10(σc) -
 3.884 log10(V)
```

It was found that, at 0% cement content confining stress plays the significant role but at higher cement contents the effect of deviator stress is more pronounced. This indicates that at higher cement content the specimens are stiff and strong enough to be influenced by confining stress. This is why the regression equation for 0% cement content included the confining stress as an independent variable thought; in other cases deviator stress was included.

At 0% cement content,

M_R (psi) = $10^{13.779} \sigma_c^{-0.381} V^{-3.884} \theta^{0.845}$ (Adjusted R^2= 87.26%) (4.22)

At 2% cement content,

M_R (psi) = $10^{7.561} \sigma_d^{0.2193} V^{-1.353} \theta^{0.3411}$ (Adjusted R^2= 92.47%) (4.23)

At 4% cement content,

M_R (psi) = $10^{-4.91} \sigma_d^{0.75} V^{2.699} \theta^{-0.056}$ (Adjusted R^2= 77.71%) (4.24)

Where, θ= Bulk stress in psi

V= P- wave velocity in ft/sec

σ_c= Confining pressure in psi

σ_d= Deviator pressure in psi

4.7.3.1 Validation of the Prediction Model

It was intended to test the prediction models as the correlations between the resilient modulus, P-wave velocity, bulk stress and confining/ deviator stress were found to be quite satisfactory. Average resilient modulus at 5 different confining stresses each with three different deviator stresses found from the testing of Grade-2 materials from Source 2 treated with 6% cement were used. In almost all cases, predicted values were within 5% range of the actual test values as shown in Figure 4-39. Relatively higher variations were observed at higher confinement associated with higher deviator stress, but still the variations are within the range of 6- 7% of actual conditions.

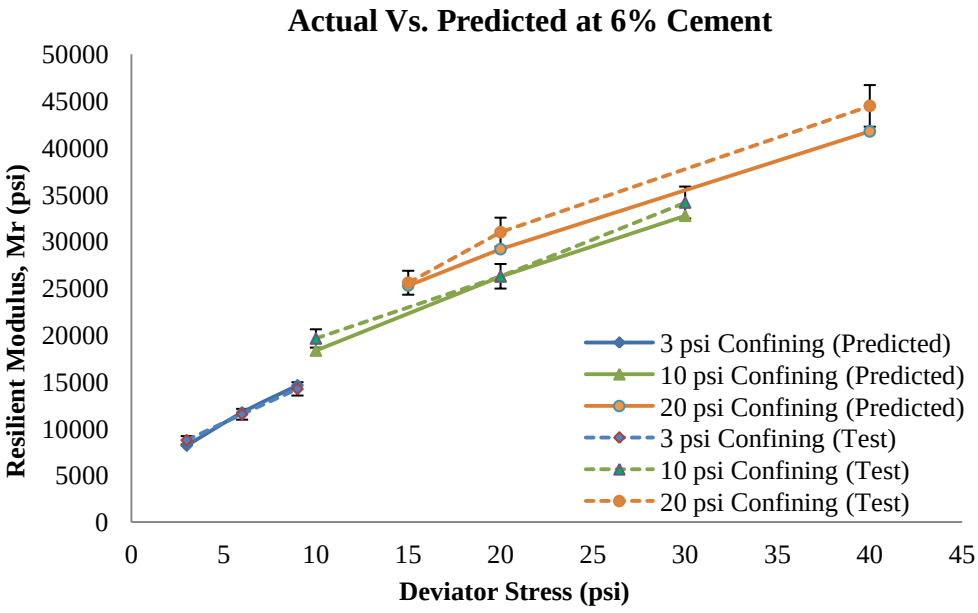

(a)

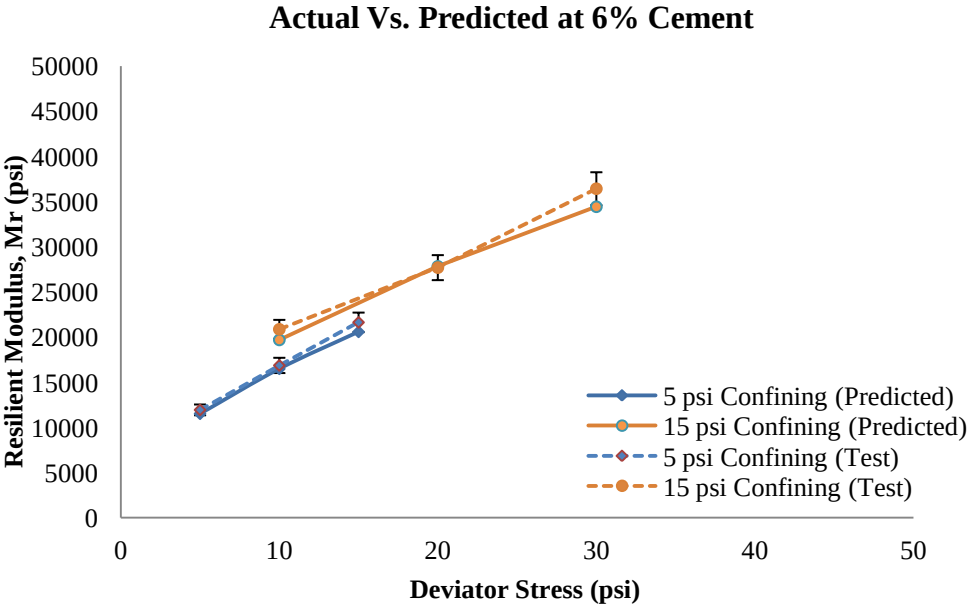

(b)

Figure 4-39 Comparison between predicted and actual Resilient Modulus at 6% cement content (a) 3, 10 and 20 psi (b) 5 and 15 psi confining pressure

At 4% cement content, higher variations were observed between actual test values and predicted values as the correlation was not that strong. Variations are significant, especially at lower confinements with higher deviator stresses and also at higher confinements with lower deviator stresses. In almost all these cases predicted values were within 7 to 18% range of the actual test values as shown in Figure 4-40 and Figure 4-41.

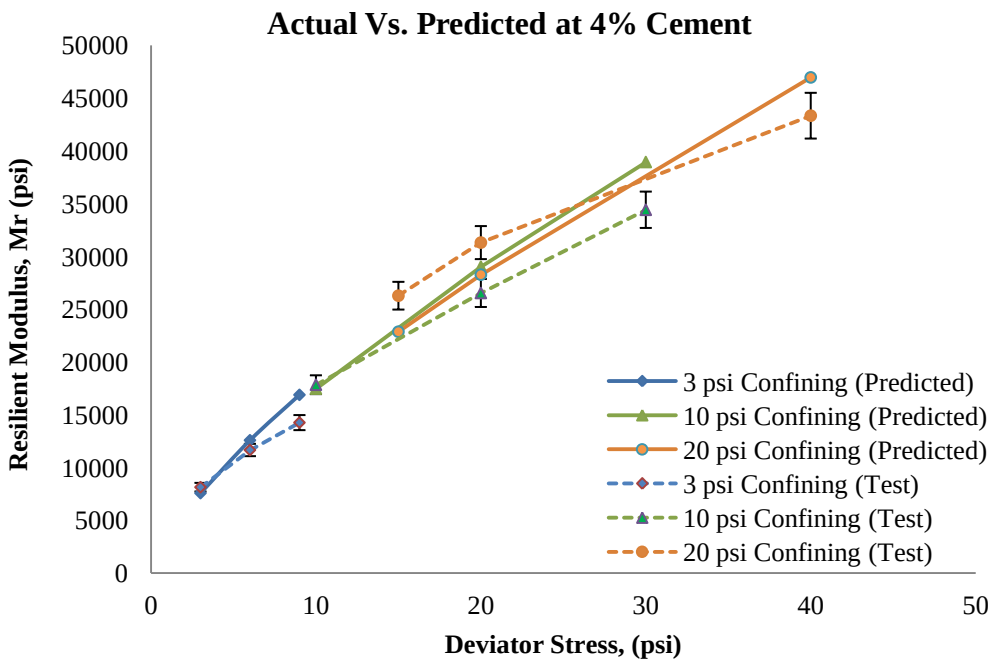

Figure 4-40 Comparison between predicted and actual Resilient Modulus at 4% cement content at 3, 10 and 20 psi confining pressure

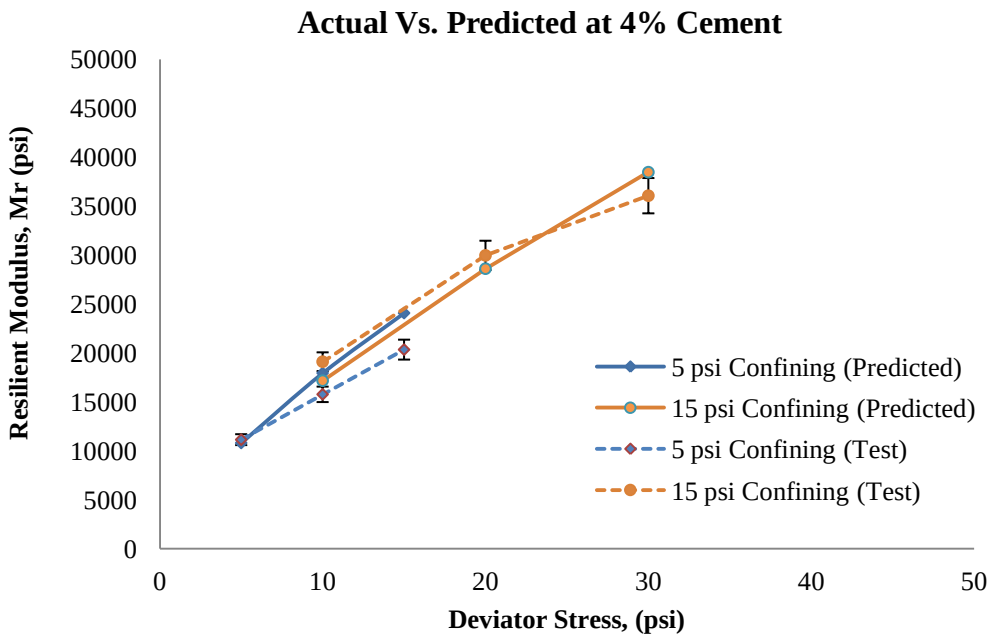

Figure 4-41 Comparison between predicted and actual Resilient Modulus at 4% cement content at 5 and 15 psi confining pressure

Predicted values at 2% cement content varied significantly from the actual conditions, especially for the cases of lower confinements with higher deviator stresses. At higher confinements with low deviator stresses, variations were also significant. In other cases, predicted values were within 10% range of the actual test values as shown in Figure 4-42.

Higher variations between the predicted and actual values were observed for 0% cement content which has been shown in Figure 4-43. Variations exceed 10% when the lower confining stresses were associated with higher deviator stresses. The same trend was also observed at higher confinements with lower deviator stresses. In other cases, variations were not that significant.

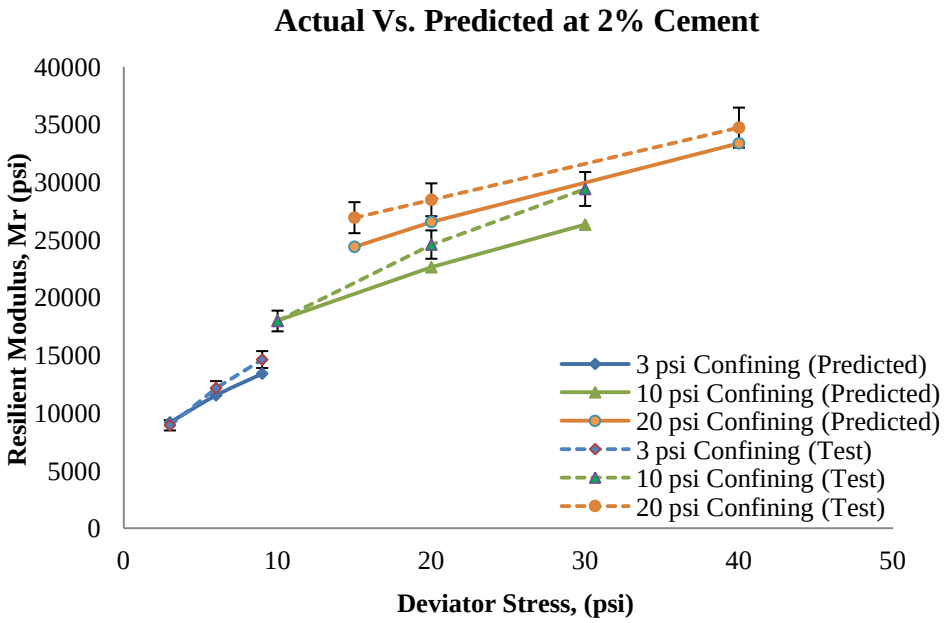

(a)

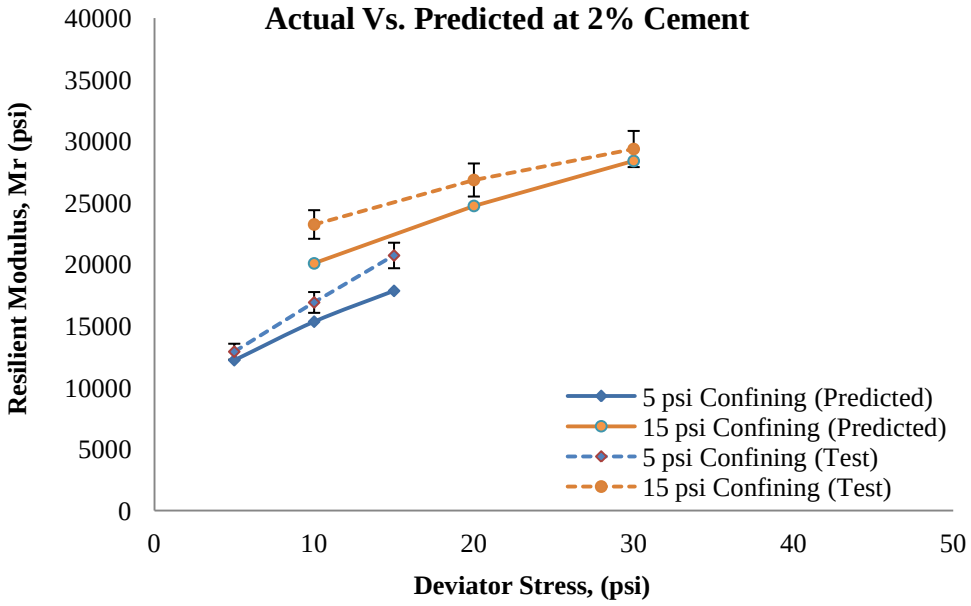

(b)

Figure 4-42 Comparison between predicted and actual Resilient Modulus at 2% cement content (a) 3, 10 and 20 psi (b) 5 and 15 psi confining pressure

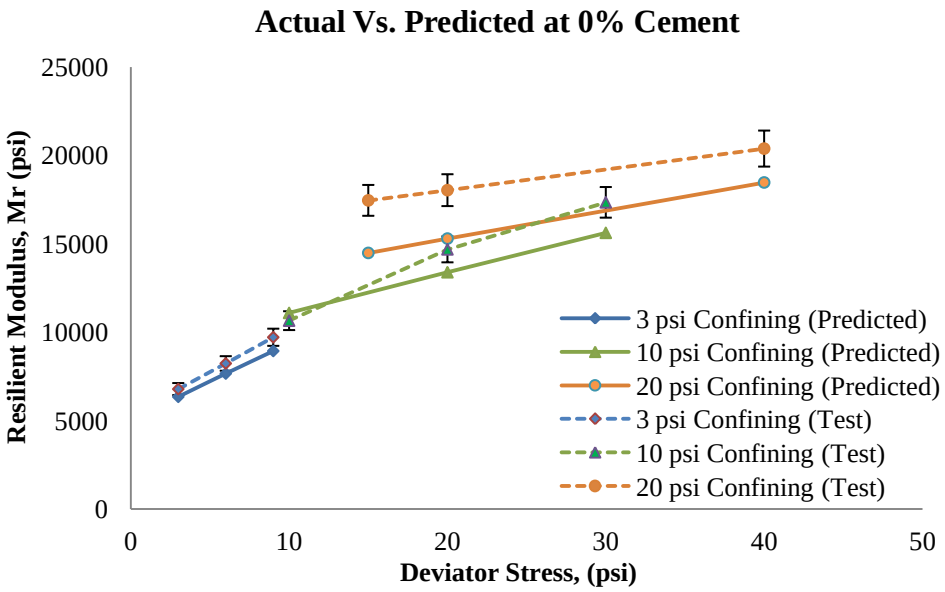

(a)

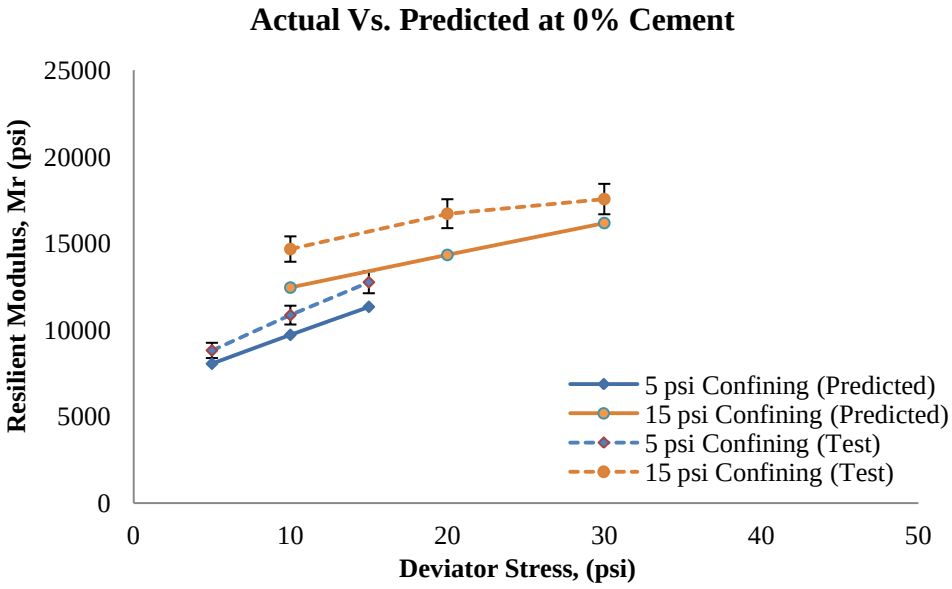

(b)

Figure 4-43 Comparison between predicted and actual Resilient Modulus at 0% cement content (a) 3, 10 and 20 psi (b) 5 and 15 psi confining pressure

Table 4-19 shows the percent difference between the actual and predicted resilient modulus response of cement treated Grade-2 (source 2) materials. For bulk stress modeling, average variations were found in between 10-16%, whereas; in four parameter modeling average variations were found to be in 3-11% range.

Table 4-19 Percent difference between the actual and predicted M_R response

Confining (psi)	Deviator (psi)	Bulk (psi)	Bulk Stress Modeling				Four Parameter Modeling			
			0%	2%	4%	6%	0%	2%	4%	6%
3	3	12	2.29	3.59	20.04	10.99	6.47	2.79	6.91	6.48
	6	15	6.89	13.97	4.67	3.24	6.94	5.13	7.93	1.65
	9	18	14.40	21.01	13.36	12.31	8.00	8.34	18.43	2.69
5	5	20	1.07	5.17	17.86	11.49	8.73	5.37	3.03	3.57
	10	25	11.25	18.16	5.27	9.34	10.50	9.24	13.79	2.23
	15	30	18.07	26.20	18.38	20.86	11.15	13.87	18.37	4.86
10	10	40	11.48	0.30	9.84	4.25	4.11	0.26	2.07	6.57
	20	50	10.67	17.66	15.96	10.59	8.82	7.98	9.38	0.09
	30	60	17.96	23.90	28.00	23.00	9.95	10.50	13.14	4.09
15	10	55	6.62	8.20	23.35	19.38	15.17	13.60	10.14	5.62
	20	65	11.69	12.91	13.37	0.25	14.25	7.85	4.53	0.52
	30	75	10.39	13.86	21.81	17.14	7.89	3.30	6.66	5.48
20	15	75	9.94	6.03	7.29	17.99	17.03	9.39	12.98	1.12
	20	80	10.28	7.94	6.53	1.39	15.19	6.71	9.70	5.86
	40	100	12.31	14.68	23.16	18.92	9.40	3.91	8.37	6.13
Average % Variation			10.35	12.91	15.26	12.08	10.24	7.22	9.70	3.80

4.7.3.2 Statistical Evaluation of Actual and Predicted Values

Figure 4-44 represents the comparison between the actual resilient modulus with the predicted values at all cement contents. Trend follows the straight line pattern along with 1:1 line, indicating good agreement between the actual and predicted values. In most cases, predicted values were found to be lower than those of the actual values providing a safety margin of using the predictive models.

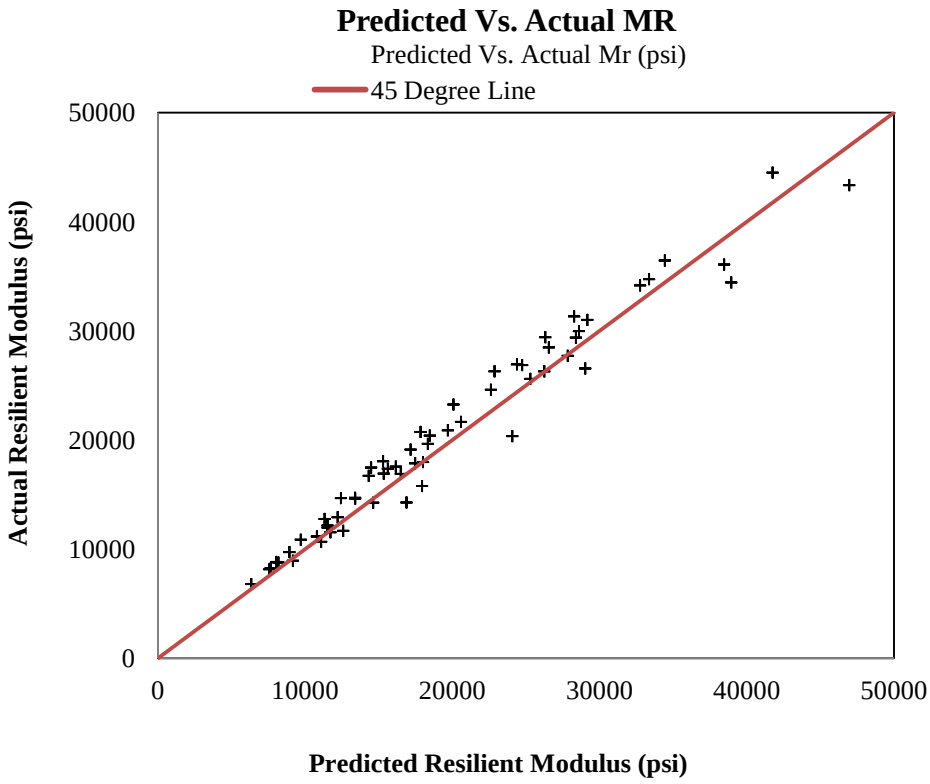

Figure 4-44 Comparison between the actual resilient modulus with the predicted values at all cement contents

Independent two sample t-test assuming unequal variance was performed to determine whether there are any significant differences between the actual and predicted values. Independent two sample t-test was preferred as the sample size was higher and also

there was no dependence between the predicted and actual test values. In t-test, the mean values of resilient modulus found from the tests were compared with the mean values of the predicted resilient modulus. Risk level of claiming equivalence or P-value was taken as 0.05. Basic hypothesizes of the t-test can be described as follow:

$H_0 : m_1 - m_2 = 0$

$H_a : m_1 - m_2 \neq 0$

Where,

m_1 = Mean of the actual resilient modulus values

m_2 = Mean of the predicted resilient modulus values

The result of t-test has been presented in Table 4-20. The t-Stat found from the analysis was lower than the critical value of two-tail test. Also, the P-value for two-tail test was higher than the risk level of 0.05. Hence, the null hypothesis cannot be rejected stating with 95% confidence that, any difference between the actual and predicted values occurred by chance.

Table 4-20 t-Test: Two-Sample Assuming Unequal Variances

	Actual MR	Predicted MR
Mean	20495.75	19729.01
Variance	84894666	87565871
Observations	60	60
Hypothesized Mean Difference	0	
df	118	
t Stat	0.452248	
P(T<=t) one-tail	0.32596	
t Critical one-tail	1.65787	
P(T<=t) two-tail	0.65192	
t Critical two-tail	1.980272	

Chapter 5

CONCLUSION AND RECOMMENDATION

5.1 Introduction

Non-destructive test methods such as stress wave velocity, cross-hole, short-pulse radar, pulse velocity etc. have been using successfully for years in assessing pavement material properties. Among these, the use of stress wave velocity method is increasing significantly due to its non-destructive and easy to use nature. In recent times, noteworthy advancements of stress wave velocity method in theoretical and experimental domains are offering a new standard of non-destructive tests. In this present study, this method was devoted to characterize the strength and stiffness properties of cement treated base materials. Different combination of reclaimed asphalt pavement (RAP) with Grade-1 and Grade-2 materials were considered separately to evaluate the applicability of stress wave velocity method on pavement base materials. It was found that the stress wave velocity method is excellent in characterizing strength properties of cement treated base materials which has presented in chapter 3. Some of the salient findings of this research are presented in the following section:

5.2 Summary and Conclusions

In accessing the suitability of cement stabilized RAP and RAP- Grade-2 mixes as a structurally sound alternative, the following considerations should also be taken into account as, these summarize the findings of this study:

- P-wave velocity, unconfined compressive strength and modulus of elasticity decrease with the increases of RAP percentage but, no significant decrease in P-wave velocity is observed, if RAP materials are used up to 30% in the mix. Inclusion of cement has significant affect on velocity, strength and stiffness response. Higher percentage of cement offers higher strength therefore; different strength

requirements for pavement base construction can be achieved with RAP and recycled crushed concrete mixtures by utilizing varying percentage of cement.

- At higher cement contents (4% and 6%), modulus of elasticity found by P-wave velocity falls within 10% range of the modulus of elasticity determined by UCS test. But at lower cement contents (0% and 2%), variations were higher compared with the variations found at higher cement contents. Inadequate fines to fill the voids might be the reason of lesser P-wave velocity at lower cement contents which eventually predicted lower moduli values.
- On the basis of strength and stiffness requirements, Figure 4-12 and Figure 4-15 can be used in pavement design for fixing an economic but satisfactory aggregate blend with appropriate amount of cement content.
- Inclusion of cement causes significant increase in resilient modulus response of every aggregate blends. At low cement content confining stress plays the vital role in resilient modulus response, though at higher cement contents deviator stress is more significant.
- It is anticipated that, Equation 4.4 can be useful in estimating the stiffness response of cement treated base materials, if RAP or recycled crushed concrete is used. Equation 4.7 is expected to predict the unconfined compression strength from P-wave velocity measurements with satisfactory level of confidence. Both the regression correlations are likely to hold good agreement with actual strength and stiffness values if the P-wave velocity remains within the range of 500 ft/sec to 1500 ft/sec.
- As presented by Equation 4.10, a weak correlation was found between the P-wave velocity and the resilient modulus response at 10 psi confining stress and 30 psi deviator stress, regardless the amount of cement was used. This equation

can be used for the initial approximation of resilient modulus at 10 psi confining and 30 psi deviator stress.

- Bulk stress modeling was done for the estimation of resilient modulus from P-wave velocity measurements at different pressure sequences. Regardless the amount of cement percentage, a weak correlation with low value of coefficient of determination was found. But the situation changed when the modeling was done at four different cement contents separately indicating the massive influence of cement content. Regression equations between bulk stress, P-wave velocity and resilient modulus at four different cement contents are presented by the Equation 4.14, 4.15, 4.16 and 4.17.
- To identify the influence of deviator stress and confining stress on resilient modulus response separately, four parameter modeling was done considering P-wave velocity, bulk stress, confining stress or deviator stress as the independent variable. Four different correlations depending on cement content are presented by Equation 4.21, 4.22, 4.23 and 4.24 which are expected to predict the resilient moduli values more accurately. It was found that, deviator stress plays most significant role rather than the confining stress, except for the case of 0% cement, supporting the fact that at higher cement content the specimens are stiff and strong enough to be influenced by confining stress. This is why the regression equation for 0% cement content included the confining stress as an independent variable thought in other cases deviator stress was included.

5.3 Recommendations

For the deeper state of understanding of the behavior of cement stabilized RAP and RAP-aggregate mixtures, the following recommendations were identified for further research work:

A) To achieve a comprehensive understanding of stress wave velocity, strength and stiffness development of base materials, it is recommended to evaluate the P-wave velocity, strength and stiffness response of different mixes if those are stabilized with lime. Same procedure as described in this study could be adopted in evaluating the strength and stiffness properties of different lime treated aggregate blends.

B) To increase the coherence of the equations and graphs proposed in this study, more samples should be tested with materials from varying sources. Investigation of other different cement contents and some more combinations will increase the reliability of the proposed equations and graphs of this study.

C) Inclusion of fiber might have significant influence on wave velocity, strength and stiffness response of the mixtures. So the investigation on the effects of different fiber types and fiber dosages on the behavioral response of cement or lime treated aggregate blends is recommended.

Appendix A

Resilient Modulus Data

Table A-1 Resilient modulus response of 100% Grade-2 (source 1) materials treated at four different cement contents

Confining (psi)	Deviator (psi)	100% Grade- 2			
		0%	2%	4%	6%
3	3	7923	13182	11163	9653
	6	7744	14326	12254	10254
	9	7748	15906	14776	12035
5	5	8101	15404	11322	10845
	10	8781	18577	18247	12547
	15	9806	21299	22535	16604
10	10	9577	21443	18215	15906
	20	12703	25790	27668	26357
	30	15341	27995	38907	32568
15	10	10828	25563	16130	26587
	20	11261	28186	21904	30124
	30	20810	31425	38285	38657
20	15	11747	30505	20552	32198
	20	14124	32836	25647	35871
	40	20810	34183	43884	45687

Table A-2 Resilient modulus response of 50% RAP + 50% Grade-2 materials treated at four different cement contents

Confining (psi)	Deviator (psi)	50% RAP + 50% Grade-2			
		0%	2%	4%	6%
3	3	8075	12694	3590	8786
	6	14727	14366	8366	15820
	9	17589	15299	10299	17062
5	5	15752	14921	8092	15188
	10	22643	16327	11327	18432
	15	24478	21247	21247	24990
10	10	21659	18893	10521	18691
	20	28387	23204	18204	27598
	30	29401	25216	35216	33611
15	10	22226	24417	9884	21176
	20	34934	31477	17477	23296
	30	46499	38265	30265	41009
20	15	33176	24404	19198	25593
	20	43791	32906	26906	35867
	40	47915	38978	38978	48623

Table A-3 Resilient modulus response of 70% RAP + 30% Grade-2 materials treated at four different cement contents

Confining (psi)	Deviator (psi)	70% RAP + 30% Grade-2			
		0%	2%	4%	6%
3	3	10260	10117	6555	10527
	6	15181	16219	7147	14765
	9	18270	22247	8708	17761
5	5	14984	15187	6914	14905
	10	20129	25596	9538	19511
	15	25420	36108	14542	27515
10	10	21563	28522	9994	20885
	20	30203	42322	18437	31668
	30	23567	35494	30439	44581
15	10	27191	31208	9809	21108
	20	36339	46461	12902	25681
	30	46791	58210	26656	48636
20	15	31902	28036	13232	27051
	20	41385	34260	17282	34669
	40	45988	52987	35550	50920

Table A-4 Resilient modulus response of 100% Grade-1 materials treated at four different cement contents

Confining (psi)	Deviator (psi)	100% Grade-1			
		0%	2%	4%	6%
3	3	11087	8925	14665	14757
	6	12035	13147	19580	11531
	9	13474	14623	21764	14242
5	5	15425	14907	19439	14957
	10	15005	18506	24364	17879
	15	16436	20721	28367	21644
10	10	16792	22965	24791	20631
	20	16792	26589	30482	26276
	30	17983	33406	35668	34155
15	10	16792	24239	23615	21875
	20	15627	26052	26484	23702
	30	20559	35669	35663	36437
20	15	16578	28821	26070	25587
	20	21333	32471	28514	30990
	40	25408	41724	41234	45486

Table A-5 Resilient modulus response of 100% Grade-2 (source 2) materials treated at four different cement contents

Confining (psi)	Deviator (psi)	100% Grade-2 (source 2)			
		0%	2%	4%	6%
3	3	6783	8925	8142	8757
	6	8232	12147	11664	11531
	9	9714	14623	14261	14242
5	5	8809	12907	11142	11957
	10	10845	16906	15771	16879
	15	12748	20721	20340	21644
10	10	10653	17965	17849	19631
	20	14688	24589	26541	26276
	30	17349	29406	34425	34155
15	10	14662	23239	19107	20875
	20	16704	26852	29966	27702
	30	17548	29369	36065	36437
20	15	17460	26921	26283	25587
	20	18038	28471	31315	30990
	40	20390	34724	43339	44486

References

1. Texas Department of Transportation. (1999c). "Particle size analysis of soils." *Tex-110-E,* Austin, TX.
2. Texas Department of Transportation. (1999b). "Laboratory compaction characteristics and moisture-density relationship of base materials." *Tex-113-E,* Austin, TX.
3. Texas Department of Transportation. (1999c). "Soil-cement testing procedure." *Tex-120-E,* Austin, TX.
4. ASTM. (2002b). "Standard test method for compressive strength of molded soil- cement cylinders." *ASTM D1633-00,* West Conshohocken, PA.
5. ASTM. (2010). "Standard test method for measuring the P-Wave speed and the thickness of concrete plates using the impact-echo method." ASTM C1383-04*,* West Conshohocken, PA.
6. ASTM. (2010). C1740-10. "Standard Practice for Evaluating the Condition of Concrete Plates Using the Impulse-Response Method." *ASTM C1740-10*, West Conshohocken, PA.
7. ASTM. (2002). "Standard Test Method for Pulse Velocity Through Concrete." *ASTM C 597–02,* West Conshohocken, PA.
8. British Standard, "Recommendations for the measurement of dynamic modulus of elasticity." *BSI 881: Part 209:1990*, U.K., 1986.
9. AASHTO T 307-99 "Determining the Resilient Modulus of Soils and Aggregate Materials" (2003).
10. Faysal, M., Mahedi, M., Aramoon, A., Thian, B., Hossain, M.S., Khan, M.S., (2015), "*Strength Characterization of Untreated and Cement Treated Recycled Flex-Base Materials*", GeoCongress 2016, February 14-17, Phoenix, Arizona.

11. Faysal, M., Mahedi, M., Aramoon, A., Thian, B., Hossain, M.S., Khan, M.A., Khan, M.S., (2015), "*Determination of Structural Coefficient of Different Combinations of Cement Treated/ Untreated Recycled Base Materials*", accepted for GeoCongress 2016, February 1417, Phoenix, Arizona.
12. Graveen, Cole. *Nondestructive test methods to assess pavement quality for use in a performance-related specification*. Diss. Purdue University, 2001.
13. Sansalone, M., and N. J. Carino. "Laboratory and field studies of the impact-echo method for flaw detection in concrete." *ACI Special Publication* 112 (1989).
14. Qasrawi, Hisham Y. "Concrete strength by combined nondestructive methods simply and reliably predicted." *Cement and Concrete Research* 30.5 (2000): 739-746.
15. American Association of State Highway Transportation Official. (1993). AASHTO Guide for Design of Pavement Structures, American Association of State Highway and Transportation Officials, Washington, D. C.
16. Hoyos, Laureano R., Anand J. Puppala, and Carlos A. Ordonez. "Characterization of cement-fiber-treated reclaimed asphalt pavement aggregates: Preliminary investigation." *Journal of Materials in Civil Engineering* (2011).
17. Sherwood, P. (1995). Alternate Materials in Road Construction: A Guide to the Use of Recycled and Secondary Aggregates, 1995.
18. Popovics, J. S., et al. "One-sided stress wave velocity measurement in concrete." *Journal of Engineering Mechanics* 124.12 (1998): 1346-1353.
19. Carino, N.J., “Laboratory Study of Flaw Detection in Concrete by the Pulse-Echo Method”, In Situ/Nondestructive Testing of Concrete, Malhotra, V.M., Ed., American Concrete Institute, SP-82, Detroit, 1984(a).

20. Olson, Larry D., Marwan F. Aouad, and Dennis A. Sack. "NDT Diagnosis of Drilled Shaft Foundations." *Transportation Research Board 77th Annual Meeting*. No. 9.8-0595. 1998.
21. Qixian, Luo, and J. H. Bungey. "Using compression wave ultrasonic transducers to measure the velocity of surface waves and hence determine dynamic modulus of elasticity for concrete." *Construction and building materials* 10.4 (1996): 237-242.
22. Sturrup, V. R., F. J. Vecchio, and H. Caratin. "Pulse velocity as a measure of concrete compressive strength." *ACI Special Publication* 82 (1984).
23. Carino, N.J., Sansalone, M., and Hsu, N. N., “Flaw Detection in Concrete by Frequency Spectrum Analysis of Impact-Echo Waveforms”, International Advances in Nondestructive Testing, W.J. McGonnagle, Ed., Gordon & Breach, New York, 1986, pp. 117-146.
24. Lin, J. and Sansalone, M., “Impact-Echo Response of Hollow Cylindrical Concrete Structures Surrounded by Soil and Rock: Part 1-Numerical Studies”, Geotechnical Testing Journal, Vol. 17, No. 2, 1994, pp. 207-219.
25. Lin, J. and Sansalone, M., “Impact-Echo studies of Interfacial Bond Quality in Concrete. 1. Effects of Unbonded Fraction of Area”, ACI Materials Journal, Vol. 93, No. 3, 1996, pp. 223-232.
26. Lin, J. and Sansalone, M., “A Procedure for Determining P-Wave Speed in Concrete for Use in Impact-Echo Testing Using a Rayleigh Wave Speed Measurement Technique”, Innovations in Non-Destructive Testing of Concrete, Pessiki, S. and Olson, L., Ed., American Concrete Institute, SP-168, Michigan, 1997, pp. 137-165.
27. Limbachiya, M. C., T. Leelawat, and R. K. Dhir. "Use of recycled concrete aggregate in high-strength concrete." *Materials and structures* 33.9 (2000): 574-580.

28. Gnanendran, C. T. and Woodburn, L. J. (2003). Recycled Aggregate for Pavement Construction and the Influence of Stabilization. Proceedings- Conference of the Australian Road Research Board, v 21, 2003, p 1755-1768.
29. Proctor Jr, Thomas M. "An improved piezoelectric acoustic emission transducer." *The Journal of the Acoustical Society of America* 71.5 (1982): 1163-1168.
30. Puppala, Anand J., Laureano R. Hoyos, and Ajay K. Potturi. "Resilient moduli response of moderately cement-treated reclaimed asphalt pavement aggregates." *Journal of Materials in Civil Engineering* 23.7 (2011): 990-998.
31. Brand, A. (2012). Fractionated reclaimed asphalt pavement as a coarse aggregate replacement in a ternary blended concrete pavement.
32. Euch Khay, S. E., Euch Ben Said, S. E., Loulizi, A., &Neji, J. (2014). Laboratory Investigation of Cement-Treated Reclaimed Asphalt Pavement Material. *Journal of Materials in Civil Engineering*.
33. Grilli, A., Bocci, E., & Graziani, A. (2013). Influence of reclaimed asphalt content on the mechanical behaviour of cement-treated mixtures. *Road Materials and Pavement Design*, *14*(3), 666-678.
34. Guthrie, W. S., Brown, A. V., & Eggett, D. L. (2007). Cement stabilization of aggregate base material blended with reclaimed asphalt pavement. *Transportation Research Record: Journal of the Transportation Research Board*, *2026*(1), 47-53.
35. Hansen, K. R., and Copeland, A.(2014). "Annual Asphalt Pavement Industry Survey on Recycled Materials and Warm-Mix Asphalt Usage: 2009–2013." *No. IS-138.*
36. Croney, David, and Paul Croney. *The design and performance of road pavements*. 1991.
37. George, K. P. "Prediction of resilient modulus from soil index properties." (2004).

38. Lotfi, H. and Witczak, M. W. (1985). Dynamic Characterization of Cement Treated Base and Subbase Materials. Transportation Research Record, n 1031, 1985, p 41-48

39. Janoo, V. C. (1994). Layer Coefficients for NHDOT Pavement Materials. Prepared for New Hampshire Department of Transportation and U.S. Department of Transportation, Special Report 94-30, September 1994.

40. Jones, D., Wu, R., & Louw, S. (2014). Full-Depth Recycling Study: Test Track Construction and First Level Analysis of Phase 1 HVS and Laboratory Testing.

41. Kim, S., Byron, T., and Sholar, G. A. "Evaluation of use of high percentage of reclaimed asphalt pavement (RAP) for Superpave mixtures."*FDOT/SMO/07-507* (2007).

42. Kolias, S. (1996). Mechanical properties of cement-treated mixtures of milled bituminous concrete and crushed aggregates. *Materials and Structures*, *29*(7), 411-417.

43. Hansen, Torben C., ed. *Recycling of demolished concrete and masonry*. Vol. 6. CRC Press, 2004.

44. Wilburn, D. R. and Goonam T. G. (1998). Aggregates from Natural and Recycled Sources: Economic Assessments for Construction Applications-A Materials Flow Analysis. U. S. Geological Survey Circular, 1176

45. Griffiths, Carolyn T., and J. M. Krstulovich Jr. *Utilization of Recycled Materials in Illinois Highway Construction*. No. IL-PRR-142,. 2002.

46. Lim, S., & Zollinger, D. G. (2003). Estimation of the compressive strength and modulus of elasticity of cement-treated aggregate base materials. Transportation Research Record: Journal of the Transportation Research Board, 1837(1), 30-38.

47. Nazarian, S., Yuan, D., Hoyos, L., and Puppala, A. "Laboratory and field evaluation of cement- treated reclaimed asphalt pavement blends as roadway base material." J. ASTM Int., 2(9), 437- 453.
48. Puppala, Anand J., Laureano R. Hoyos, and Ajay K. Potturi. "Resilient moduli response of moderately cement-treated reclaimed asphalt pavement aggregates." *Journal of Materials in Civil Engineering* 23.7 (2011): 990-998.
49. Taha, R., Al-Harthy, A., Al-Shamsi, K., & Al-Zubeidi, M. (2002). Cement stabilization of reclaimed asphalt pavement aggregate for road bases and subbases. Journal of Materials in Civil Engineering, 14(3), 239-245. Texas Department of Transportation. (1999a). "Determining the specific gravity of soils." *Tex-108-E, Austin, TX.*
50. Tia, M., Hossiney, N., Chen, Y., Do, T. A. (2012). Use of Reclaimed Asphalt Pavement in Concrete Pavement Slabs. No. 00088115.
51. Yuan, D., Nazarian, S., Hoyos, L. R., & Puppala, A. J. (2011). Evaluation and Mix Design of Cement-Treated Base Materials with High RAP Content. In Proceedings (CD), 90 th Annual Meeting, Transportation Research Board, Washington, DC.
52. Sansalone, M. and Carino, N.J., “Stress Wave Propagation Methods”, CRC Handbook on Nondestructive Testing of Concrete, Malhotra, V.M. and Carino, N.J., Ed., CRC Press, Florida, 1991, pp. 275-304.
53. Sansalone, M. and Pratt, D.G., “Theory and Operation Manual for the Impact-Echo Field System”, Vol. 1, 2nd Edition, Jan. 1993.
54. Sansalone, M., Lin, J., and Streett, W.B., “A Procedure for Determining Concrete Pavement Thickness Using P-Wave Speed Measurements and the Impact- Echo Method”, Innovations in Non-Destructive Testing of Concrete, Pessiki, S. and Olson, L., Ed., American Concrete Institute, SP-168, Michigan, 1997, pp. 167-184.

55. Sansalone, M., Lin, J., and Streett, W. B., “A Procedure for Determining P-Wave Speed in Concrete for Use in Impact-echo Testing Using a P-Wave Speed Measurement Technique”, ACI Materials Journal 1997, Vol. 94, Iss. 6, pp. 531-539.
56. Briaud, Jean-Louis. "Defect And Length Predictions By NDT Methods For Nine Bored Piles Jean-Louis Briaud,* Marc Ballouz,♦♦ and George Nasr**** Spencer J. Buchanan Professor, Department of Civil Engineering, Texas A&M University, College Station, TX, 77843-3136, USA." *Deep Foundations 2002: An International Perspective on Theory, Design, Construction, and Performance: Proceedings of the International Deep Foundations Congress 2002, Februery 14-16, 2002, Orlando, Florida*. Vol. 1. American Society of Civil Engineers, 2002.
57. Pessiki, S. P. and Carino, N. J., “Measurement of the Setting Time and Strength of Concrete by the Impact-Echo Method”, Report No. NBSIR 87-3575, National Bureau of Standards, Washington, D.C., July 1987, 109 pages.
58. Pessiki, S. P. and Carino, N. J., Setting Time and Strength of Concrete Using the Impact Echo Test Method”, ACI Materials Journal 1988, Vol. 85, Iss. 5, pp. 389-399.
59. Pessiki, S. P. and Johnson, M. R., “Nondestructive Evaluation of Early-Age Concrete Strength in Plate Structures by the Impact-Echo Method”, ACI Materials Jour nal 1996, Vol. 93, No. 3, pp. 260-271.
60. Popovics, J. S., Song, W., Achenbach, J. D., Lee, J. H., and Andre, R. F., “One-Sided Stress Wave Velocity Measurement in Concrete”, Journal of Engineering Mechanics, Vol. 124, Iss. 12, 1998, pp. 1346-1353.
61. Olson, Larry D., and Clifford C. Wright. "Non-destructive testing for repair and rehabilitation." *Concrete International* 12.3 (1990): 58-64.
62. Amick, Hal, et al. "Voids Beneath Slabs-on-Ground." *Concrete international* 31.7 (2009): 29-33.

63. Davis, Allen G. "The nondestructive impulse response test in North America: 1985–2001." *NDT & E International* 36.4 (2003): 185-193.

64. Naik, T. R., and Malhotra, V. M., “The Ultrasonic Pulse Velocity Method”, CRC Handbook on Nondestructive Testing of Concrete, Malhotra, V.M. and Carino, N. J., Ed., CRC Press, Florida, 1991, pp. 169-188.

Biographical Information

Masrur Mahedi graduated with a Bachelor of Science in Civil Engineering from Bangladesh University of Engineering and Technology, Dhaka, Bangladesh in February 2013. After graduation, he started his career as a Lecturer in European University of Bangladesh (EUB), Civil Engineering Department, Dhaka, Bangladesh. He started his graduate studies at The University of Texas at Arlington in Summer 2014. During his study, he got the opportunity to work as a graduate research assistant under the supervision of Dr. Sahadat Hossain. The author's research interests include Recycled Materials, Non-destructive Test (NDT) Methods, Structural Health Monitoring, Slope Stability Analysis, Numerical Modeling and Bioreactor Landfills.